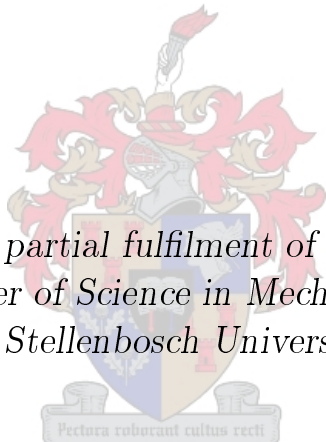


A Study for the Development of a Laser Tracking System Utilizing Multilateration for High Accuracy Dimensional Metrology

by

Gabriel Pieter Greeff



*Thesis presented in partial fulfilment of the requirements for
the degree of Master of Science in Mechatronic Engineering
at Stellenbosch University*

Department of Mechanical and Mechatronics Engineering,
University of Stellenbosch,
Private Bag X1, Matieland 7602, South Africa.

Supervisor: Prof. K Schreve

March 2010

Declaration

By submitting this thesis electronically, I declare that the entirety of the work contained therein is my own, original work, that I am the owner of the copyright thereof (unless to the extent explicitly otherwise stated) and that I have not previously in its entirety or in part submitted it for obtaining any qualification.

Signature:

G.P. Greeff

Date:

Copyright © 2010 Stellenbosch University
All rights reserved.

Abstract

A Study for the Development of a Laser Tracking System Utilizing Multilateration for High Accuracy Dimensional Metrology

G.P. Greeff

*Department of Mechanical and Mechatronics Engineering,
University of Stellenbosch,
Private Bag X1, Matieland 7602, South Africa.*

Thesis: MScEng (Mechatronic)

March 2010

Accurate dimensional measurement devices are critical for international industrial competitiveness for South Africa. An overview of all the necessary components of a laser tracking system using a multilateration technique for very accurate dimensional metrology is presented.

A prototype laser tracker station was built to further investigate this type of system. The prototype successfully tracks a target within a volume of at least $200 \times 200 \times 200 \text{ mm}^3$, approximately 300 mm away from the tracker. This system includes the mechanical design of a prototype tracker station, electronic implementation of amplification and motor control circuits, a tracking control algorithm, microcontroller programming and interfacing, as well as a user interface.

Kinematic modelling along with Monte Carlo analyses find the main error source of such a tracker as the beam steering mechanism gimbal axes misalignment. Multilateration is also motivated by the results found by the analysis.

Furthermore, an initial sequential multilateration algorithm is developed and tested. The results of these tests are promising and motivate the use of multilateration over a single beam laser tracking system.

Uittreksel

'n Studie vir die Ontwikkeling van 'n Laser Volgsisteem deur middel van Multilaterasie vir Akkurate Dimensionele Metrologie

(“A Study for the Development of a Laser Tracking System Utilizing Multilateration
for High Accuracy Dimensional Metrology”)

G.P. Greeff

Departement Meganiese en Megatroniese Ingenieurswese,
Universiteit van Stellenbosch,
Privaatsak X1, Matieland 7602, Suid Afrika.

Tesis: MScIng (Megatronies)

Maart 2010

Dit is van kritieke belang dat Suid-Afrika akkurate dimensionele metingstoestelle ontwikkel vir internasionale industriële medding. 'n Oorsig van al die nodige komponente vir 'n Laser-Volgsisteem, wat slegs van multilaterasie gebruik maak om baie akkurate drie dimensionele metings te kan neem, word in hierdie projek voorgestel.

'n Prototipe Laser-Volgsisteem-stasie word gebou om so 'n sisteem verder te ondersoek. Die prototipe slaag wel daarin om 'n teiken, binne 'n volume van $200 \times 200 \times 200 \text{ mm}^3$ op 'n afstand van omtrent 300 mm te volg. Die sisteem sluit die meganiese ontwerp van die sodanige stasie, elektroniese seinversterking, motorbeheer, 'n volgingsbeheer algoritme, mikroverwerker programmeering en intergrasie, asook 'n gebruikerskoppelvlak program in.

Kinematiese modelering, tesame met Monte Carlo simulasies, toon aan dat die hoof oorsaak van metingsfoute by so 'n stasie by die rotasie-asse van die laserstraal-stuurmechanisme, wat nie haaks is nie, lê. Die multilaterasie metode word ook verder ondersteun deur dié modelering.

'n Algoritme wat sekwensiële multilateratsie toepas word boonop ontwikkel en getoets. Die resultate van die toetse dui daarop dat die algoritme funksioneer en dat daar voordele daarin kan wees om so 'n metode in plaas van 'n Enkelstraal-Volgsisteem te gebruik.

Acknowledgements

I would like to express my sincere gratitude to the following people and organisations:

- The NMISA, for sponsoring this project.
- O.A. Kruger, from NMISA, for motivation and advice.
- Prof. K. Schreve, my supervisor, for crucial guidance and motivation.
- E.C. Strydom, my lovely girlfriend, for vital encouragement.
- And my hardworking fellow students.

Above all I thank our Father in heaven, whose grace is sufficient, through Jesus Christ.

Contents

Declaration	i
Abstract	ii
Uittreksel	iii
Acknowledgements	iv
Contents	v
List of Figures	vii
List of Tables	x
Nomenclature	xi
1 Introduction	1
2 Literature Review	5
2.1 Dimensional Metrology and Measurement System Selection	5
2.2 Laser Trackers	8
2.3 Laser Tracker Components	11
2.4 Main Uncertainty sources	23
2.5 Kinematic Model	28
2.6 LTS with Multilateration	34
2.7 CMM Calibration with a LTS	37
3 Laser Tracker Design	38
3.1 Design Process Description	38
3.2 System Requirements	39
3.3 Beam Steering Mechanism Design	39
3.4 Actuator Selection and Control	44
3.5 Sensor Amplification	48
3.6 Embedded Controller Design and Programming	53
3.7 Calibration Concepts	58

4	Laser Tracker Kinematic Model Simulations	60
4.1	Simulation Process and Algorithm	60
4.2	Simulations	61
4.3	Implications of the Simulation Results	65
5	Sequential Multilateration Algorithm Tests	66
5.1	Experiment Introduction	66
5.2	The Algorithm	67
5.3	The Experiments	68
5.4	Experiments with Setup One	69
5.5	Experiments with Setup Two	73
5.6	Discussion of Results	78
6	Conclusion	79
Appendices		81
A	Mathematics and Other Kinematic Models	82
A.1	Note on Homogeneous Transformations	82
A.2	Kinematic Modeling: Other Models	84
B	Summary of All Relevant Datasheets	89
C	PCB Schematics	91
D	Gimbal Prototype 2 Drawings	99
E	Cost Summary	115
List of References		116

List of Figures

1.1	Traceability Measurement Chart	2
2.1	A Laser Tracker made by Leica Geosystems	9
2.2	Schematic of a Laser Tracker with Main Components	10
2.3	Schematic of the Tracking Principle	11
2.4	Schematic of the Twyman-Green Interferometer	15
2.5	Schematic of a Heterodyne Interferometer	16
2.6	Commercially Available Gimbal Mount from Aerotech	18
2.7	Schematic of an Articulating Hemisphere with a Mirror	18
2.8	Schematic of a Tracker Using a Sphere as a Bearing	19
2.9	Schematic of the Pivoting Interferometer	19
2.10	Photo of a Segmented PSD	21
2.11	Photo of a SMR	22
2.12	Schematic of a Hemispherical Retroreflector	22
2.13	Schematic of Installation Errors for a Interferometer	25
2.14	Ideal Tracker Model	29
2.15	Mirror Centre Offset with Target and Reference Position	31
2.16	Mirror Centre Offset Detail	32
2.17	Multilateration Setup for Irregularly Placed Trackers	36
3.1	Time Line of the Design Process	39
3.2	The Two Gimbal Prototypes	42
(a)	Prototype 1	42
(b)	Prototype 2	42
3.3	Illustration of the Effect of Axes Misalignment	43
3.4	Mirror Position and Horizontal Axis Adjustment	43
(a)	Horizontal Axis Adjustment	43
(b)	Mirror Position Adjustment	43
3.5	Illustration of Mirror Offset	44
3.6	Photo of Prototype 2	45
3.7	PWM and Microstepping	47
(a)	PWM Signal	47
(b)	Resulting Current per Phase	47
3.8	Schematic of a Pincushion Type PSD	49

3.9	The Third Prototype Amplification Circuit	50
3.10	Photos of the Final Prototype	51
(a)	Sensor with Amplifier Circuit and 12bit, Faster movement	51
(b)	Sensor with Cover	51
(c)	Sensor with Setup	51
3.11	Sensor Range Tests	52
(a)	Range with 12 bit, Faster movement	52
(b)	Range with 12 bit, Slower Movement	52
(c)	Range with 10 bit	52
3.12	Photo of the Microprocessor and main PCB	54
3.13	Diagram of the Main PCB	55
3.14	Process Flow of Main Program	56
3.15	Change of Spot Position and Size Due to Centre Offset	58
4.1	Example of TP Set	61
4.2	Total Individual Error per Parameter	62
4.3	Total Individual Error per Parameter per Point	63
4.4	Principle Component Analysis	63
(a)	Covariance Ellipsoid	63
(b)	XY Plane Ellipse ($Z = -100$)	63
4.5	Error Contour	64
4.6	Measurement Error Analysis	65
(a)	Effect of Measurement Errors	65
(b)	Magnitude Effect of Measurement and Gimbal Errors	65
5.1	Overall Multilateration Algorithm Process	68
5.2	Final Error for the Fit (Experiment 1)	70
5.3	Three Dimensional Error Analysis (Tracker Position 1)	71
5.4	Three Dimensional Plot (Experiment 1)	71
5.5	Final Error for the Fit (Experiment 2)	72
5.6	A Target Coordinate Set Created by CMM Movement	74
5.7	Setup for Experiment Three	74
5.8	Example of the Average Error for the Fit and Laser Trackers for the Five Distances	76
(a)	Difference with First 700mm Distance	76
(b)	Difference with 450mm Distance	76
(c)	Difference with Second 700mm Distance	76
(d)	Difference with 416mm Distance	76
(e)	Difference with 200mm Distance	76
5.9	Repeated Measurements for Tracker Position One	77
C.1	Amplification Prototype Schematic 1 and 2	91
C.2	Amplification With a Instrumentation Amplifier	92
C.3	Low Pass Anti-Aliasing Filter	92

C.4 Main Board Schematic	93
C.5 Main Board Schematic	94
C.6 First Amplifier Schematic	95
C.7 Final Amplifier Schematic	96
C.8 Final Amplifier Schematic	97
C.9 Stepper Motor Controller Schematic	98
D.1 Gimbal Prototype 2 Drawing Tree	99
D.2 A001 Gimbal Assembly p1	100
D.3 A001 Gimbal Assembly p2	101
D.4 B001 Laser Cut Base	102
D.5 B001 Machined Base	103
D.6 B002 Bearing Support	104
D.7 C001 Z Axis Bush	105
D.8 C002 Laser Cut Z Axis Arm	106
D.9 C002 Machined Z Axis Arm	107
D.10 D001 Laser Cut Y Axis Support	108
D.11 D001 Machined Y Axis Support	109
D.12 D002 Y Axis Mount	110
D.13 D003 Y Axis Bush	111
D.14 D004 Y Axis Shaft	112
D.15 E001 Mirror Support	113
D.16 E002 Mirror Holder	114
E.1 Summary of the Project Costs	115

List of Tables

2.1	SMX Laser Tracker Specifications	9
2.2	API SMR Specifications	27
3.1	Sample Tracking Speeds	40
3.2	Comparison Between Various Beam Steering Mechanisms	41
5.1	SMR Tests	77
B.1	Summary of All Relevant Datasheets	90

Nomenclature

Abbreviations

SMR	Spherically Mounted Retroreflector
OPD	Optical Path Distance
PSD	Position Sensitive Diode
LTS	Laser Tracking System
I	Intensity

Chapter 1

Introduction

The main focus of this thesis is to start the development of a multilateration based Laser Tracking System (LTS), which can determine three dimensional coordinates. This study aims to provide a foundation for the development of a sub-micron accuracy LTS for NMISA¹, which can be used to calibrate conventional bridge type CMMs (Coordinate Measuring Machines).

The project is placed in context by understanding the necessity of highly accurate dimensional measurements or dimensional metrology in industry. Consider, for example, an automated manufacturing and assembly process. All the robots in the process must be calibrated and the manufactured components themselves need to be measured to determine whether they comply with the design specifications. Quality inspection, calibration, assembly and reverse engineering are just some fields where the accuracy and speed of coordinate metrology is vital. Some example applications of dimensional metrology (specifically with a LTS) are the inspection of aircraft components, rotor blades and satellite dish antennas. They are also used in the assembly of large structures (aerospace industry) and even for patient positioning. The level of the required accuracy of dimensional metrology in these industries are increasing and this is the core motivation for the project; i.e. the need for more accurate coordinate metrology for NMISA (Takatsuji *et al.*, 1998; Zhang *et al.*, 2005; Zhuang and Roth, 1995; Lin *et al.*, 2005).

Furthermore, note that all length measurement devices should be calibrated relative to the length standard. This requirement results in a traceability chain, all the way from the definition of the unit for length to machines used on the factory floor. However, with each calibration step away from the length

¹The National Metrology Institute of South Africa (NMISA) is mandated by the Measurement Units and National Measurement Standards Act, No 18 of 2006, under the auspices of the Department of Trade and Industry (the DTI) to maintain, develop and disseminate the National Measurement Standards for South Africa. NMISA is therefore responsible for maintaining the SI units and to maintain and develop primary scientific standards of physical quantities for SA and compare those standards with other national standards to ensure global measurement equivalence. NMISA also provides reference analysis in the case of a measurement disputes (NMISA, 2008).

standard, the uncertainty of the calibrated measuring device increases, which motivates the use of a multilateration based laser measurement system which is directly traceable to the length standard (Umetsu *et al.*, 2005).

The traceability to the length standard determines the theoretical relative accuracy of a LTS. The international length standard, the metre, was defined in 1983 as follows (BIPM, 2006):

“The metre is the length of the path traveled by light in vacuum during a time interval of 1/299 792 458 of a second.”

Figure 1.1 shows the traceability chain in South Africa, with specific focus on the automobile industry, which also places the project into financial context for NMISA (Kruger, 2004). This chart depicts that the annual automotive exports requires CMM measurements, which necessitates at least 350 CMM calibrations per year. For an estimated export of *R65Billion*, the cost of the CMM measurements are estimated to be over *R50Million*, with a total calibration cost in the order of *R3.5Million* per year.

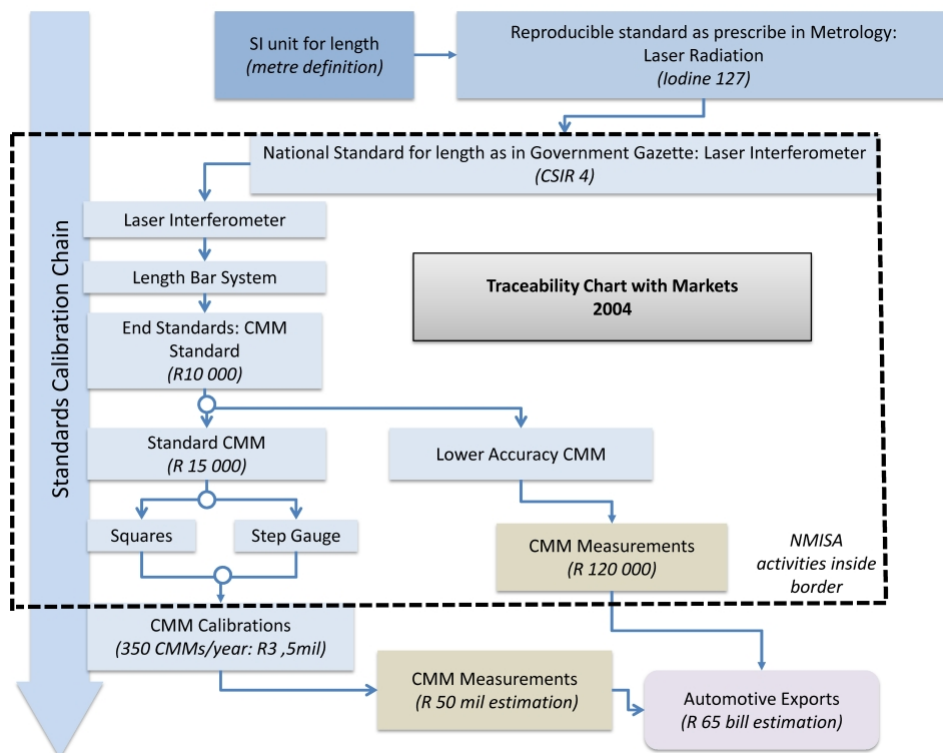


Figure 1.1: Traceability Measurement Chart (Kruger, 2004)

For this thesis a LTS is defined as an integrated system consisting of one or more laser trackers. A laser tracker is a three dimensional measurement system

which uses two angle encoders and a laser interferometric length measurement to determine the target point coordinates.

A laser tracker points the laser beam emitted by a heterodyne laser source with beam steering mechanism to a special retroreflective target. This target returns the incident beam back to the beam steering mechanism. A laser tracker uses a heterodyne laser interferometer to determine the relative distance to the target from a calibrated home point, defined as the default origin of the coordinate system. Along with the two rotary encoders for the angular rotations (azimuth and elevation) of the beam steering mechanism, the three dimensional coordinates of the target can be determined.

Note that the target must be tracked, since the interferometer only measures relative displacement. If the tracker station loses the target at any point the interferometer will lose its *reference* distance and will not be able to determine the current distance to the target.

If more than three laser trackers are used to measure the same target points, only the displacement measurement of each laser tracker could be used to determine the target coordinates (Takatsuji *et al.*, 1998). This calculation is called multilateration and, as only the laser interferometric distance measurements are used, the measurement will be directly traceable to the length standard.

Multilateration is a mathematical technique, similar to trilateration. Trilateration determines the coordinates of a point by only using three distances, taken from three different points to the desired target point. With multilateration however more than three distances per target point are used and this creates a useful redundancy. If a system has several target points and there are more than three measuring stations, all of them measuring simultaneously the distance between them and each target point, the redundant measurement can be used to solve both the target coordinates and the measuring stations coordinates, relative to an arbitrary origin.

This concept of multilateration provides the theoretical tool enabling a LTS to only use laser length measurements to determine the target and measuring station origins. Again, this then promises theoretically to be very accurate as it will be directly traceable to the length standard.

The main motivation for using a LTS in dimensional metrology is that a LTS satisfies Abbe's principle (explained in chapter 2.4), has direct traceability to the length standard, can be self-calibrated and is potentially superior to the conventional bridge-type CMMs (Takatsuji *et al.*, 1998; Lin *et al.*, 2005). The self-calibration of a LTS also creates a virtual metrology frame, making it more portable (Hughes *et al.*, 2000).

The development of a multilateration LTS is the greater project for NMISA. The current concept for such a system is to use one laser source split into four beams, each with its own tracking and interferometry subsystem. The greater system can be divided into three main sub-projects: (1) a tracking and interferometry subsystem, including its calibration, modelling and testing, (2)

multilateration simulation, algorithm and tests, which includes modelling the effect of individual tracker station errors, (3) and lastly the development of an advanced control system. Each of these sub-projects will however require intensive studies and this brings the current study into perspective for the greater project planned by NMISA.

The goal of this thesis is to start with the development of such a system. The final thesis outcome has three main components:

1. provide a starting point for LTS development for NMISA
2. build and test a prototype laser tracker
3. develop a sequential multilateration² algorithm for NMISA

These components are derived from the three main sub-projects of the bigger project. Each component will provide a platform from which these sub-projects can be launched. The design, construction and testing of a prototype laser tracker was also selected as a main component to gain practical insight into the construction and part procurement challenges of a tracker station, since it is the fundamental building block, along with multilateration algorithm, of the bigger project. With any measuring system there are various sources of uncertainty and noise. This also forms part of the system's design specifications.

The layout of the thesis starts with the literature review. This will give the reader a foundation for the project. It includes a general overview of work done in dimensional measurement concerning laser trackers. The review explains the basic concepts, components and error sources of laser tracking and provides a kinematic model for a laser tracker. From the review the reader will gain a clear context for this thesis. It is also aimed to give a background of references for those who will continue work on this project. Part (1) of the thesis' outcome is fulfilled by the Literature Review.

The laser tracker design done for part (2) is presented after the Literature Review and is followed with the simulations done for the tracker and the test results.

Sequential multilateration tests and multilateration simulations continue the discussion and are done with regards to part (3) of the thesis' outcome.

The report is completed by a Conclusion chapter.

²Sequential multilateration is a technique where multilateration is performed using only a single Laser Tracker

Chapter 2

Literature Review

This chapter's main goal is to provide a starting point for the development of a LTS. It starts with a section containing a general overview of current coordinate metrology. From the overview it is clear that metrology plays a very important role in industry. This section will also be used to compare other possible measurement systems to a LTS, motivating the use of LTS for this project. More detail on current laser trackers are given next, as well as detail on the operation of a laser tracker. The operation of the main components of a laser tracker is explained, the errors caused by these components are discussed and an overview of a kinematic model found in literature is provided.

This chapter is completed with a review concerning multilateration and calibration of a bridge type CMM with a LTS.

2.1 Dimensional Metrology and Measurement System Selection

The coordinate system was invented by René Descartes and published in 1637. This system, along with definition of the unit of length, makes theoretical coordinate metrology possible. The necessity of measurable coordinate systems abounds in many fields and the ability to measure various objects relative a coordinate system is vital. From every day articles such as rulers and tape measures, to high accuracy and also large scale metrology devices, the ability to measure coordinates relative to an international standard is critical (Bridges and Hagan, 2001).

Many devices have been produced to perform measurements for specific applications. Examples of such devices are conventional bridge type CMMs, theodolites, photogrammetry techniques, linear scales or rulers, length bars and various LRF (Laser Range Finding) devices. Three methods for determining three dimensional coordinates are by measuring: (1) two angles and one distance to the target, (2) multiple angles to the target (triangulation),

or (3) by measuring multiple lengths (trilateration and multilateration) to the target point (Cuypers *et al.*, 2009).

Choosing the best device not only depends on the device's ability, but also on the measurement requirements. Cuypers *et al.* (2009) defines three categories, apart from cost, for the selection of mobile CMMs: (1) task requirements, (2) part restrictions and (3) environmental restrictions.

For this project the general requirement is that the system should be able to calibrate a bridge type CMM. This implies that there are no part restrictions and that the environmental conditions are controlled. Therefore accuracy is the most important requirement for this project. The measurement range must only be within a bridge type CMM movement range ($3 \times 2 \times 2$ m).

The selection criteria for this project's measurement device is that it should be the most accurate general purpose dimensional metrology system possible, within cost constraints, for a measurement volume of bridge type CMM. The rest of this section will investigate these selection criteria relative to some of the above-mentioned devices.

2.1.1 Bridge Type CMM

The conventional bridge type CMM is used for coordinate metrology in production lines and is highly accurate (Takatsushi *et al.*, 1998).¹ A bridge type CMM however uses linear scales and therefore does not satisfy Abbé's principle, which requires that all displacements are along the measurement axis (Fan *et al.*, 2007), reducing its theoretical accuracy limits. Furthermore, its measurement volume is limited and it is a solid stationary structure, limiting part size and therefore making it a less general type of measurement system.

An example where large scale metrology is required is large scale assemblies, as found in the aerospace industry. A bridge type CMM measuring volume is limited in comparison to a commercial laser tracker, which has a range up to 35 metres. A laser tracker is also portable and only has two measurement constraints: (1) direct line of sight between the target and tracker (this can be overcome by using multiple trackers) and (2) the laser tracker must never lose track of the target (Gallagher, 2003; Zhang *et al.*, 2005). Some laser trackers do however have a less accurate absolute measurement system, which can be used to partially overcome constraint number (2).

This loss of general application and theoretical accuracy limits motivates the selection of LTS above a CMM for this project.

2.1.2 Theodolites and Photogrammetry

Devices such as theodolites and systems using photogrammetry are also used for large scale measurements. These devices are tailor made for specific sit-

¹The CMM currently in use by the NMISA has an accuracy in the order of magnitude of $1 \mu\text{m}$.

uations though, while a LTS is more versatile in that it can make close and longer range measurements, as well as both dynamic and static measurements, within an accuracy of at least $25 \mu\text{m}$ (Gallagher, 2003).

A LTS therefore has a more dynamic resolution range (more general application) than theodolites and photogrammetry techniques, motivating its selection for this project

2.1.3 Absolute or Relative Displacement Measurement Devices

A LTS can use either absolute distance range finders or interferometers. A heterodyne laser interferometry based system has the limitation that the beam must at all times have a direct line of sight to the target. Absolute distance measurements overcome this limitation. Most of these devices however still require a special cooperative target, except for Coherent Laser Radar (CLR). Furthermore the use of such a laser, is motivated (instead of radio or sonic waves) by Jain (2003), stating that these waves cannot be focused adequately, while a laser beam can be focused and has low divergence.

TOF (Time of Flight) is an absolute distance measurement method that measures the time a light pulse takes to travel to the target and back. Light though travels extremely fast and to measure the flight time is exceedingly difficult, limiting the distance resolution to a few millimetres and making TOF devices impractical for this project. The concept of TOF however has been improved by various means, e.g. absolute distance interferometry, FMCW (Frequency Modulated Continuous Wave) or source modulation type range finders and CLR. These methods modulate the various components of the beam, such as frequency, amplitude and polarisation (Estler *et al.*, 2002). Currently however heterodyne laser interferometry still has the finest resolution, with manufacturing claims in the range of 10 nm (Gallagher, 2003).

2.1.4 LTS Selection Motivation

In conclusion of this section, the decision to use a LTS type system for this project is supported based on the general review above, which compared other solutions to a LTS. Zhuang *et al.* (2003) reports that for:

“Robot performance measurements and standardization, LTS technology provides the speed, accuracy, flexibility and range that no other coordinate measuring system can.”

Zhuang *et al.* (2003) also states that a LTS is the preferred calibration tool for CNC (Computer Numerical Control) machines.

Since a bridge type CMM is a type of robot, the LTS are clearly distinguished from all other measurements systems for this thesis goal, defined as a

system which could be the most accurate general purpose coordinate metrology system possible, within constraints, for the later objective of bridge type CMM calibration.

2.2 Laser Trackers

Single beam laser trackers are reviewed, before multiple beam or multilateration LTS. A short history of laser trackers is given, as well as some information of commercial laser trackers, after which the operational principle is explained.

2.2.1 History

The first laser trackers, which utilised TOF to track missiles or airplanes, were built in the 1960's. However in 1980 Allen Greenleaf from Itek Optical Systems proposed a surface profile measurement system, which used four distance measuring interferometers and a tracking system (see also Watson (s.a.)), and in 1986 Kam Lau filed a US Patent (Lau *et al.*, 1987), which was derived from Greenleaf's system. This new system used a distance measuring interferometer, as well as an azimuth and an elevation encoder, which made the new invention more portable, but still an accurate coordinate measurement system, capable of both static and dynamic measurements (Gallagher, 2003).

Vincze *et al.* (1994) later added a CCD sensor to the laser tracker concept with which the 6 DOF (degrees of freedom) or pose (position and orientation) of a robot manipulator can be determined. Takatsuji *et al.* (1998) measured target points with trilateration with separate trackers and Hughes *et al.* (2000) report work on a LTS, which they tested with sequential multilateration, with measurement results indicating an uncertainty of 200 nm.

2.2.2 Commercial Laser Trackers

Three producers of laser trackers are Leica Geosystems (Figure 2.1), FARO Inc. (formerly SMX), and API (Automated Precision Incorporated). By considering the products of these companies and their claimed accuracy specifications for their products (see Table 2.1), it is clear that the market for these systems is already well-developed and that there is currently well-funded research and development in this field. Many universities and metrology laboratories have also constructed laser trackers or LTS for their own purposes (Gallagher, 2003).

Also available are absolute and non-tracking laser trackers, which use ADM (Absolute Distance Meter). A non-tracking laser tracker station search in a programmable area for the target, instead of tracking it through space (Cuypers *et al.*, 2009).



Figure 2.1: A Laser Tracker made by Leica Geosystems (Geosystems, 2009)

SMX Tracker Measurement Specifications			
Category	Specification	Radial (Interferometer)	Transverse (Encoders)
General			
	Resolution	0.16 μm	0.25 arcseconds
	Repeatability	1 μm +1 $\mu\text{m}/\text{m}$	3 μm +1 $\mu\text{m}/\text{m}$
Accuracy			
	Encoder	N/A	18 μm +4 $\mu\text{m}/\text{m}$
	Bucketed in Distance	2 μm +0.8 $\mu\text{m}/\text{m}$	N/A
	Radial Distance	10 μm +0.8 $\mu\text{m}/\text{m}$	N/A
Tracking			
	Speed	4.0 m/s	180°/s
	Acceleration	unlimited	180°/s ²
	Error	negligible	5 arcseconds
Working Range			
	Upright Mount	35 m	280° horizontal 115° vertical
	Side Mount	35 m	280° vertical 115° horizontal
Laser			
	Power	0.5 mW, Helium Neon	
	Class	Class 2	

*Repeatability and accuracy at 1 sigma for a second observation of a stationary target
in a stable environment*

Table 2.1: SMX Laser Tracker Specifications (Taken from data supplied with the Tracker, also see FARO (2009))

2.2.3 Working Principle

A typical commercial laser tracker consist of the following main components: a laser source, a beam steering mechanism with angle encoders, interferometer block, an optical Position Sensitive Diode (PSD) sensor, beam splitting optics,

a retroreflector, a control unit and software. These components work together and are used to both track the target and measure the coordinates of the target (see Figure 2.2).

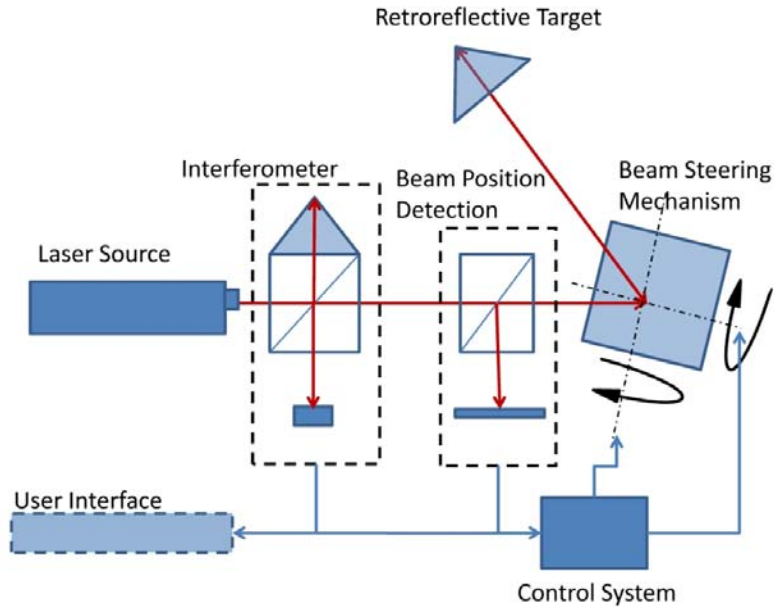


Figure 2.2: Schematic of a Laser Tracker with Main Components (Based on Lau *et al.* (1987))

The source beam is split with a beamsplitter into a measurement and reference beam. The measurement beam travels from this beamsplitter to the target and back. After returning from the target it will interfere with the reference leg of the original beam, and this interference will be used to determine the change in displacement of the target.

The measurement beam is steered towards the target with a mirror mechanism. The mirror must reflect the measurement beam coming from the source towards the target, and therefore must be able to rotate about two axes.

The target must reflect the measurement beam back towards the mirror where it can be reflected all the way back towards the first beam splitter. If the returning measurement beam does not return properly onto the reference beam the interferometer will not be able to determine the change in distance to the target, since it's only able to measure the change in distance from one point to another. The crucial concept of the laser tracker operation is that the measurement beam must always return onto the reference beam without disruption or too much offset. The target then needs to be tracked. And this is done by minimizing the measured displacement between the outgoing and returning measurement beam (see Figure 2.3).

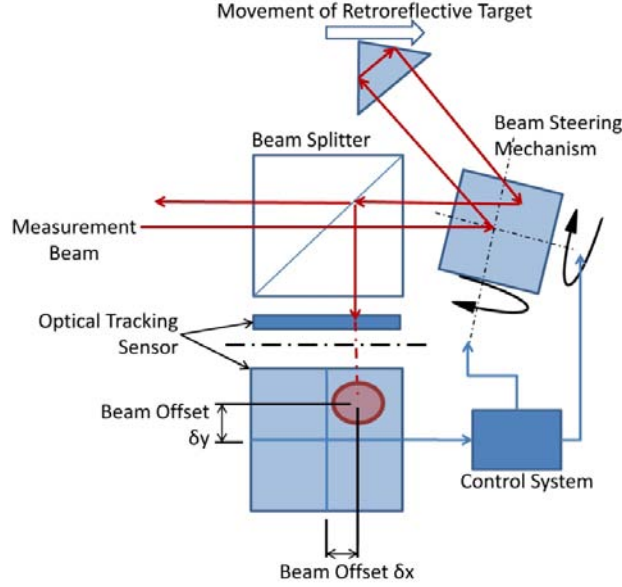


Figure 2.3: Schematic of the Tracking Principle

This displacement is detected by deflecting some of the returning measurement beam unto a PSD with another beamsplitter. This optical sensor has four electrodes, each of them producing an amount of photo-current relative to the distance of the electrode to the centre of the beam spot. These photo-currents are amplified and converted to form four voltages, which are used to determine the position of the centre of the beam on the sensor's active area. If the system is calibrated so that the returning beam hits the centre of the PSD when the outgoing measurement beam hits the centre of target, for example, the deviation from the centre of target can be detected with the PSD.

The controller can use the detected offsets to minimize the tracking error by rotating the beam steering mirror to re-centre the beam on the PSD, which will also point the measurement beam towards the centre of the target. When this is done continuously the target will be tracked and this tracking is what enables the laser tracker to measure the interferometric length.

The coordinates of the target is finally determined with the two encoder readings and interferometric length measurement. This length is relative to a *home position* and is equal to the difference between the distance from the measurement beam incident point to the target point and from the same incidence point to the home position.

2.3 Laser Tracker Components

The various components of a laser tracker, including concepts found in literature, are discussed next. For this project it is defined that a laser tracker

consists of the following main functional components: the target, PSD, beam steering mechanism and interferometer.

2.3.1 Interferometer

The laser interferometer comprises of the laser source, necessary beamsplitters, reflectors, photo detector or fringe counter, electronics (which both power the laser head and count the fringes), as well as software used to interpret the measurement, which produces the final interferometric length measurement.

The interferometer operational principle will be discussed first, by giving a mathematical description of light and interference, after which the development of the interferometer will be briefly presented. This will help to explain how the interferometer works and what affects its accuracy.

2.3.1.1 Description of a Light Beam

For the purpose of this project light can be seen as a transverse electromagnetic wave, modelled as a second order homogeneous, linear, partial differential equation, in the general form of (Hecht, 1997):

$$\frac{\partial^2 \Psi}{\partial x^2} + \frac{\partial^2 \Psi}{\partial y^2} + \frac{\partial^2 \Psi}{\partial z^2} = \frac{1}{v^2} \frac{\partial^2 \Psi}{\partial t^2} \quad (2.3.1)$$

where, for a vacuum:

$$v = 1/\sqrt{\epsilon_0 \mu_0} \quad (2.3.2)$$

ϵ_0 is the electric constant called the *permittivity of free space (or vacuum)* given by $\epsilon_0 = 8.8542 \times 10^{-12} \text{ C}^2/\text{N m}^2$, and μ_0 is the magnetic constant called the *permeability of free space* defined as $\mu_0 = 4\pi \times 10^{-7} \text{ N s}^2/\text{C}^2$.

For free space the speed (c) of any electromagnetic wave can then be predicted by v , where c is the speed of light and is used to fix the definition of the metre. This relation also shows that the medium through which light travels affects the speed of light or its propagation.

For further illustration, a harmonic wave in one dimension can be described as:

$$\frac{\partial^2 \Psi}{\partial x^2} = \frac{1}{v^2} \frac{\partial^2 \Psi}{\partial t^2} \quad (2.3.3)$$

where:

$$\Psi(x, t) = f(x - vt) = A \sin k(x \mp vt) = A \sin(kx \mp \omega t) \quad (2.3.4)$$

with the spatial period λ (wavelength) and temporal period τ . The propagation number (k), the temporal frequency (ν , or the number of waves per unit time), and the angular frequency (ω), is now defined as (Hecht, 1997):

$$k = 2\pi/\lambda\tau = \lambda/v\nu = 1/\tau\omega = 2\pi\nu \quad (2.3.5)$$

The wave can also be presented in complex numbers, with $\psi = \omega t - kx + \varepsilon$ and ε is the initial phase, as:

$$\Psi(x, t) = A \cos(\omega t - kx + \varepsilon) = Ae^{i\psi} \quad (2.3.6)$$

Finally, a plane harmonic wave can now be described as:

$$\Psi(x, y, z, t) = Ae^{i(\mathbf{k}\cdot\mathbf{r} \mp \omega t)} \quad (2.3.7)$$

where \mathbf{k} is the propagation vector with magnitude k (the propagation number) and \mathbf{r} equal to $\alpha i + \beta j + \gamma k$. Plane harmonic waves are essential since any three dimensional wave can be constructed by superposition of plane waves. And superposition creates the effect of interference, or as Hecht (1997) states (where irradiance implies intensity):

“Optical interference corresponds to the irradiance of two or more light waves yielding a resultant irradiance that deviates from the sum of the component irradiance’s.”

This deviation term is described next, and how it is used to measure displacement as result of interference.

2.3.1.2 Wave Superposition and Resulting Intensity

The wave model just described obeys the superposition principle, which implies that the light field could be used to measure the resulting interference, since for two waves:

$$\mathbf{E} = \mathbf{E}_1 + \mathbf{E}_2 \quad (2.3.8)$$

The electric field (\mathbf{E}) varies in time very rapidly though, making it impractical to detect. The intensity (I) however, can be measured directly. Interference as a result of wave superposition is then best detected by measuring this intensity. This intensity is given by $\epsilon\nu\langle\mathbf{E}^2\rangle$, which means that $\langle\mathbf{E}^2\rangle$ can be taken as the measure for intensity, or (as shown by Hecht (1997)):

$$I = \langle\mathbf{E}^2\rangle_T \quad (2.3.9)$$

$$\mathbf{E}^2 = \mathbf{E} \cdot \mathbf{E} \quad (2.3.10)$$

And with the superposition principle for two monochromatic waves, at the same frequency:

$$\mathbf{E}^2 = (\mathbf{E}_1 + \mathbf{E}_2) \cdot (\mathbf{E}_1 + \mathbf{E}_2) \quad (2.3.11)$$

$$\mathbf{E}^2 = \mathbf{E}_1^2 + \mathbf{E}_2^2 + 2\mathbf{E}_1 \cdot \mathbf{E}_2 \quad (2.3.12)$$

By taking the time average, it is then found that:

$$I = I_1 + I_2 + I_{12} \quad (2.3.13)$$

with the interference term of:

$$I_{12} = 2\langle \mathbf{E}_1 \cdot \mathbf{E}_2 \rangle_T \quad (2.3.14)$$

which is simplified to:

$$I_{12} = \mathbf{E}_1 \cdot \mathbf{E}_2 \cos(\delta) \quad (2.3.15)$$

with δ equal to $(\mathbf{k}_1 \cdot \mathbf{r} - \mathbf{k}_2 \cdot \mathbf{r} + \varepsilon_1 + \varepsilon_2)$ and is then the phase difference resulting from the combined path length and initial phase difference. Note that if the two waves are perpendicular, the interference term will be zero (Hecht, 1997).

2.3.1.3 The Development of Interferometry

For interference to occur between two light sources, the sources must be separate, yet still coherent, where coherence refers to the waves having the same wavelength and phase or constant difference in phase. It could be said that “*the waves from these sources are not in step, but are marching together*” (Hecht, 1997). All interferometric devices can be placed into two categories: wavefront or amplitude splitting. The challenge for an interferometer is to create these sources.

Thomas Young (1773-1829) first demonstrated, with the wavefront splitting double-slit experiment, the interference of light. In 1880 A.A. Michelson constructed an amplitude splitting interferometer, which used light interference to measure displacement. The Michelson interferometer however is superseded by the Twyman-Green interferometer (see Figure 2.4). The main difference between the Michelson and Twyman-Green interferometers is that the light source is a collimated monochromatic source for a Twyman-Green interferometer (Gallagher, 2003).

Figure 2.4 shows a schematic of such an interferometer. Notice how the source is split into two beams: a reference beam and a measurement beam. A compensation plate is used to ensure that both beams are refracted by the same amount. Only the one mirror is actuated, changing the optical path difference (OPD) between the two beams of the interferometer. The interferometer measures the change in the OPD. Once these two beams are recombined interference fringes are created. These interference fringes are areas of minimum to maximum intensity, seen as dark and light zones, and are created as result of the wave superposition. Hecht (1997) shows how a displacement δd can be calculated from these fringes. The following equation is cited, for wavelength λ and number of fringes N :

$$\delta d = N(\lambda/2) \quad (2.3.16)$$

A change of λ of the OPD generates interference fringes and a displacement of the actuated mirror of $\lambda/2$ will cause a OPD of λ . As the reference mirror

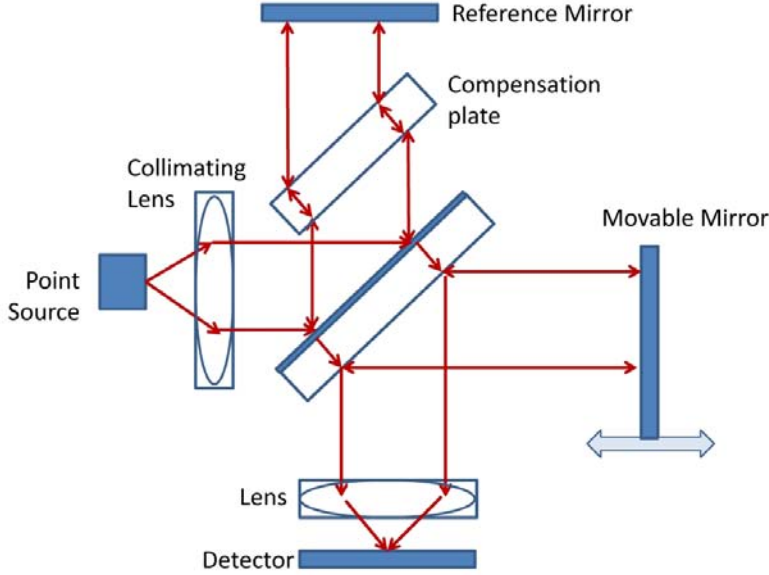


Figure 2.4: Schematic of the Twyman-Green Interferometer (Based on Born and Wolf (1999))

moves a fringe counter counts the creation of new fringes. The displacement is then computed by multiplying the number of fringes by $\lambda/2$. Note that the interferometer only measures the difference in OPD, and that it is not an absolute distance measurement device (Gallagher, 2003).

Yu and Yang (1997) shows that, instead of counting the fringes, that the Doppler shifted frequency can be measured. This results in a velocity measuring interferometer and the displacement can be obtained by integrating the velocity. The Doppler effect causes the detected frequency (ω) to shift from the initial frequency with:

$$\omega = \omega_o (1 \pm V/c) \quad (2.3.17)$$

where ω_o is the original frequency, V the light source velocity (or detector velocity) and c the speed of light in a vacuum. The sign of the division operation is determined by the direction of movement of the mirror. If the mirror is displaced with a velocity of V toward the beamsplitter, which result in an effective light source velocity of $2V$, a frequency difference ($\Delta\omega$) between the light reflected from the two mirrors will exist, equal to:

$$\Delta\omega = \omega_o 2V/c = 4\pi V/\lambda \quad (2.3.18)$$

A *beat* is seen if these two frequencies are mixed in a photodiode. The intensity cycles within a period T can now be expressed as (with d the displacement):

$$N = 1/2\omega \int_0^T \Delta\omega dt = 2d/\lambda \quad (2.3.19)$$

The Twyman-Green interferometer however has two restrictions: (1) it cannot detect the direction into which the target mirror is moved and (2) the measurement resolution is limited to only $\lambda/2$. These restrictions are overcome by using either homodyne or heterodyne interferometers (Gallagher, 2003).

A homodyne (single frequency) interferometer is similar to the Twyman-Green interferometer, since its source beam also has a single frequency. It differs in that a polarizing beam splitter, two quarter wave plates, and two linear polarisers are added.

The homodyne interferometer analyzes the fringe intensity, which enables it to measure the displacement with a resolution less than $\lambda/2$. It also splits the return beam onto two detectors used to determine the direction of the movable mirror's displacement, since a lag or lead between the two beams will be detected. This type of interferometer is limited, as fluctuation of source intensity could be interpreted as displacement. This necessitates that the power of the laser source must be rigorously controlled (Gallagher, 2003).

Heterodyne (dual frequency) interferometers improve on the homodyne interferometers. It utilizes two sensors: one to measure the frequency difference between the two frequencies of the bi-frequency source beam, as it leaves the laser, which then forms the reference signal. And the other sensor measures the frequency difference of the recombined beam. When the measurement mirror is displaced the frequency of the light reflected off this mirror will be Doppler shifted. By comparing the two sensors the direction of displacement can be determined. The measurement resolution is also made finer than $\lambda/2$ (Gallagher, 2003).

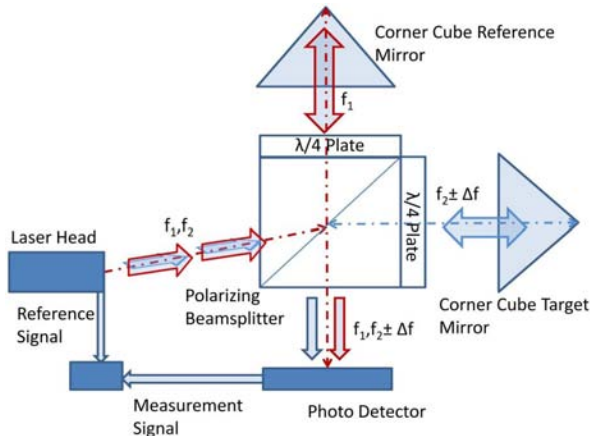


Figure 2.5: Schematic of a Heterodyne Interferometer (Based on Zhuang and Roth (1995))

A Zeeman split is typically used to split a single laser source into two frequencies (f_1 and f_2 usually with a $20MHz$ difference). Opposite circular polarizations are also induced in the two frequencies. Note that a light wave can be polarized in a certain orientation. A requirement though for interference is that the interfering waves must have the same polarization, i.e. waves with perpendicular angled polarization states has no interference (Hecht, 1997). The heterodyne interferometers uses a polarizing beamsplitter, which with the quarter wave ($\lambda/4$) plate (see Figure 2.5), allow the one beam (f_1) to travel to the reference reflector and the other beam (f_2) to the target reflector. The quarter wave plate has the function of changing the wave polarization. Therefore the quarter wave plates allow the two waves, after passing twice through their respective quarter wave plates (which induces a combined 90° change in polarization) to interfere with each other.

For this project a heterodyne interferometer (Zygo ZMI 2000, displacement interferometer) is used. This interferometer has the advantage that it processes the electric signals instead of the laser source intensity, which is not subject to drift, to determine the distance and direction of the displacement (Gallagher, 2003).

2.3.2 Beam Steering Mechanism

The beam steering mechanism includes the actuators, angular position encoders, reflecting mirror, mounting for the mirror and control of the actuators. Four different types of steering mechanisms were found in literature and are discussed next.

A gimbal mechanism, as described by Lau *et al.* (1987), can rotate a mirror simultaneously in the two required axes. Expensive (in the range of US\$11 600 to US\$100 000) high accuracy gimbals for optics can be procured from Aerotech (see Aerotech (2009)). Figure 2.6 shows the A360D available from Aerotech. This mount is similar to the one used by Zhuang and Roth (1995). It is also possible to separate the two axes, mounting a mirror for each axis on a separate rotation stage (called scanning mirrors) and an example of this is found in Teoh *et al.* (2002).

According to Jiang *et al.* (2002) the misalignment of the two gimbal axes causes a considerable error for a laser tracker measurement. They present an articulating hemisphere mechanism (Figure 2.7). The mirror is mounted on a half sphere which rests on three small steel balls and is actuated by a pin connected to a motorized XY stage. Jiang *et al.* (2002) states that this method is simple and inexpensive and, in principle, is almost free from this misalignment.

Jiang *et al.* (2002) also do an uncertainty analysis on this type of tracker and in Umetsu *et al.* (2005) it is stated that the total mechanical error contribution to the measurement uncertainty for a tracker of this type was determined as $0.3 \mu m$.



Figure 2.6: Commercially Available Gimbal Mount from Aerotech (Aerotech, 2009)

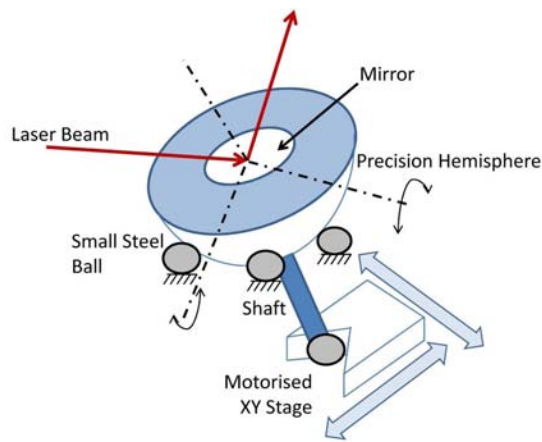


Figure 2.7: Schematic of an Articulating Hemisphere with a Mirror (Based on Jiang *et al.* (2002))

The last alternative found is called a *laser tracer* and is described in Hughes *et al.* (2000) and Schneider (2004). It uses a reference sphere and the whole interferometer block rotates about this sphere (Figure 2.8). The source beam consists of two orthogonal polarisations. These two polarisations are separated with the polarising beamsplitter. One passes straight through this beamsplitter and acts as the reference component, while the other component is deflected towards the reference sphere, from where it is reflected to the centre of the target retroreflector. As the reference beam is reflected back from the target, the polarising beam splitter deflects this beam onto the reference beam producing the required interference. As with all the tracking type laser trackers, a part of the measurement beam is deflected with a beamsplitter (2), onto a PSD sensor. The readings of this sensor are used to rotate the interferometer block around the reference sphere and thereby track the target.

Hughes *et al.* (2000) report that the PSD and interferometer were mounted to form a single block, approximately $50 \times 45 \times 10$ mm³. This block is then

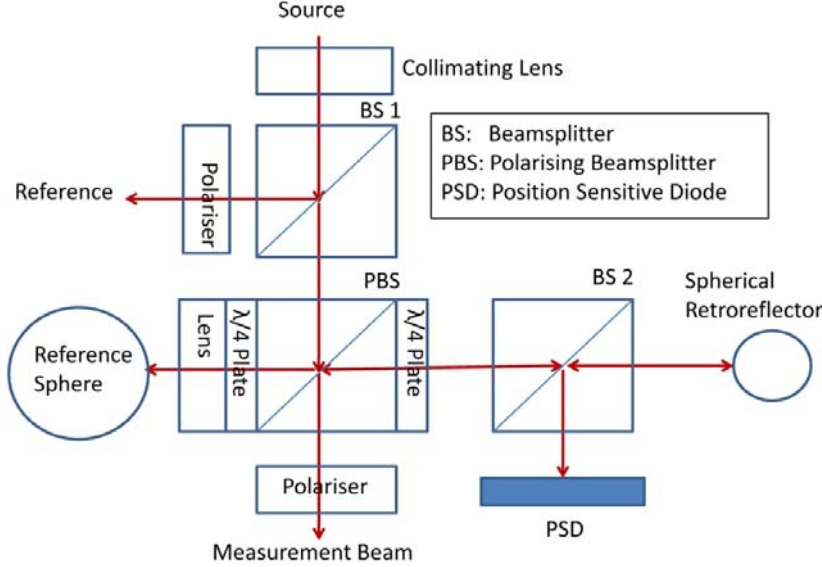


Figure 2.8: Schematic of a Tracker Using a Sphere as a Bearing (Based on Hughes *et al.* (2000))

gimbal mounted and rotated around the reference sphere (Figure 2.9), where either the sphere's surface or its virtual centre can be used as the reference for the interferometer.

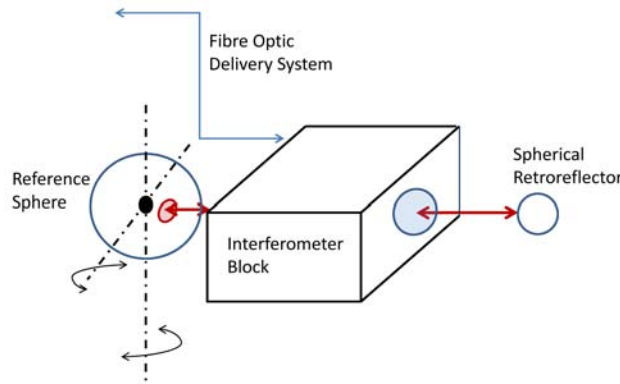


Figure 2.9: Schematic of the Pivoting Interferometer (Based on Schneider (2004))

Schneider (2004) states that as the interferometer block moves around the fixed reference sphere, radial and lateral deviations of the mechanical axes of rotation do not significantly affect the measurement accuracy. Hughes *et al.* (2000) adds that another advantage of this tracking system is that the heat of the laser head is kept away from the tracker optics, since the beams are delivered with polarisation maintaining fibre optics. Furthermore, an uncer-

tainty of $60 \text{ nm} \pm 2L$ per $L \text{ nm}$ (which is the interferometric measurement plus deadpath length) is estimated.

2.3.3 Position Sensitive Diode

The position sensitive diode (PSD) is a critical component of a laser tracker, since the displacement between the measurement beam incident point on the target and target centre is measured by the sensor. Note that it also has an effect on how fast the target can be tracked. A PSD is a continuous silicon photodetector used for optical position sensing and basically consists of a uniform resistive layer, which is formed on a silicon substrate. A pair of electrodes is formed at the ends of the resistive layer from which photo-currents are measured. These photo-currents are generated as a result of the photovoltaic effect and their magnitude is relative to the distance of the electrode to the centre of the beam spot on the sensor's active area. The photo-currents are typically amplified and converted to form the measured voltage signal used by the control system.

A PSD is preferred above other continuous position sensors (for example a charge-coupled device (CCD)), as a PSD has nanometre position resolution, sub-microsecond response times, relatively simple interface circuits and high reliability (Johnson and Lentz, 2003). PSDs can also be divided into two general groups: segmented PSDs and lateral effect PSDs.

2.3.3.1 Segmented Position Sensitive Diodes

Segmented PSDs are discussed next. A two dimensional segmented or quadrature PSD is divided into four segments, which are separated by a small gap, called the dead region. The sensor is used for positioning by measuring each segment's photocurrent. A symmetrical beam is positioned at the centre of the PSD if all these currents are equal (OSI, 2007).

Segmented PSDs have a higher accuracy level than the lateral effect PSDs, due to the superior responsitivity match between the elements. A segmented PSD's resolution is independent of the signal to noise ratio (S/N) of the system, enabling them to detect very low light levels. This group of PSDs is limited though, since the beam spot must be bigger than the dead region and must also overlap all the segments at all times and a uniform beam spot intensity is also required (OSI, 2007). For example, if the beam only falls on the two upper segments, only the spot's X position can be determined. A displacement of more than 10% of the beam diameter will also cause the measurement to become non-linear. These limitations restrict the beam spot displacement measurements to a small and narrow the tracking range (Shirinzadeh, 1998; Edwards, 1988). Figure 2.10 shows a picture of three four segmented, quadrant, silicon photodiodes: the S5890, S5891 and S5870, available from Hamamatsu Photonics (Hamamatsu, 2002).

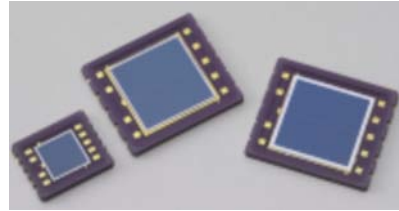


Figure 2.10: The S5890, S5891 and S5870 Segmented PSDs from Hamamatsu (Hamamatsu, 2002)

2.3.3.2 Lateral Effect Position Sensitive Diodes

The other group is the lateral effect photodiodes, which can be either one or two dimensional and are continuous single element PSDs, i.e. they have no dead areas. The beam spot position can be calculated with their photocurrents over the entire active area. Lateral effect photodiodes have the main advantage of a wide dynamic range and that the measured position is independent of the light spot intensity distribution (unlike segmented PSDs), the resolution however is detector (or circuit) signal to noise ratio dependent (OSI, 2007). This sensor is also more expensive (Shirinzadeh, 1998). There are three different types of lateral effect PSDs: (1) duolateral, (2) tetralateral and (3) pincushion (Johnson and Lentz, 2003).

The duolateral type has the highest position detecting ability, but is also the most expensive. The pincushion type is an improved tetralateral PSD, as it has a bigger high linearity region than the tetralateral type PSD. Both of these though have a simpler bias scheme, smaller dark current and faster response time than the duolateral type.

2.3.3.3 The Photovoltaic and Photoconductive Mode

There are two methods by which a photodiode can be used: (1) the photovoltaic- and (2) the photoconductive mode. The difference between these modes is found in how the diode is biased. With the photovoltaic mode the diode is grounded, but with the photoconductive mode a reverse bias is applied. The photovoltaic mode is used when precision is more important and the photoconductive mode when speed is rather required (Rako, 2004).

2.3.4 Target

Two main types of retroreflecting targets are found in literature: a corner cube and a *cat's eye*. The requirements for an ideal retroreflector are: (1) it must provide high parallelism, i.e. the incident beam is reflected and returned in 180° , regardless of the orientation of the target and the incident beam direction, (2) the centre of the target must be in the centre of incident and reflected beams, (3) the target must be lightweight and (4) must have as wide as

possible acceptance angle for the incoming beam (Teoh *et al.*, 2002; Yongbing *et al.*, 2003).

There are two types of corner cube targets, also called SMRs (Spherically Mounted Retroreflector): an air path type (hollow front surface mirror) and solid glass corner cube. Lin *et al.* (2005) show that the air path SMR is preferred since it is free from refractive effects. Such a type of SMR is basically a small steel like ball, with a corner of a near perfect cube cut out of it, in such a way that the corner point is ideally exactly at the centre of the sphere. The resulting three orthogonal sides in the cut out area have highly reflective mirrors on them (see Figure 2.11), giving the target the property of reflective parallelism.



Figure 2.11: A SMR made by API (API, 2008)

A cat's eye type retroreflector is usually made from two glass hemispheres with the same refractive index, but different radii, with their flat sides joined together to form the target (see Figure 2.12). The rear hemisphere is coated with a highly reflective coating. The beam is focussed by the front hemisphere, as the beam enters the target, on the surface of the rear hemisphere. There the beam is internally reflected, after which the front one again refracts the beam, so that it returns parallel to the incident beam (Yongbing *et al.*, 2003).

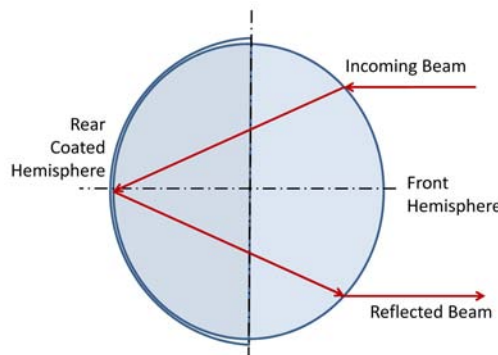


Figure 2.12: Schematic of a Hemispherical Retroreflector (Based on Yongbing *et al.* (2003))

However, if the refractive indices of the hemisphere are close to two, the target becomes a single sphere, this according to Yongbing *et al.* (2003) has three advantages (spherical over hemispherical): (1) simplified production, (2)

higher accuracy and (3) an increased incident beam acceptance angle. This angle, with a spherical target, can be 360° in principle, making a *whole view angle cat's eye*. This will reduce LTS tracker position restrictions.

Yongbing *et al.* (2003) also states that a cat's eye target has a larger acceptance angle, higher accuracy and a lower sensitivity to the direction of the incoming beam, than a corner cube target. Note that the acceptance angle is a critical specification for the target, especially for multilateration, as this requires that the target is tracked simultaneously from various angles.

2.4 Main Uncertainty sources

It is important to know the error sources of a measurement system, that is, what the different sources are and what influences they have on the final measurement, and under which conditions they are observed. In general, there are two different types of errors: errors for which the system can be compensated for, and random errors. Both these errors have the effect of making the resulting measurement more uncertain. Each component of the laser tracker adds an uncertainty to the final measured coordinates. The whole system can also be influenced by the environment. Watson (s.a.) points towards thermal expansion, vibrations and air turbulence.

Teoh *et al.* (2002) defines the following categories for uncertainty sources: environmental effects, measurement acquisition and approximation effects, as well as the uncertainty of the reference materials used for the calibration and then investigates each of the following components: the laser interferometer, environment, motors with angular encoders and the PSD.

Gallagher (2003) differentiates between the following error sources: angular encoders, tracking system, orthogonality, distance measurement and beam misalignment. The orthogonality error is unique since it is a surveying error, which occurs when the true vertical deviates from the nominal vertical axis, and is therefore not perpendicular with the horizontal axis. The curvature of the earth causes this difference to occur for the measurement range of a laser tracker. Gallagher (2003) then proposes that by keeping the measurement range between 60° to 120° ($\pm 30^\circ$ from horizontal), that the effect of this error can then be reduced.

Each component's uncertainty is discussed next along with steps, which can be taken to compensate for them, based on the reports found in literature.

2.4.1 Errors Due to the Laser Interferometer and Optics

Note that for this project the interferometer and optics are used as complete modular components and therefore it is not part of the design scope. The errors caused by these components can however be understood and steps can be taken to reduce their influence.

2.4.1.1 Types of Influences

Vincze *et al.* (1994) report geometric aberrations of the target, non-ideal optical components and deviation of laser beam from a mathematically straight path as error sources, and the laser interferometer according to Teoh *et al.* (2002), is influenced by three factors: environmental, geometric and instrument errors. Gallagher (2003) also cites installation errors such as: deadpath error, cosine error, and Abbé error. Environmental effects include material expansion, optical thermal drift and temperature gradients.

2.4.1.2 Environmental Influences

According to Estler *et al.* (2002) three atmospheric effects, which affect light propagation, are refraction, variation of the speed of light² and turbulence caused by time-dependant refractive variations. The first order approximation, that the laser beam travels at a constant speed in a straight line, is not valid for non-laboratory conditions. This is true as the ambient conditions affects the refractive index of the air the laser beam travels through. This change in refractive index results in an error in the wavelength of laser, causing the laser beam to bend, which results in a variation in the displacement measured (Gallagher, 2003). The three factors influencing the refractive index are temperature, pressure and humidity.

The influence of the temperature, pressure and humidity on the refractive index can be reduced by controlling the environment. For example, by using specially designed cooling, which creates laminar flow over heat sources and by using air homogenizers. Watson (s.a.) proposes that a stable fixed path interferometer operating in the same environment can also be used to remove errors due to the change in the refractive index. The error in the laser beam wavelength can be compensated for with a modified Edlén's equation (Gallagher, 2003). For this purpose commercial laser trackers are equipped with small *weather stations*, which measures the temperature, humidity and pressure to compensate for different conditions.

Estler *et al.* (2002) shows that temperature gradients have the greatest effect on measurement deviation and describes two areas of research for the compensation for first order atmospheric correction: one is based on two beam interference and the other is based on the variation of optical refraction with wavelength. Gallagher (2003) points out that temperature also causes thermal expansion of optics.

2.4.1.3 Installation and Calibration Influences

The interferometer only measures a displacement relative to a calibrated distance, or home position. Error in this calibration value will propagate into all

²The speed of light affects only time of flight devices

measurements. Gallagher (2003) states that the effect of this error propagation will be more severe at extreme angles away from the horizontal. Furthermore, its proposed that if the measurement range is kept between 30° from the horizontal and the calibration is done with as little error as possible, that the effect of this calibration error can be reduced.

The installation errors for the interferometer are deadpath error, cosine error and Abbé error, as shown in Figure 2.13.

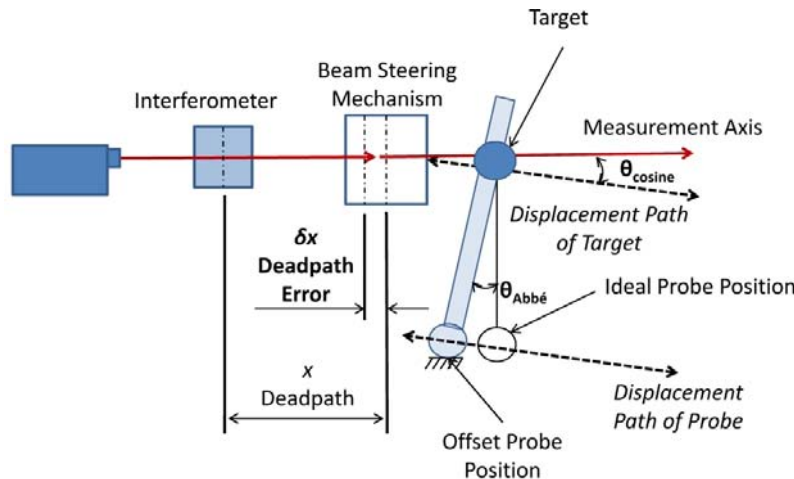


Figure 2.13: Schematic of Installation Errors for a Interferometer (Based on Gallagher (2003))

The cosine error occurs when the target does not move parallel to the measurement axis. Abbé's error occurs when the measured point's displacement is not along the measurement axis and the probe is offset from the expected position. A deadpath length exists when the interferometer is not located at the measurement origin and a deadpath error is caused when there is variation in this offset during measurement. Deadpath errors can be caused by refractive index errors or thermal expansion effects (Gallagher, 2003). For a laser tracker the beam steering mechanism's centre of rotation is defined as the origin for the measurement and is not fixed in space due to geometric errors and causes this error as well. It will be shown (Section 2.5) that changes in the centre of rotation have a major detrimental effect on measurement certainty.

The optical setup must ensure that the reference and measurement beam travel the same optical distance through the interferometer, so that the only difference in the optical path is as result of the displacement of the measured point. The target should also be placed as close as possible to the actuated mirror to reduce the deadpath.

2.4.2 Errors Due to the Beam Steering Mechanism

The interferometric length measurement process requires that the beam is never broken, always point towards the centre of the target and hit the mirror steering mechanism in the centre of rotation. The last point is extremely important with regard to the design of this mechanism. Zhuang *et al.* (1992) show that there is a measurement error δl due to the mirror centre offset, which is equal to:

$$\delta l = b|\sin(\theta_{out}) + \sin(\theta_{in})| \quad (2.4.1)$$

where θ_{out} and θ_{in} is the incident and reflected angles with the mirror. The order of magnitude of the error is equal to b , which is the beam incident point offset from the centre of rotation. This error is caused since the measurement assumes that the distance from the laser source to the incident point is fixed, and that the measured distance is strictly the distance from centre of rotation to the target centre.

There are three possible reasons why the beam steering mechanism has this error: (1) there is an offset of the incident point from the centre of rotation, (2) the centre of rotation is not constant due to the axes being non-perpendicular and (3) the axes do not intersect. The effect of reason number two is cited by Zhuang and Roth (1995) as:

$$\delta l = \frac{r(\frac{1}{\cos(\omega)} - 1)}{1 + \tan(\omega)\tan(\theta_{in})} \left(\frac{1}{\cos(\omega)} + \cos(\theta_{out})(1 + \tan(\omega)\tan(\theta_{in})) \right) \quad (2.4.2)$$

where $\omega = 0.5(\theta_{out} + \theta_{in})$, and r is the radius of uncertainty of a sphere centred at the origin. Zhuang and Roth (1995) then states that r is inversely proportional to the cost of the gimbal system and that there is no mechanical adjustment procedure, which can reduce r , with such systems.

Both the mirror centre offset and the gimbal axis misalignment is modelled by Zhuang and Roth (1995) for a gimbal beam steering mechanism. A kinematic model can be used to compensate for geometric errors and this modelling is discussed later in the chapter.

Teoh *et al.* (2002) also identifies backlash from gears, friction between moving parts, shaft misalignment with angular encoders and weight of the mirrors (which causes a bending and tumbling of motors) as sources of errors. These errors are non-geometric and cannot be modelled and calibrated for. They can only be included in the final uncertainty budget and reduced by careful component selection, design and assembly procedures.

2.4.3 Errors Due to the Position Sensitive Diode

Teoh *et al.* (2002) state that the main sources of error are the PSD resolution and calibration procedure, which was used to determine the relationship between the sensor output and beam offset from the centre of the target. Note

that the PSD offset is used in the determination of the target point calculation. For the calibration Teoh *et al.* (2002) mounted the PSD on a rotation stage (for elimination of the cosine error) and a translation stage independently.

The amplification and conversion electronics also introduced uncertainty with PSD measurement. The digital resolution of the ADC (Analogue to Digital Conversion) also reduces the sensor resolution.

2.4.4 Errors Due to the Target

According to Hughes *et al.* (2000), the retroreflecting target is a critical component for a LTS. The target can cause a measurement error, by for example, not reflecting the beam through an angle of 180° , i.e. a non-parallel return beam, or by adding to the uncertainty of the PSD offset.

For a spherical retroreflector measurement uncertainty can be caused as the optical path length is varied by the target when the beam has different incident angles on the target. This can arise as a result of form errors, spherical aberration and material inhomogeneity (Hughes *et al.*, 2000). For a corner cube it can be caused by the mirrors not being orthogonal. Also, if the mirrors are not intersecting in one point, the measured offset would be erroneous (Teoh *et al.*, 2002).

An example of claimed specifications of commercially available corner cubes is given in Table 2.2. From this table an example of the centring accuracy difference between the air path type (hollow) and solid (prismatic) corner cubes can be seen.

SMR Specifications			
Diameter (mm)	Type	Centring (μm)	Accuracy
38.1	40 m, Hollow	± 12.7	
38.1	40 m, Hollow Precision	± 2.5	
38.1	40 m, Prismatic	± 25	
38.1	60 m, Prismatic	± 25	
12.7	40 m, Hollow	± 12.7	
12.7	40 m, Prismatic	± 25	

All SMRs are specified with a roundness of (Grade 50) $\pm 1.3 \mu\text{m}$

Table 2.2: API SMR Specifications (API, 2008)

2.5 Kinematic Model

This section reviews a kinematic model of Zhuang and Roth (1995) with which the geometric uncertainty of a gimbal type beam steering mechanism can be modelled. Other models are also derived in Vincze *et al.* (1994), Teoh *et al.* (2002) and Lin *et al.* (2005). A motivation for a kinematic model of a laser tracker of LTS is given next, after which the model is presented. This model of Zhuang and Roth (1995) was used for simulation studies to study the effects of the various identified parameters of a laser tracker (the simulations are discussed in Chapter 4).

2.5.1 Purpose and Requirements of a Kinematic Model

The LTS has geometric errors, which necessitates a kinematic model describing the laser tracker beam path. With such a model the measured point's coordinates can not only be calculated, but must also be adjusted for the geometric errors. Random errors also exist though, and cannot be compensated for with a kinematic model (Teoh *et al.*, 2002).

Vincze *et al.* (1994) state that the aim of such a model is to describe all linear and angular relationships between the mechanical parts. To accomplish this, a laser tracker can be compared to a sequential robot arm, where the arms are laser beam paths, assuming that the laser beam travels a mathematical straight path. Zhuang and Roth (1995) add that a model can be used for both calibration and for tracking purposes, and that such a model should have no redundant parameters.

The requirements of a kinematic model are therefore a minimal, yet a complete set of parameters, which can be used for LTS calibration, testing and for insight into limitations of a LTS, by providing a theoretical estimate of the LTS accuracy.

For a laser tracker using a gimbal type mount, the mirror centre offset and gimbal axis misalignment should be modelled (Zhuang and Roth, 1995). Gimbal axis misalignment causes a mirror centre offset and the mirror centre offset causes a deadpath error as the measurement assumes a constant distance from the laser source to the mirror.

2.5.2 Single Beam Model

The single beam model of a laser tracker from Zhuang and Roth (1995) is presented next. A single beam tracker consists of a gimbal mounted with a mirror. The model develops in three steps: first the laser tracker is modelled for the ideal case, then the mirror centre offset is added and finally, the gimbal axis misalignment is incorporated as well (this section is based on Zhuang and Roth (1995))

2.5.2.1 Ideal model

The gimbal is treated as a two degree of freedom manipulator and for the ideal model the following assumptions are made:

1. The two axes of the gimbal are intersecting, perpendicular and the second axis is on the mirror surface.
2. The incident beam hits the mirror centre of rotation.
3. The mirror centre of rotation is on the mirror front face.

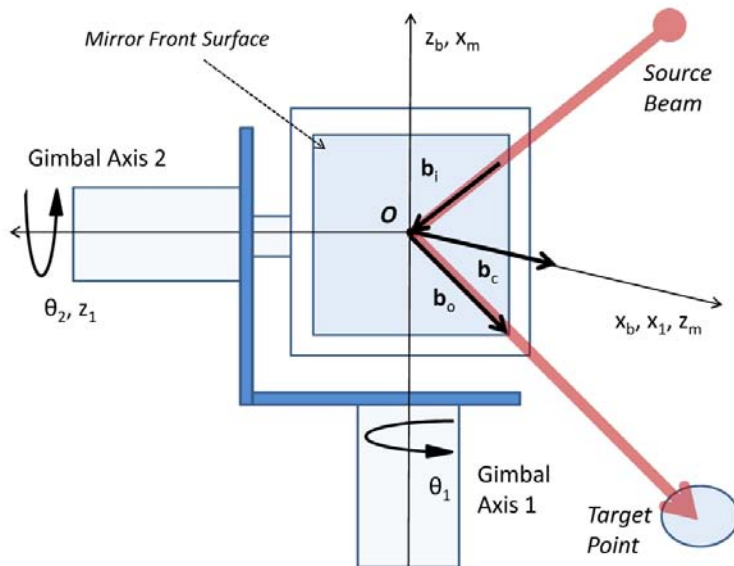


Figure 2.14: Ideal Tracker Model (Zhuang and Roth, 1995)

For the first step a Cartesian coordinate system (frames) is attached to each component or axis of rotation, the definitions (see Figure 2.14) of the frames used are:

1. $\{x_b, y_b, z_b\}$: Base frame
2. $\{x_1, y_1, z_1\}$: First link frame
3. $\{x_m, y_m, z_m\}$: Mirror frame

Now, all three frames are placed with their origins at the mirror centre of rotation, O . Where z_b is the rotation axis of the first joint (gimbal axis 2), z_1 . The rotation axis of the second joint and z_m is the normal to the mirror surface. At the home position ($\theta_1 = \theta_2 = 0$) the x axes of the first two frames

are coincident with z_m . The base frame can be rotated around its x axis with a 3D rotation matrix ($\text{Rot}(x, 90^\circ)$) to align it with the first link frame (see Appendix A, for details on the rotation matrix). Rotation of the first link frame around its z and x axes will align the first link frame with the mirror frame. The base frame can then be aligned to the mirror frame with a 4×4 homogeneous transformation, given by:

$${}^b\mathbf{T}_m = \text{Rot}(z, \theta_1)\text{Rot}(x, 90^\circ)\text{Rot}(z, \theta_2)\text{Rot}(z, 90^\circ)\text{Rot}(x, 90^\circ) \quad (2.5.1)$$

The unit mirror surface normal vector can now be presented in the base frame as (see Appendix A):

$$\mathbf{b}_c \equiv [b_{c,x}, b_{c,y}, b_{c,z}]^T \quad (2.5.2)$$

which is obtained from the first three elements of the third column of bT_m . If the fixed incident beam direction (\mathbf{b}_i) and mirror surface normal is known, the reflected beam direction (\mathbf{b}_o) can be determined with the following optical reflection relationships:

$$\mathbf{b}_i \times \mathbf{b}_c = \mathbf{b}_o \times \mathbf{b}_c \quad (2.5.3)$$

$$\mathbf{b}_i \cdot \mathbf{b}_c = \mathbf{b}_o \cdot \mathbf{b}_c \quad (2.5.4)$$

It can then be shown that (Zhuang and Roth, 1995):

$$\mathbf{b}_o = -B(\mathbf{b}_c)\mathbf{b}_i \quad (2.5.5)$$

where

$$B(\mathbf{b}_c) = \begin{bmatrix} 2b_{c,x}^2 - 1 & 2b_{c,x}b_{c,y} & 2b_{c,x}b_{c,z} \\ 2b_{c,x}b_{c,y} & 2b_{c,y}^2 - 1 & 2b_{c,y}b_{c,z} \\ 2b_{c,x}b_{c,z} & 2b_{c,y}b_{c,z} & 2b_{c,z}^2 - 1 \end{bmatrix} \quad (2.5.6)$$

The target position (\mathbf{r}_p) can be determined, if the reference distance, l_r , from point \mathbf{O} to point \mathbf{R} (a reference point at $\theta_1 = \theta_2 = 0$) and the incident beam direction is known (as well as the relative measured distance, l_m , and the gimbal angles):

$$\mathbf{r}_p = -(l_m + l_r)B(\mathbf{b}_c)\mathbf{b}_i \quad (2.5.7)$$

For the ideal tracker, the target positions can only be measured, if the initial distance to \mathbf{R} and the incident beam direction are calibrated.

2.5.2.2 Extended Model

The ideal model can be extended to incorporate the mirror centre offset. The extended model however is also valid for gimbal axis misalignment, as long as

the transformation matrix (${}^b\mathbf{T}_m$) is adapted (Zhuang and Roth, 1995). Note that the fundamental error source in this model is the deadpath error. Only the transformation matrix (${}^b\mathbf{T}_m$) is modified for the offset incorporation.

The mirror centre offset is then modelled as seen in Figure 2.15. From this model Zhuang and Roth (1995) show that, if \mathbf{r} is the position vector of \mathbf{P} (the target point) in the base frame, that:

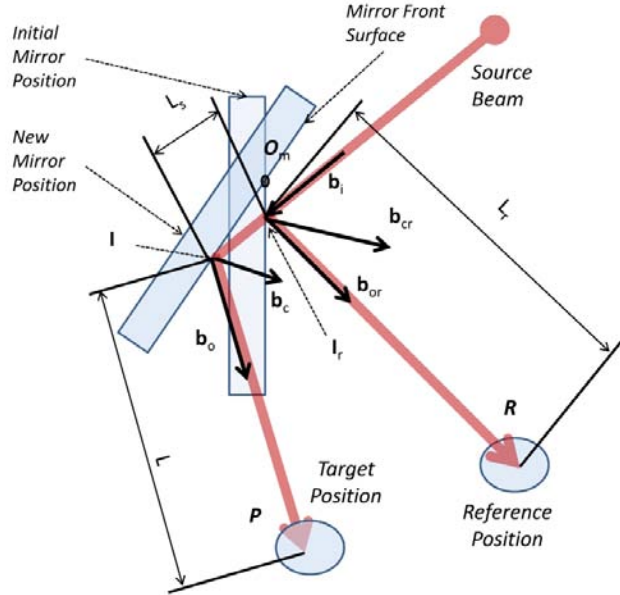


Figure 2.15: Mirror Centre Offset with Target and Reference Position (Zhuang and Roth, 1995)

$$\mathbf{r} = \mathbf{R}_{ir}^m \mathbf{r}_{ir} + \mathbf{t}_{ir} - (l_m + l_r - l_s) B(\mathbf{b}_c) \mathbf{b}_i + l_s \mathbf{b}_i \quad (2.5.8)$$

and

$$l_s = -\mathbf{b}_c \cdot (\mathbf{R}_{ir}^m \mathbf{r}_{ir} + \mathbf{t}_{ir} - \mathbf{r}_m) / (\mathbf{b}_c \cdot \mathbf{b}_i) \quad (2.5.9)$$

where \mathbf{R}_{ir} and \mathbf{t}_{ir} are the rotation and translation sub-matrix of ${}^b\mathbf{T}_m$, respectively, when $\theta_1 = \theta_2 = 0$. With the initial point of incidence, \mathbf{I}_r , (which describes the centre offset) defined as:

$${}^m\mathbf{r}_{ir} \equiv [c_x, c_y, 0] \quad (2.5.10)$$

\mathbf{r}_{ir} is determined by transforming ${}^m\mathbf{r}_{ir}$ from the mirror frame to the base frame, which then is:

$$\mathbf{r}_{ir} = \mathbf{R}_{ir}^m \mathbf{r}_{ir} + \mathbf{t}_{ir} \quad (2.5.11)$$

The other parameters are defined as previously noted. The axes misalignment can be modelled next by adapting the current transformation matrix by

realizing that the origins of the three frames are not coincident. Let \mathbf{O}_b , \mathbf{O}_1 and \mathbf{O}_m be the origin of each frame (see Figure 2.16).

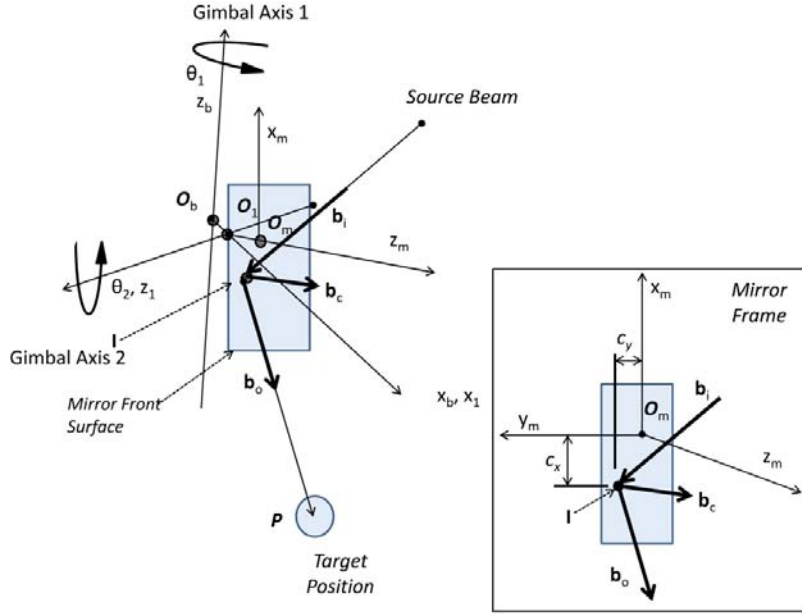


Figure 2.16: Mirror Centre Offset Detail (Zhuang and Roth, 1995)

By assuming that the tracker is at its home position for frame $\{b\}$ and $\{1\}$, x_b and x_1 are coincident and that the axes are normal with the z_b and z_1 axes when z_b and z_1 cross, then x_b and x_1 are perpendicular on z_b and z_1 , respectively. Let \mathbf{O}_b and \mathbf{O}_1 be the intersection points of the normal of the axis (z_b and z_1) and axes self.

The angle α_1 and translation a_1 is now sufficient to model the gimbal axis misalignment, this is done with the rotation matrix $Rot(x, \alpha_1)$, which aligns $\{b\}$ with $\{1\}$ and the translation matrix (see Appendix A) $Trans(a_1, 0, 0)$, which makes the rotated frame coincident with $\{1\}$.

Next, let the z_m axis be parallel with the mirror surface normal and make it pass through the origin \mathbf{O}_1 . \mathbf{O}_m is the intersection point of the z_m axis and the mirror surface. Note that the second axis does not necessarily lie on the mirror surface, but that x_m is on the mirror surface itself. $Rot(z, \theta_2 + \Delta\theta_2)Rot(x, \alpha_2)$ aligns frame $\{1\}$ with $\{m\}$ and $Trans(0, 0, e_2)$ moves the rotated frame to be coincident with $\{m\}$.

For the ideal case the parameters are: $\alpha_1 = 90^\circ$, $a_1 = 0$, $\Delta\theta_2 = 90^\circ$, $\alpha_2 = 90^\circ$ and $e_2 = 0$. The transformation bT_m can now be generalized to include the axis misalignment as follows:

$${}^bT_m = Rot(z, \theta_1)Rot(x, \alpha)Trans(a_1, 0, 0)Rot(z, \theta_2 + \Delta\theta_2)Rot(x, \alpha_2)Trans(0, 0, e_2) \quad (2.5.12)$$

This is done as the three frames' origins are not in general coincident. The angular parameter α_1 and translation parameter a_1 model the gimbal axis misalignment, while the two angular parameters ($\Delta\theta_2$ and α_2), with one translation parameter e_2 , model the offset between the second mirror axis and the mirror surface.

For a single beam laser tracker three dimensional measurement the following ten parameters must therefore be calibrated: c_x , c_y , l_r , α_1 , a_1 , $\Delta\theta_2$, α_2 , e_2 , as well as, the two components of the incoming beam's unit direction vector (\mathbf{b}_i). For a calibrated coordinate measurement, the following steps must be taken with this model:

1. Compute ${}^b\mathbf{T}_m$ at $\theta_1 = \theta_2 = 0$, with the reference point, before measurement starts.
2. Take measurements of the relative distance (l_m) and the two gimbal angles (θ_1 , θ_2).
3. Compute ${}^b\mathbf{T}_m$ and $B(\mathbf{b}_c)$ and then l_s .
4. Finally determine \mathbf{r} : the target position (for the next point return to step 2).

2.5.2.3 Error Model

An error model is also derived by Zhuang and Roth (1995), which gives a representation of the errors on the coordinates of the target, in terms of the internal measuring and kinematic parameter errors. This is done by differentiating the kinematic model for the target point \mathbf{r} , with respect to c_x , c_y , l_r , \mathbf{r}_m , \mathbf{b}_c , and \mathbf{b}_i .

For example, this model can be used to estimate the required measurement accuracy for system calibration. The error model can be used to determine the parameters, with a non-linear least-squares technique. This model can also be used for optimal selection of target points for calibration and be reordered in such a way to aid the design of a single beam laser tracker. The error model results shown by Zhuang and Roth (1995) were compared to the kinematic simulations done in this project. Chapter 4 numerically investigated the errors (instead of analytically) and focusses on the parameter effects.

2.5.2.4 Multiple Beam Model

A multiple beam model was derived by Zhuang *et al.* (2003), which used multiple planer constraints surfaces for the self-calibration of a LTS (see Appendix A.2.3.1). The relatively less accurate gimbal angle measurements are also incorporated for calibration. It is then shown that large errors can be avoided, by using angular measurements to predict the mirror centre offset.

2.6 LTS with Multilateration

This section describes multilateration. Lewis (2006) states that multilateration is:

“A measuring system that determines either two or three dimensional coordinates by combining only length measurements made from fixed points.”

Watson (s.a.) describe a dimensional measurement using four tracking laser interferometers, with fixed distances between each laser tracker. Takatsuji *et al.* (1998) show the first practical coordinate measurement by utilizing the trilateration principle, where the placement of the laser trackers is arbitrary. The optimal placement or arrangement of the laser tracker stations and measurement volume are discussed by Takatsuji *et al.* (2000), Zhang *et al.* (2003) and Zhang *et al.* (2005). Zhuang *et al.* (2003) also propose using the less accurate angular encoder measurements to help improve the calibration accuracy.

2.6.1 Advantages and Disadvantages of Multilateration

As stated previously, a LTS using multilateration satisfies Abbe’s principle, has direct traceability to the length standard, can be self-calibrated and is potentially superior to the conventional bridge-type CMMs (Takatsuji *et al.*, 1998; Lin *et al.*, 2005). The self-calibration of a LTS also creates a virtual metrology frame, making it more portable (Hughes *et al.*, 2000).

Zhang *et al.* (2003) add that such a system (after self calibration) can determine the position of the target or initial distance for a laser tracker, in the event of one of the trackers losing the target for a moment. This overcomes the main limitation of an interferometric laser tracker: that the target must be tracked at all times. The measurement range can be extended by only moving one tracker base station at a time. The new base coordinates can be determined by using the other calibrated base coordinates. This allows, for example, the measurement of an object from all sides. Self calibration is also a major advantage, since it negates the requirement for tedious measurement preparations (Takatsuji *et al.*, 1998)

A disadvantage of such a system is that the measurement volume is limited, compared to a single beam system (Vincze *et al.*, 1994). And as high speed is vital for LTS tracking, an advanced control system is necessary, as shown by Bai *et al.* (2005).

2.6.2 Non-Linear Least Squares Formulation

The measuring system determines the coordinates of the targets and tracking stations by using a non-linear least squares algorithm.

The least squares algorithm tries to fit all the *measurement* variables to all the *system* variables. The measurement variables are defined as all the distances from tracker mirror centre of rotation to all the targets and the system variables as the four laser tracker base coordinates, the initial (reference) length of each tracker and the *target* variables (x, y and z target point coordinates).

This is done by minimizing the error term (or residual) of the cost function. The residual e_{ij} , for the j 'th measurement station and i 'th target point, is (Takatsuji *et al.*, 1998):

$$e_{ij} = \sqrt{(x_j - X_i)^2 + (y_j - Y_i)^2 + (z_j - Z_i)^2 - (l_{ij} - L_i)} \quad (2.6.1)$$

with the target coordinates $((x, y, z)_i)$, the measurement station coordinates $((X, Y, Z)_j)$ and the distance measured (l_{ij}) . Note that all the length measurements (l_{ij}) are relative to an initial length (L_i) , for each tracker. The length measurements are therefore given by $L_i + L_{\text{measured}}$, where L_{measured} is the actual interferometric length measurement.

The coordinate system can be fixed, as well as the number of system variables required for the base stations' coordinates reduced, without loss of generality, by four assumptions regarding the positions of the tracking stations: the first station is at the origin, the second tracker is only displaced in the x direction, the third tracker is in the x - y plane and lastly, the fourth tracker is positioned anywhere in space (Takatsuji *et al.*, 1998).

The coordinate system can then be fixed in space by only six coordinates and only ten system variables are therefore required. These variables are the six for the system coordinates $(X_2, X_3, X_4, Y_3, Y_4, Z_4)$ and the four for the initial lengths (L_1, L_2, L_3, L_4) (see Figure 2.17).

Therefore for n target points, there are $3n$ target variables and $4n$ known measurements values. This implies that at least ten target points are required to solve the whole system (see Figure 2.17).

The unknown variables (for n target points and four tracker stations) can now be solved, given the required initial values for system variables, using the non-linear least square method, by minimizing the cost function defined as:

$$E = \sum_{i=0}^4 \sum_{j=0}^n e_{ij}^2 \quad (2.6.2)$$

The measurement of the first tracker can be used for the initial target point coordinates. Each tracker's first length measurement can be used as its initial length. The position of each tracker station relative to the other stations also needs to be roughly measured and is used to provide the initial stations' coordinates.

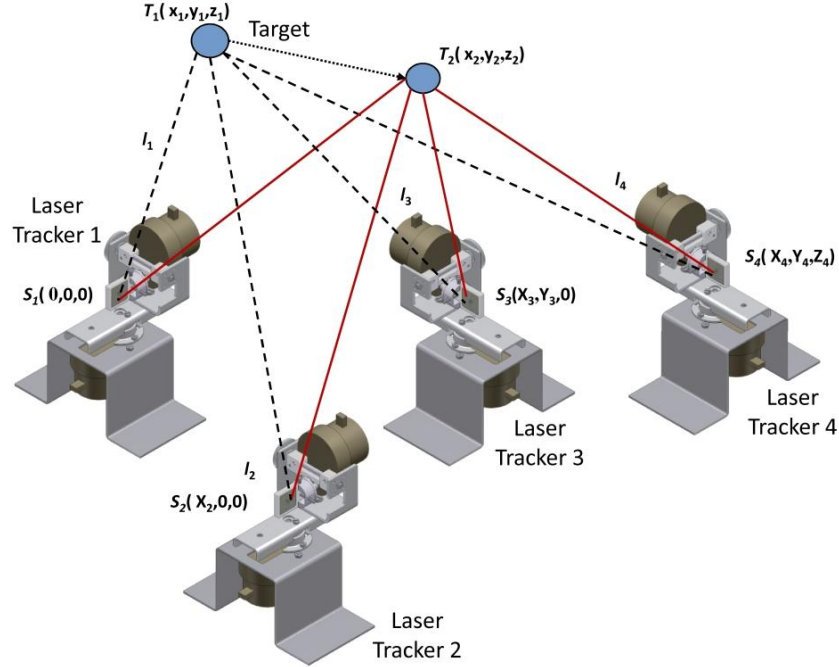


Figure 2.17: Multilateration Setup for Irregularly Placed Trackers (Based on Umetsu *et al.* (2005))

2.6.3 Ideal Arrangement of Base Stations and Target Points for Self-Calibration

Firstly, Takatsuji *et al.* (1998) state that for the improvement of LTS measurements that the optimal relationship between the tracker stations should be investigated. Zhang *et al.* (2003) show that there is a magnification error, which differs for different tracker arrangements. This error is shown to be minimal when the 4 stations are arranged in a regular tetrahedron.

Some rules are given by Zhang *et al.* (2003) for optimized self-calibration for the self-calibration target points:

1. the points should not lie on the same line
2. the points could lie in the same plane perpendicular to the principle axis
3. the points should not be located close to the plane formed by base points
4. increasing the number of points increases accuracy
5. the initial point, used for the reference lengths, should not lie in the target point plane, but in the direction away from the base points.

It is also stated that by using a weighted (relative to the tracker position) least square fit, that the self-calibrated uncertainty can be reduced.

Zhang *et al.* (2005) developed a computer simulation technique from which recommendations are made for tracker positions of a LTS with 5 or 6 stations. Takatsuji *et al.* (2000) also add that the four base stations should not be in the same plane and that the regular tetrahedron, which are formed by the trackers, should also cover the measurement volume.

2.6.4 Other Multilateration LTS Concepts

Literature also reports on non-laser tracking type multilateration systems (Fletcher *et al.*, 2005). For example systems which use absolute measurement techniques (Norgia *et al.*, 2007; Rhee and Kim, 2002), since these technologies are improving it could be feasible to develop an accurate CMM with them. This is out of scope of this project, but it can be included as future work to consider such systems.

2.7 CMM Calibration with a LTS

The bridge type CMM has 21 geometric parameters, which mathematically describes the kinematic errors of the CMM. These errors must be calibrated. This is currently this is done in industry with step gauges or ball plates. This type of calibration procedures though has drawbacks, for example, it takes an extremely long time for this procedure, which ultimately means machine down time (Jiang *et al.*, 2002).

Schwenke *et al.* (2005) show how to map a CMM with a specially designed laser tracker, called the *laserTRACER* (also described by Hughes *et al.* (2000)). Results from testing with a high accuracy CMM with a working volume of $1200 \times 1000 \times 600 \text{ mm}^3$ are shown to have uncertainties in the range of $1 \mu\text{m}$ and $2 \mu\text{rad}$. Note that this method is called sequential multilateration, since only a single station is used. For this procedure the target must be moved back and forth to all the desired target points, for the different tracker positions.

Schwenke *et al.* (2005) note that drift as a result of the target repositioning, for the different tracker positions, can be minimized. This can be done by retracing the target path each time, instead of moving the target from the last target point straight back to the first target point.

Jiang *et al.* (2002) report design work on a LTS specifically for CMM calibration and Umetsu *et al.* (2005) describe using their LTS for this purpose. A single laser tracker is also used and the reported tests show a residual error of less than $0.5 \mu\text{m}$. Umetsu *et al.* (2005) propose using two laser trackers instead of using the trilateration principle as the working volume is limited for the multilateration principle, due to limitations of the acceptance angle of the target. It is suggested that the retroreflector is attached to the CMM ram with an offset and the orientation of the offset is changed at each coordinate. With this added redundancy the target points can be solved.

Chapter 3

Laser Tracker Design

This chapter reports the design work done for the project. It mainly fulfills part (2) of the thesis outcomes.

A LTS is an interdisciplinary system, requiring expertise in various fields, including electronics, optics, precision mechanics, control systems, numerical computation and integrated computer control techniques (Gallagher, 2003). The aim therefore of the tracker design was not to perform a detail design for a tracker, but rather to develop an understanding of the design requirements for such an advanced mechatronic system, by designing, constructing and testing a prototype. This being so, two prototypes were constructed and the second one was tested and shown to successfully track a corner-cube target.

This chapter shortly describes the design process undertaken, specifications and requirements developed for the system. The mechanical, electronic and programming interface is presented, along with the control method and sensor system integration.

3.1 Design Process Description

The steps taking during the design process is shown in Figure 3.1. The project had four main phases (A to D). The D phase also has 4 sub-phases.

Phase A involved work on a sequential multilateration algorithm (see Chapter 5) after which the system as a whole was considered (phase B). From phase B concepts for the whole system were developed, by defining three main components requiring design. These components are the BSM (Beam Steering Mechanism), the PSD sensor and the microcontroller. Suppliers for the necessary components were also contacted for quotes, to determine the financial feasibility of the concepts (phase C). Only then did the design process start (after elimination of non-feasible solutions). The design process involved specification development, concept generations, detail design, assembly and finally testing.

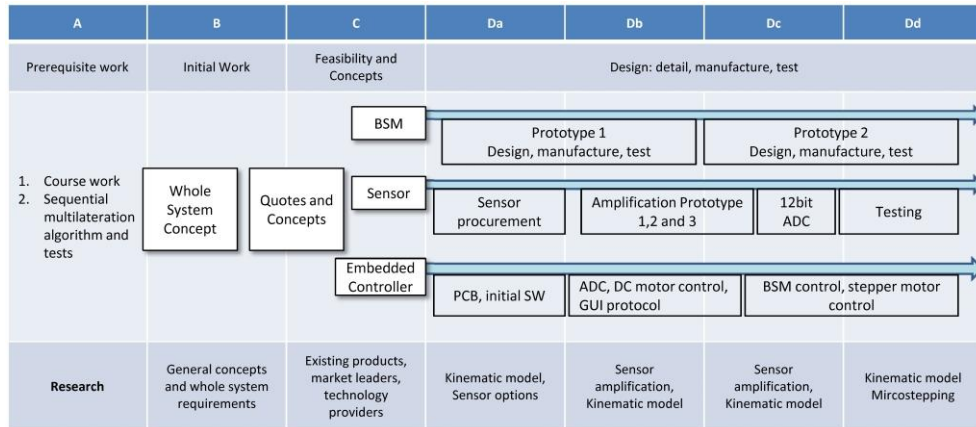


Figure 3.1: Time Line of the Design Process (BSM: Beam Steering Mechanism, PCB: Printed Circuit Board, ADC: Analogue to Digital Conversion)

Each component's design will be discussed, after the system requirements section. Note that other components such as the interferometer and the target are defined as outside of the scope for this project design.

3.2 System Requirements

After communications with the NMISA and the literature study, the following was decided: the LTS must be a coordinate measuring device, which should be designed for high accuracy measurements, within cost constraints, with the final objective of calibrating a bridge type CMM.

From the literature study the following requirements for a tracker station was derived:

1. the station must use a heterodyne interferometer
2. the beam steering mechanism must be designed to reduce any deadpath errors
3. the station must be able to track the target accurately enough so that the returning measurement beam interferes sufficiently with the reference beam for successful distance measurement.

3.3 Beam Steering Mechanism Design

The beam steering mechanism must be able to both redirect the source beam to the target and the returning beam to interferometer and PSD. This must be done smoothly and accurately, ideally without causing any deadpath error in the length measurement.

Some example specifications for the tracking speed was found in literature, and shown in Table 3.1.

Tracking Speeds			
Reference	Speed (m/s)	Acceleration (m/s ²)	Type
Vincze <i>et al.</i> (1994)	6	25	Gimbal
Geosystems (2009)	6	19	Gimbal
API (2009)	3	19	Gimbal

Table 3.1: Sample Tracking Speeds

3.3.1 Concept and Selection

The literature study showed that there are four different existing concepts for the beam steering mechanism, defined as a: (1) single mirror gimbal, (2) multiple mirror gimbal, (3) hemispherical and (4) a spherical beam steering mechanism.

During the design process other concepts was also considered, for example a hexapod (parallel manipulator) mount, but this was not included in the final concept selection process. A proven concept though was preferred negating the risk of an unproven concept. This increased the feasibility of a functional prototype. The remaining concepts are compared in Table 3.2.

Various aspects need to be considered for concept selection. Firstly, cost is discussed. Cost of buying an *off the shelf* high accuracy gimbal mount was found high (see Section 2.3.2). Both the spherical and hemispherical mounts require high precision spheres though, with form errors below 50 nm (Schwenke *et al.*, 2005) and $\pm 0.1 \mu\text{m}$ (Jiang *et al.*, 2002). The multiple mirror concept requires two motorized high accuracy rotary mounts, with a resolution of at least 0.007° and a velocity of 1 rev/s (Shirinzadeh, 1998).

Second is the theoretical accuracy. Both the spherical and hemispherical mounts are free, in principle, from axes alignment errors inherent with either the single or multiple mirror mounts. The spherical system however does not require a halved precision sphere, reducing manufacturing complexity and also making the shape error measurement easier. The hemisphere also requires that the source laser beam and the mirror intersect at the sphere centre. The patented sphere concept then seems to be the most accurate system theoretically.

Various Beam Steering Mechanisms		
Reference	Type	Notes
Zhuang and Roth (1995)	Single Mirror Gimbal	High cost of commercially available mount
Hughes <i>et al.</i> (2000), Schwenke <i>et al.</i> (2005)	Spherical	Patented, requires very high accuracy reference sphere, states that accuracy unaffected by accuracy of bearings and axes alignment
Shirinzadeh (1998), Teoh <i>et al.</i> (2002)	Multiple Mirror	Each mirror is mounted on precision rotary stage
Jiang <i>et al.</i> (2002)	Hemispherical Mount	States that accuracy is unaffected by misalignment of axes, only small uncertainty from deviation of mirror centre and it reduces tracker size

Table 3.2: Comparison Between Various Beam Steering Mechanisms

Hughes *et al.* (2000) report measurement uncertainty of 200 nm for a sequential multilateration experiment with a spherical tracker using a spherical retroreflector. The estimated uncertainty of ± 60 nm for this spherical tracker station is given. Umetsu *et al.* (2005) also report that the estimated uncertainty for a hemispherical tracker station is 300 nm.

For a first prototype a gimbal mounted single mirror concept was selected. Motivation for this choice is that it has the simplest construction and it is the least expensive. Again, this project is only an initial investigation and not a final design. These motivations are therefore justified based on time, budget and expertise constraints.

3.3.2 Single Mirror Gimbal Design

Two prototypes were designed, manufactured and assembled. The second prototype was tested and it successfully tracked a corner cube retroreflector. A special aim for the design was that it should be possible to adjust the mirror position and axes orientation so that the deadpath error can be reduced. This aim is further motivated by the kinematic model chapter (Chapter 4). Note that the axes should ideally be perfectly perpendicular and intersecting.

The design of the two prototypes are shown in Figure 3.2. Prototype 1 (Figure 3.2a) uses two small, geared brushed DC motors, while prototype 2 (Figure 3.2b) uses two geared stepper motors. Both prototypes make provision for both adjusting the horizontal axis orientation and the mirror position. The

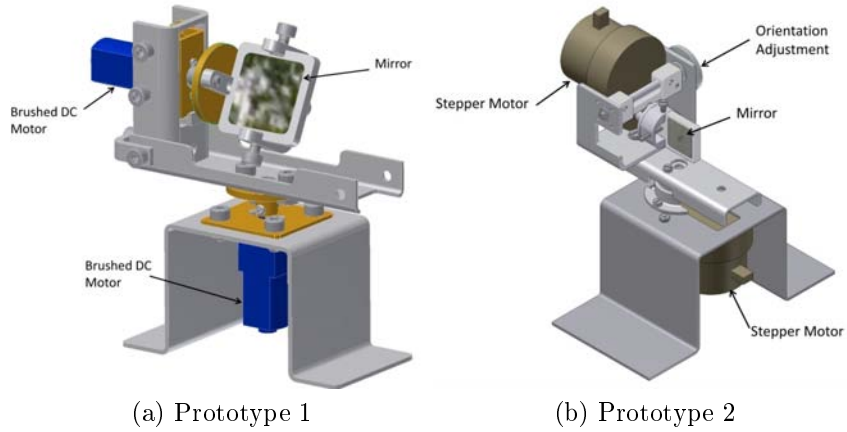


Figure 3.2: The Two Gimbal Prototypes

design decisions made to compensate for the inherent error caused by the axes misalignment, the non-intersecting axes and the mirror offset with prototype 2 are discussed next.

3.3.2.1 Axes Misalignment

Figure 3.3 shows the cumulative effect of the axes misalignment. The ideal mirror position and the actual mirror position are shown. The effects of geometric errors in the vertical axis rotation (modelled as $\delta\theta_{horizontal}$) will be reduced by minimizing the distance δy and the same is applicable for the horizontal axis rotation and distance δx .

The stepper motor used has an ovoid shaped gearbox mounted on it. There is then an offset between the motor centre and output shaft. The horizontal axis motor was mounted with the output shaft as low as possible, to reduce δy .

The horizontal axis motor orientation can also be adjusted, see Figure 3.4a. A balancing weight can be placed opposite this motor on the vertical axis arm, to reduce wobble. Finally, a thrust bearing was used to support this arm.

A bush which sit on the shaft has a tapped hole orthogonal to the shaft axis. A grub screw fastens into this hole, pushing unto the flat on the shaft, which fastens shaft to the bush and therefore the arm, for the vertical motor, or the mirror holder, for the horizontal motor.

During assembly it was important to apply pretension to reduce play in the motor output shaft and the assembly. This is done by forcing the shaft in an axial direction and then fastening the grub screws. By applying pretension during assembly the backlash, axis alignment and wobble is improved, but is not completely negated.

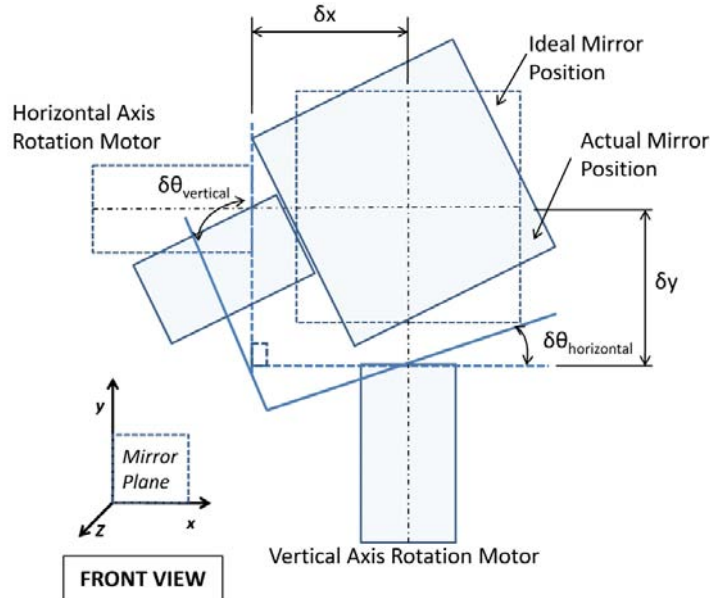


Figure 3.3: Illustration of the Effect of Axes Misalignment

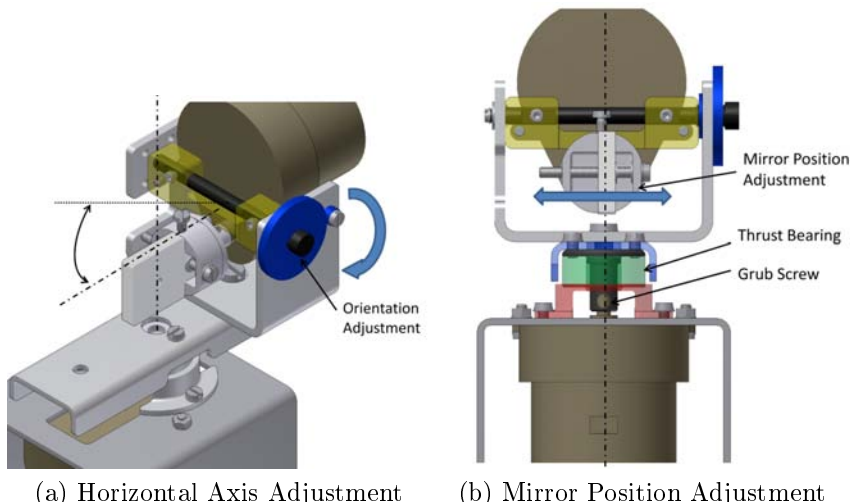


Figure 3.4: Mirror Position and Horizontal Axis Adjustment

3.3.2.2 Non-Intersecting Axes and Mirror Offset

Figure 3.5 shows the mirror being offset in the z direction, which is the direction normal to the mirror surface. Note that of all the possible translation directions, only a translation in z axis is of importance and that the mirror can be translated in the xy plane, as long as the source beam is still incident on the (assumed) perfectly flat mirror.

Figure 3.4b shows how the design of prototype 2 allows for this adjustment.

A bolt is used to make a simple linear actuator. The bolt is driven through the tapped mirror holder. A spring (not shown) presses between this component and the one mounted on the output shaft. The mirror the slides in the z direction as the bolt is turned.

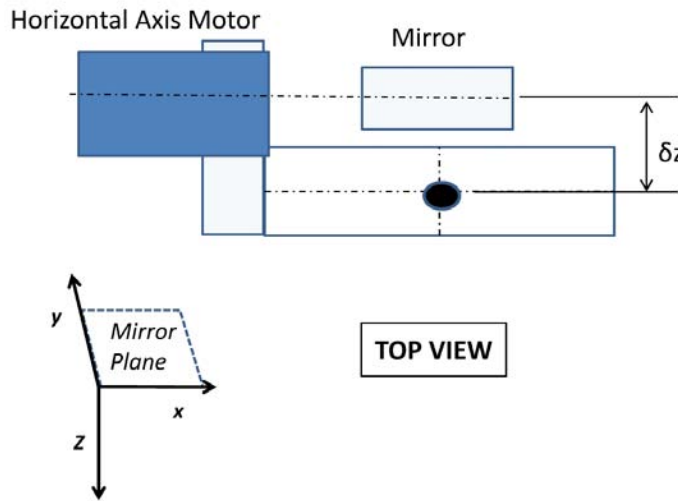


Figure 3.5: Illustration of Mirror Offset

3.3.3 Design Result and Discussion

The final version of prototype 2 is shown in Figure 3.6. It did function and the next steps for an improved beam steering mechanism will be to increase laser beam acceptance angle, improve axis adjustment, consider brushless DC motors and also to investigate the feasibility of other possible concepts.

Another feature of this design is that the thrust ball bearing can be replaced with a needle bearing, reducing the height of the horizontal axis and thereby reducing the effect of the error of axes misalignment. The design also allows for the stepper motors to be replaced with RC (Remote Control) type servo motors.

Backlash will be present since the motors are geared. The effect of the backlash though was reduced by connecting a spring between the rotating part and a point relatively stationary to the rotating part.

3.4 Actuator Selection and Control

An important step in the design process of the gimbal is the motor selection, which is discussed next along with the observed effect of the backlash.

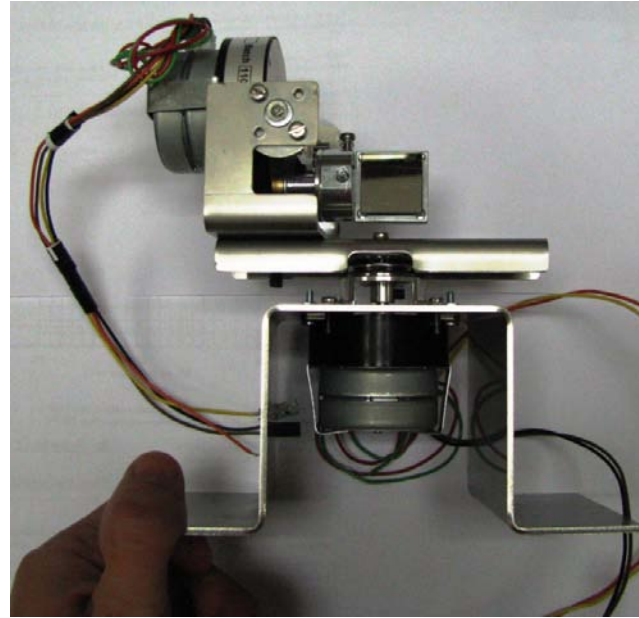


Figure 3.6: Photo of Prototype 2

Two prototypes were constructed, both using geared motors. The first prototype used brushed DC motors and the second used geared stepper motors. An important specification for the gimbal is the attainable rotational resolution or minimum attainable step size. With any type of motor there are various factors increasing the minimum step size, for example friction, inertia and the specific motor control method.

3.4.1 Motor Selection

There are two general types of gimbals: a gear driven gimbal and a direct drive gimbal. Schmidt (2006) compares these two types. Gear driven gimbals can use either servo (DC) motors or stepper motors. These gimbals are less expensive, have great in position stability and have high load bearing capacities with high stiffness. A drawback of such a gimbal though is backlash due to the gearing, resulting in a reduced bidirectional repeatability. A gear train also suffers from wear during operation, reducing system accuracy over its lifetime.

Direct drive gimbals usually use brushless DC motors. Repositioning errors are negated since this type of motor has no backlash or mechanical wear. The bidirectional repeatability for direct mount gimbals is at least two times better than geared gimbals and their rotational speed is also a lot faster (Schmidt, 2006). However direct mount gimbals lack the torque and size capability of geared gimbals.

The control system however for brushless motors is more complex than the control system for steppers and brushed DC motors. These two motors are also more readily available and are relatively less expensive. A geared brushed

motor was therefore used for the first prototype (least complex control) and a geared stepper for the second. A stepper was preferred for the second prototype, since it also has relatively simple control electronics compared to brushless motors and does not require a rotary encoder for basic position control. A stepper also has fast response times (Condit and Jones, 2004), crucial for target tracking.

After testing prototype 2 it was found that fast direction change speed, very small step size and accurate positioning is the critical parameters for the beam steering mechanism. Since the mirror is small and lightweight it can be concluded that for the next prototype (outside of scope of this project), a direct drive solution will have to be considered.

3.4.2 Stepper Motor Control

See Appendix B for specifications of the permanent magnet 6-wire unipolar stepper motor used in prototype 2. It has a theoretical step resolution of $0.06^\circ/\text{step}$. This can be theoretically reduced, with microstepping, to $0.004^\circ/\text{step}$ (with 16 bit microstep resolution). Microstepping is explained next. During gimbal tests it became clear that microstepping is necessary, since it increase both the speed and resolution of the mechanism.

A unipolar¹ permanent magnet stepper motor was used. The unipolar stepper though was driven as a 4-wire bipolar stepper, since prototype 1 used DC motors, which also required bidirectional current flow through a coil. This made the upgrade from prototype 1 to 2 faster, as no extra electronics were required.

The stepper gives a *normal* step if the current coil is deactivated and the next one is activated (switched off or on). This gives very jittery movement, if the stepping rate is low. Stepping motion can however be improved with a method like half-stepping, where the current coil is kept activated, while the next one is being energized. Only after both coils are energized, is the previous coil deactivated.

Microstepping further improves the stepping motion by using a PWM (Pulse Width Modulated) signal (see Figure 3.7a). During testing microstepping gave the best results, both for step size and speed.

Microstepping works by partially activating or deactivating each coil, see Figure 3.7b. This method varies the voltage over the coil in a sinusoidal form between completely off and fully on, rather than immediately bringing the voltage up to the maximum allowable level, as determined by the maximum allowable current limit specified for the stepper. This results in a very smooth transition between step positions. Theoretically it can give any stepper an

¹In a unipolar stepper the current always flows in the same direction in a specific coil. Bipolar steppers have bidirectional current flow through a coil.

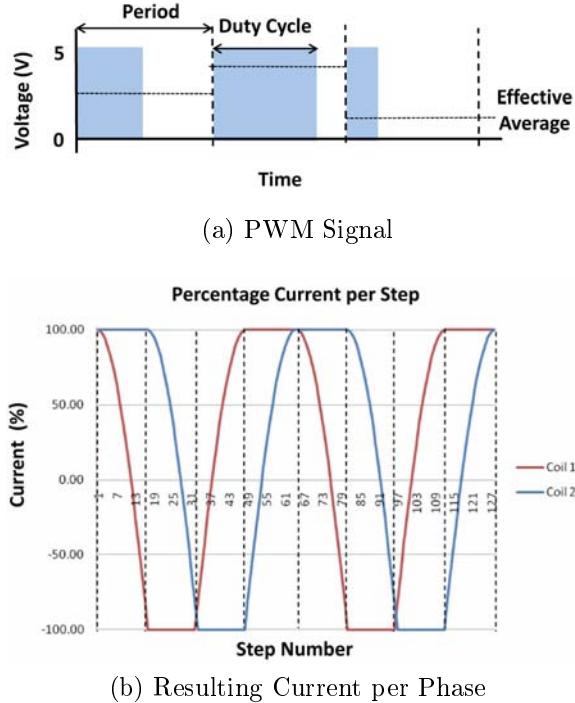


Figure 3.7: PWM and Microstepping (Based on Condit and Jones (2004))

infinitely small step size, but there are factors limiting the step resolution, such as the static friction in the system. (Condit and Jones, 2004)².

The PWM signal creates an effective, microcontroller adjustable, average voltage over the motor coil. A duty cycle of 50%, for example, ideally gives an effective average of half the applied voltage. The inertia of the motor due to a combination of the mechanical inertia and the inductance, prevents the motor from immediately responding to the *on* or *off* signals of the PWM. The output shaft will therefore not manifest any motion jitter as a result of the PWM switching, since the switching frequency of the PWM signal is at least an order of magnitude greater than the response frequency of the motor. Finally the PWM signal frequency is preferred to be higher than 10kHz, so that the switching is inaudible to a human ear.

It is possible to generate such a PWM signal with a microcontroller. Note that the microcontroller also reads the sensor values and apply the control strategy, to actuate the motors. A microcontroller though cannot source sufficient current to drive a motor. External components are therefore needed to integrate the PWM signal with a larger current source and to facilitate bidirectional current flow.

Both the brushed DC motor and the brushless bipolar stepper motor re-

²A PCB was also designed and tested with a chip made for stepper motor control (the L297), but microstepping with only the microcontroller was found to work better, even if it was more resource intensive for the microcontroller.

quire bidirectional current flow. This requires the switching of the polarity over a coil and is optimally done by using a *H-bridge*. A dual full bridge driver IC (Integrated Circuit) chip (specifically the L298, see Appendix B for details) and a few Schottky diodes were used. This bridge forms a critical part of the motor control design.

An advanced stepper motor control was designed, built and improved by implementing a microstepping algorithm, rather than a normal stepping control system. This was done with minimal cost and components.³

3.5 Sensor Amplification

The literature review found that a lateral effect pincushion type PSD sensor would be the best. These devices and amplification components are however hard to source in South Africa and also expensive. The NMISA had a segmented quadrant type silicon photodiode available and it was used for this project. An amplifier had to be built for this sensor whose output was connected to a analogue to digital converter (ADC). The amplifier PCB is discussed, after which the ADC conversion. The main difference between the PSD sensor and the quadrant detector, is that the quadrant detector has a small gap ($30\mu m$) between each quadrant, while the PSD is uniform.

3.5.1 Amplifier Selection

Three amplifier circuit prototypes were built and tested. The third one was used and is mainly based on the design done by Johnson and Lentz (2003) and the technical data as presented in OSI (2007).

A photodiode is a photoelectron converter: it produces current due to incident light, and can be modelled as a large resistor, capacitor, diode and current source, all in parallel. The current source models the amount of light converted into current (see Figure 3.8) and the amount or position of the beam spot is determined by measuring this current.

The simplest measurement circuit for this sensor would be to use a voltage divider: a very large resistor in series with the photo sensitive diode, connected to an ADC. The measured current though is not only the converted light, but also the current, which exist due to the dark current (modelled by the resistor) dependant on temperature and the applied voltage. The voltage dependent capacitance, which exist as result of the terminals of the PN junction (Hamamatsu, 2002), influences the sensor reaction speed. This technique therefore is ineffective (Rako, 2004) and calls for a more complex design.

Prototypes 1 and 2 schematics are given in Appendix C. Since very low tolerance resistors for the prototypes were however not available, variable re-

³Please see the Appendix E for cost, Appendix B for datasheets and Appendix C for circuit board schematics.

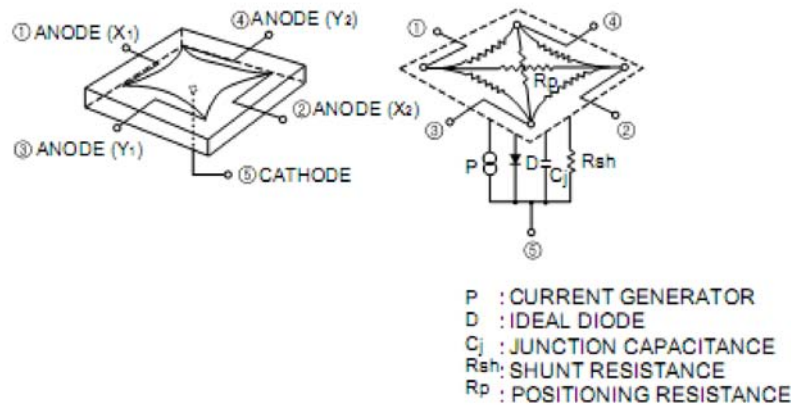


Figure 3.8: Schematic and Electronic Model of a Pincushion Type PSD (Hamamatsu, 2002)

sistors were used. Both concepts use a differential amplifier and this requires that three variable resistors are adjusted. Note that the sensor has four outputs. One for each quadrant and that it would be ideal if they responded in precisely the same way to the incident light, which requires fine adjustment of the resistors.

An instrumentation amplifier was also considered (see Appendix C), since it required only one resistor instead of three. The amount of voltage swing is a factor which determines the attainable sensor resolution with an ADC. With the help of simulation programs however, it was found that the instrumentation amplifier available has less voltage swing than the operational amplifier.

The literature review also showed that the sensor can either be used in the photovoltaic mode or photoconductive mode. The photovoltaic mode is used for more accurate, yet slower response times. In comparison, the photovoltaic mode is used for faster, but less accurate sensing. The photoconductive mode, which requires a reverse voltage was selected for prototype 3.⁴

The schematic of the third prototype for the amplification circuit is shown in Figure 3.9. The first amplifier after the sensor converts the current to a voltage, while the second one amplifies the voltage.

The effect of the capacitance on the system can be reduced, if a large constant voltage is applied. This is achieved by connecting the sensor output pin to a virtual ground, created by an operational amplifier. The amplifier was designed with the required feedback resistor with a small capacitor in parallel. This capacitor compensates for the capacitive effect of the diode and help to prevent output oscillations (Rako, 2004; Johnson and Lentz, 2003).

Johnson and Lentz (2003) also uses a 10Hz low pass anti-aliasing filter (see Appendix C). This filter was included in prototype 3, as well as a connection

⁴Prototype 3 can be modified to operate in the photovoltaic mode.

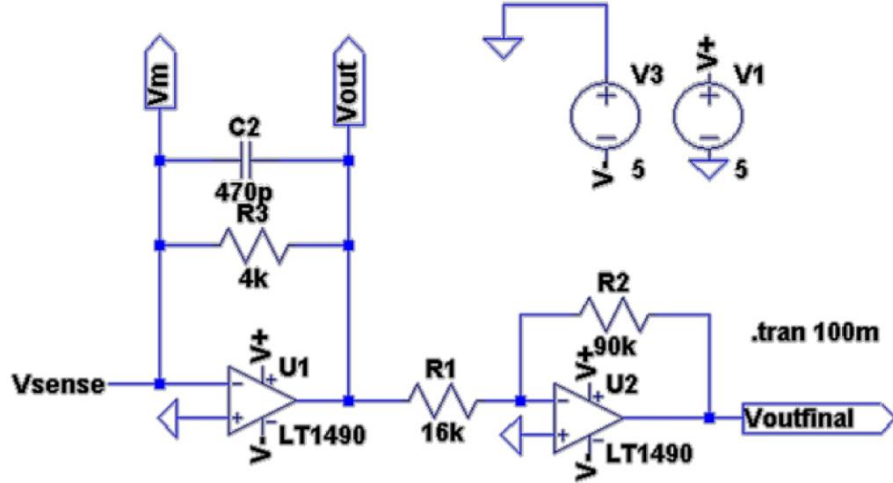


Figure 3.9: The Third Prototype Amplification Circuit (for one of the four outputs of the SiPIN)

to a 12 bit ADC. The filter was tested by measuring the voltage before and after it and the post filter signal was relatively noise free.

3.5.2 Analogue to Digital Conversion

After the photodiode has been biased, the resulting photocurrent converted, amplified and filtered, the result is converted or digitized, so that a microcontroller can react accordingly. This step though also introduces system uncertainty since it places minimum step size on all readings and adds a conversion error.

Estimations for the ADC resolution (10 and 12 bit) can be seen in Equation 3.5.1. Where the V_{swing} is the amplified voltage change as the beam moves over the linear response length L_{sensor} . This is the length from one edge, of the sensor's linear spatial response active area (L_{sensor}), to the opposite edge. The N_{Total} is the maximum counts a specific ADC can have. Since digital values are presented with only two types of digits, a 10 bit ADC will have 2^{10} or 1024 counts, which then for a 5V swing will result in 4.883 mV/count, for example.

$$\begin{aligned} R_{ADC} &\approx \left(\frac{\Delta V_{swing}}{N_{Total}} \right) \left(\frac{L_{sensor}}{\Delta V_{swing}} \right) \\ &= \frac{L_{sensor}}{N_{Total}} \end{aligned} \quad (3.5.1)$$

This conversion process however does take time, and for the microcontroller processing time and available memory are critical resources. The microcontroller used has a 10 bit ADC module, while the amplifier prototype is designed to feed a 12 bit external ADC, which is read by the microcontroller with a SPI

(Serial Peripheral Interface) bus. The speed of the conversion directly affects the control of the gimbal. This is further discussed in the microcontroller section (Section 3.6).

3.5.3 Design Results

The speed, accuracy and repeatability are the critical sensor factors. The sensor amplification design should not compromise the existing performance capabilities of the sensor, which is ultimately limited by the signal to noise ratio (resolution), dark current (accuracy) and photodiode capacitance (speed). The final prototype (Figure 3.10) was also enclosed in small metal box to reduce any EMI (Electro Magnetic Interference) noise around the sensor and amplification electronics.

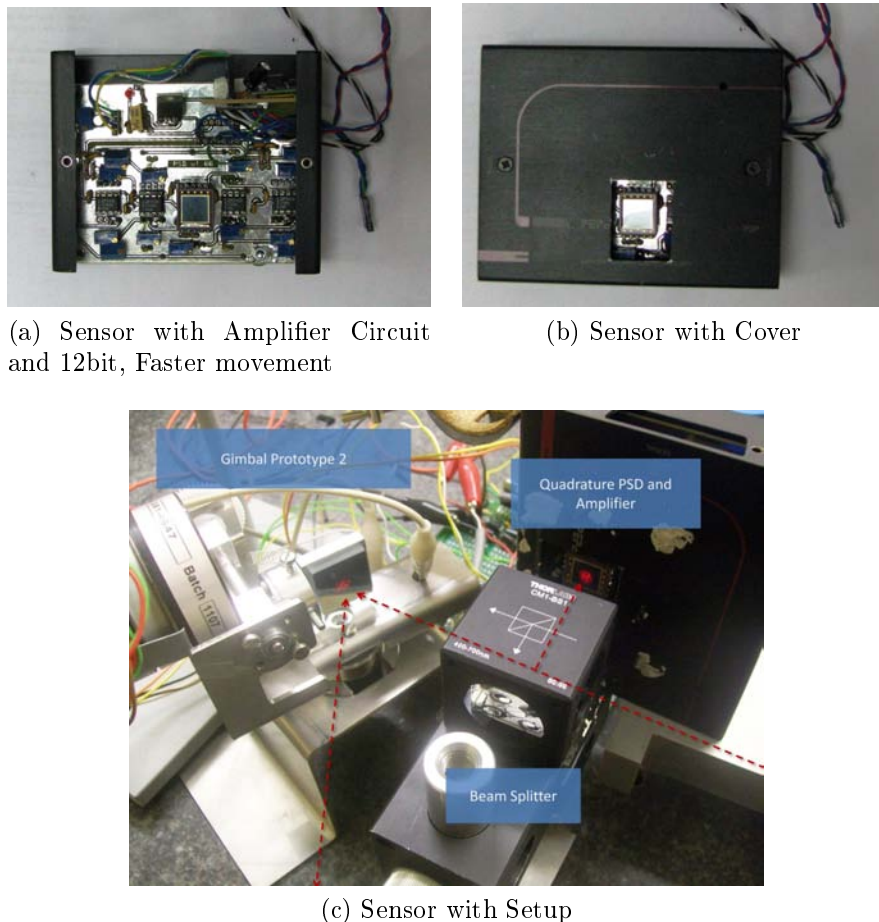


Figure 3.10: Photos of the Final Prototype

Many tests were performed and various algorithms were developed to get an understanding of the sensor and its requirements. Unfortunately the sensor,

which was available, was not a PSD (which will give greater linear range and therefore better control), yet the tracking station with the segmented quadrature detector, SiPIN photodiode, did function.

A range test was performed with the final prototype, with both the external and internal ADCs. This was done by steering the beam to the target, placed on top of a micrometer. The sensor and optics were then adjusted until the tracking spot were in the sensor's approximate centre. After turning off the tracking system and centring the tracking spot, the micrometer was adjusted, which moved the tracking spot over the sensor. The micrometer was actuated until the tracking spot touched the sensor's edge. The four resulting readings from the sensor were recorded for each time step, as the spot moved over the sensor. Figure 3.11 show the results of such a test. In each plot the *x* axis is the time in unit steps and the *y* axis is the ADC counts.

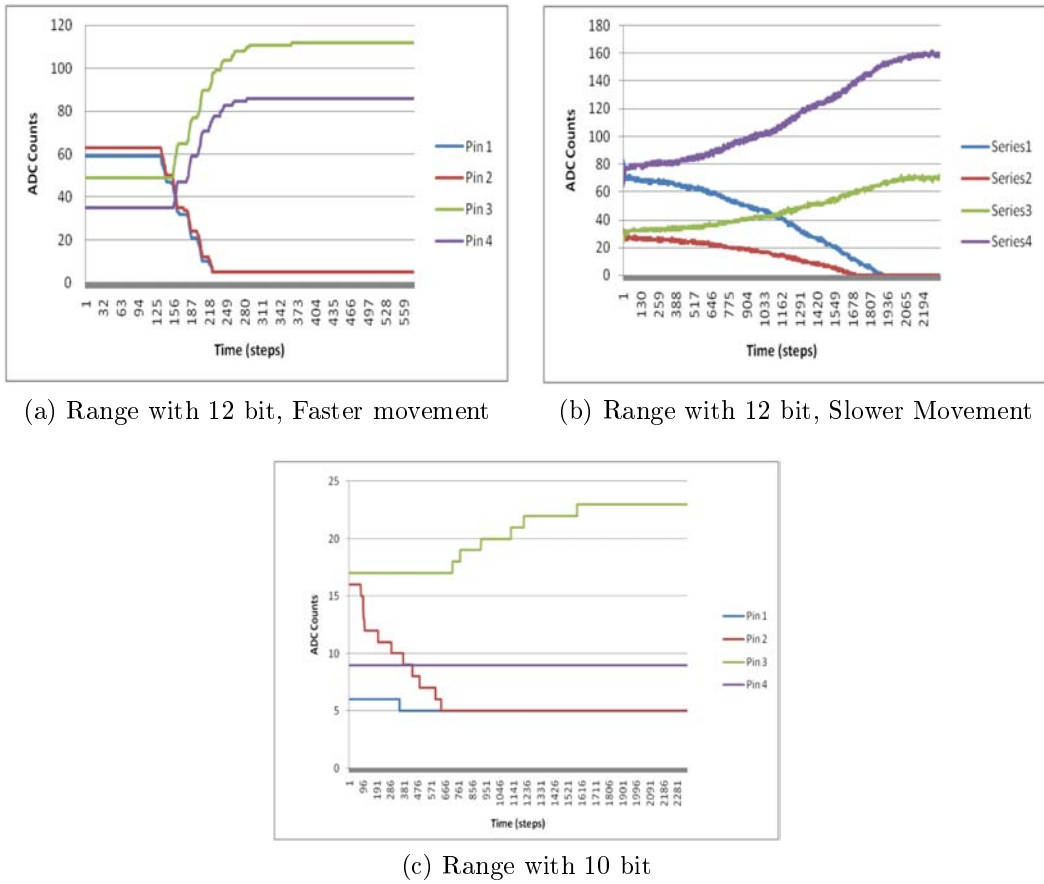


Figure 3.11: Sensor Range Tests

Figure 3.11a show the results of the spot being moved from the approximate centre to the edge of the active area with the external 12 bit ADC, and Figure 3.11b shows the same type of test while the micrometer is turned much slower.

These two can be compared to Figure 3.11c, where a result of movement over the sensor connected to the internal 10 bit ADC is shown.

The actual range⁵ found for the 12 bit ADC was around ± 50 ADC counts (implying an edge to edge range of a 100 counts), while ± 12 counts were found for the 10 bit. Since $50/2^{12} \times 2^{10}$ is equal to 12, this reduction in range is expected.

From the figures the increase in minimum detectable step size is also seen, between the 12 and 10 bit ADCs. It is estimated for the 12 bit ADC, that a resolution of $100\mu m/count$ and $500\mu m/count$ for the 12 bit and 10 bit ADCs was obtained respectfully. Only 2.4% of 4096 available counts for the 12 bit ADC was used. This can be ascribed to the ambient lighting on the sensor and that the alignment laser used during the amplification design and testing, and the interferometer laser used differed both in size and intensity. Differences in the range is due to the use of only an approximate sensor centre and the different starting positions of the target.

3.6 Embedded Controller Design and Programming

The dsPIC30f4011, a 16bit high performance digital signal controller, was selected as the microcontroller for this project, since this processor has sufficient number of PWM modules (3), ADC channels (9) and processing capabilities up to 30 MIPS (Million Instructions per Second).

3.6.1 Controller Description

A prototype PCB (Figure 3.12), which was jointly developed with the Stellenbosch Robotics Club, was used. It features a serial UART (Universal Asynchronous Receiver/Transmitter) connection, bootloader (enabling fast programming with the serial connection), 7.3728MHz oscillator, which is setup to produce a throughput of about 14.74 MIPS or an instruction cycle period of 68 nanoseconds. The PCB also has two L298 H-bridges, which can be used to control four DC motors or two steppers, bidirectionally. There is also a prototype area and header type connections to all the microcontroller pins.

With this project most of the time was used for programming purposes, as could be expected since programming motor control, gimbal control, sensor data acquisition and user control through a PC was required. All programming for the microcontroller was done in C, using a MPLAB IDE from Microchip with the C30 tool suite. The user interface was programmed in Python. The

⁵The change in ADC count, from a approximate midpoint to sensor edge, for a specific pin.

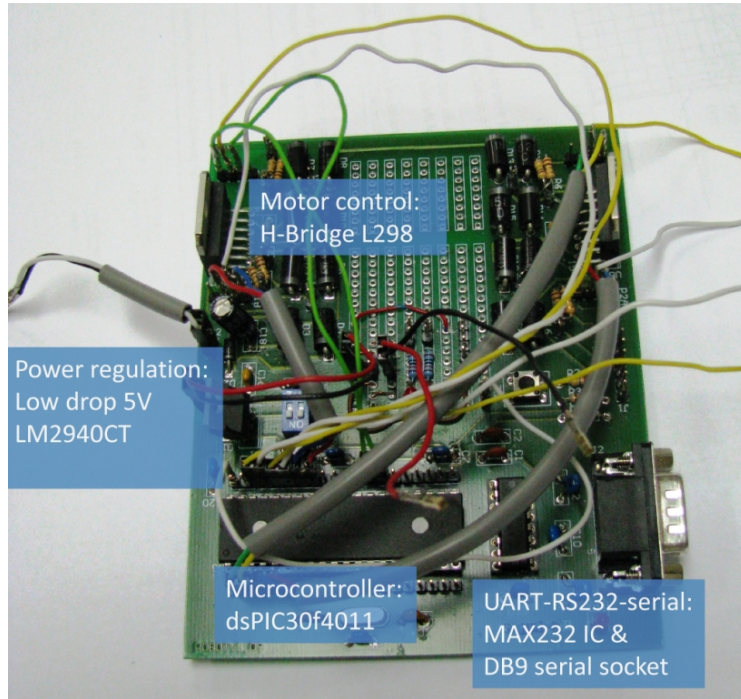


Figure 3.12: Photo of the Microprocessor and main PCB

system was therefore designed to facilitate debugging. Display LEDs, for example, would not have been able to give enough detail debug information and a LCD mounted with the PCB would have required unnecessary costs. Hence, the serial connection was preferred for debugging.

The functional layout is shown in Figure 3.13, as well as the main components. The microcontroller is the centre of the whole system, since it both receives and interprets the sensor data, controls the motors due to either the control algorithm or user commands, and it also gives feedback or debug information to the user through the serial connection. The two diamonds in the figure indicates decision blocks, where the one connected to the sensor is to show that the system can either use the 12 bit external ADC, which is connected to the microcontroller through a SPI bus or the microcontroller's onboard 10 bit ADC. The other decision block, before the serial connection, indicates that the system can be either programmed by the serial port or be used for sending commands and receiving debug information.

The microcontroller has several built in modules, which are activated for use by setting the control registers in the microcontroller flash memory to the required states. This is done with programming. Some modules used for this project are: UART, SPI, ADC, Timers, PWM and IO (Input/Output Port) modules.

The general programming backbone of the system is described next, after which the motor control and sensor data acquisition, and then GUI interface

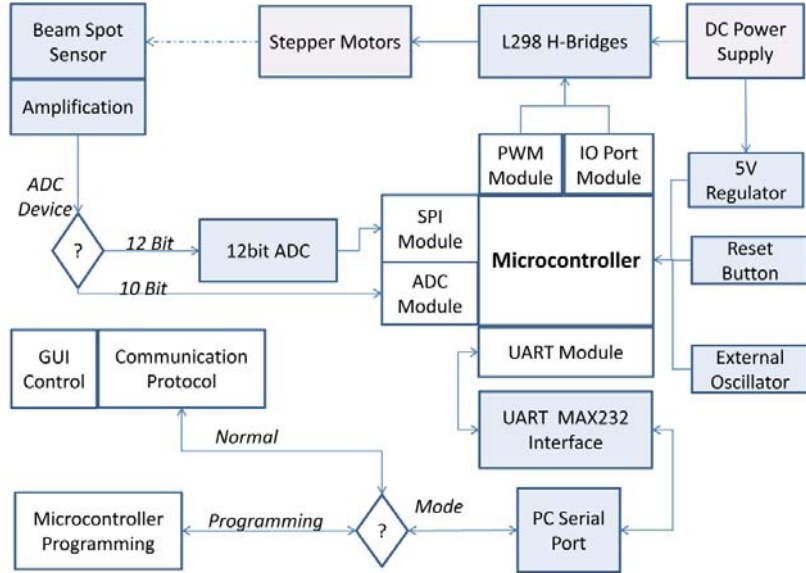


Figure 3.13: Diagram of the Main PCB

and control algorithm. A free bootloader, a software program loaded unto the microcontroller to enable programming with the serial port, the Tiny Bootloader was used (Claudiu, 2003)⁶.

3.6.2 Microprocessor Programming

As mentioned, time is a critical resource for the microcontroller, since the controller program however only consumed about 50% of the total program memory available, memory was not considered that critical.

Figure 3.14 shows the main program. The general approach to microcontroller programming is to first initialize the system (step 1), after a reset has occurred (step 0), and then to enter an infinite loop, which is shown as step 2. The processor then continually checks if either a command has been received through the serial port or whether the system is in a specific state, for example, a *print all sensor values* state.

A stepper motor however is very sensitive to the step rate. If it is stepped too fast, it will not move at all. A timer interrupt is therefore implemented, see 3.14 step 3.a and 3.b. In general, a timer interrupt works by incrementing a register every instruction cycle. If this register overflows, or matches a preset value an interrupt flag is set, and the register is reset to 0. If the timer interrupt is enabled and an ISR (Interrupt Service Routine) with a higher priority is not being executed, a specific interrupt handling function or ISR is called for the

⁶Please visit <http://www/etc.ugal.ro/cchiculita/software/picbootloader.htm> for more details on the Tiny Bootloader.

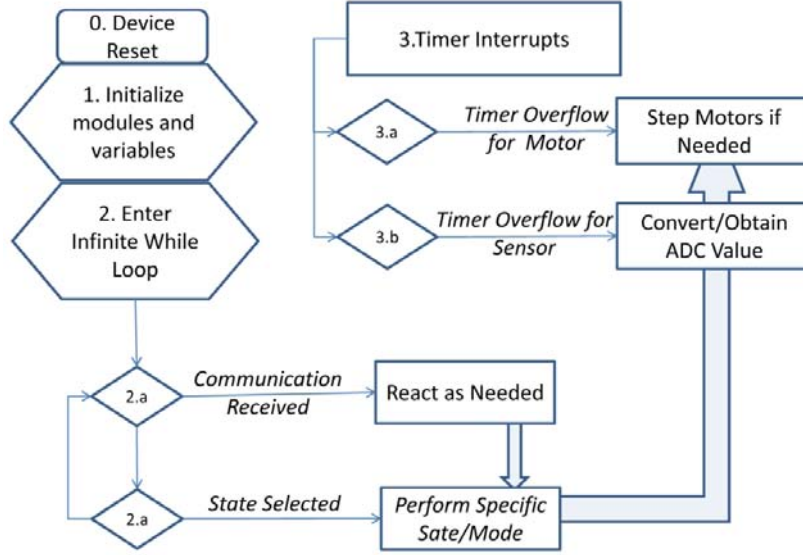


Figure 3.14: Process Flow of Main Program

tripped interrupt flag. The main program is therefore interrupted, until the ISR is completed or a higher priority ISR request occurs.

Note that interrupts have priorities, and that the most time critical interrupts must be given the highest priorities, to ensure that the desired timing is achieved.

3.6.3 Motor Control and Data Acquisition

In the case of this project a timer ISR allows for the stepping of the motor at a constant speed, and a steady rate of data acquisition from the sensor. Each ISR takes a certain number of instructions to be completed though and, if for example, the time required to complete the data acquisition ISR is longer than the period it has before the next time based ISR is needed, traffic problems can occur, resulting in the stepper motor not functioning properly. This has to be taking into account during programming, testing and debugging and places a restriction on the maximum timer frequencies.

During testing however it was found that the 8 bit SPI communications took more processing time than the internal 10 bit ADC module.

3.6.4 GUI Interface

States for the main program were defined, for example the *W* (wait), *D* (Debug) and *C*(Calibrate) state. The user can command the system to enter one of these states, and then give further commands as needed. To zero the sensor for ambient light, the user will first command the main program state to the calibrate state and only then give another command to zero the sensor. These

steps are necessary to keep the code modular and for debugging. The GUI however performs these steps in the background, allowing the user to zero the sensor for example, with only one command.

The GUI interface was written in Python, with the PyQt package. For the serial port communication threading was used, to allow the GUI to manage the main window events and check the serial port concurrently. A virtual state of the processor is kept in the GUI program and updated as new commands are sent and feedback from the microcontroller is received. The software part of the communication between the GUI and microprocessor was facilitated with a simple communication protocol, where the GUI is the master and waits for feedback or acknowledgement after each sub-command. Timing must be considered again, as well as buffer overflow.

3.6.5 Basic Control Algorithm

Two main approaches for the control algorithm were tested. The idea of both is to simply minimize the offset between a preset photodiode origin on the sensor and the current centre of gravity of the incident beam spot, by adjusting the required gimbal angles. The one approach was to calculate the $x-y$ coordinates of the incident beam spot from the four converted and amplified photocurrents of the sensor. The other approach was to use these four values and minimize the difference between them. The coordinate calculation approach failed, as this sensor is a quadrature detector.

A straightforward *bang-bang* control is implemented after the analogue to digital conversion of all the sensor outputs. The diagonal error is first minimized by rotating both axes simultaneously, to within a certain approximation level. After which only one axis is rotated per turn to minimize the x or y offset, i.e. the y axis offset is only solved after the x axis offset has been reduced below a specified level. After the diagonal offset is solved the motor speed is also reduced, creating a step like P (portioned control).

A control strategy was necessary since the spot overstepped the centre. The timing delay with 12 bit ADC conversion and SPI communication and the minimum step resolution creates this overshoot. This requires that an effective delay, by decreasing the step speed, had to be inserted between steps to ensure that the centre is detected. The overshoot is then reduced by decreasing the stepping speed.

Tracking speed however is an important requirement for the tracker. This speed is increased through the control strategy by first stepping both motors simultaneously and then each motor separately, at a reduced speed, as the spot approaches the sensor centre.

This control method did sufficiently track the retroreflector target, yet for the next prototype PID control will have to be considered since the tracking speed should then be much faster. Furthermore, for a full LTS system

with multiple trackers a fuzzy logic type control system could be necessary (Bai *et al.*, 2005).

Part of the future work of the control system could also be the development of a centre of rotation detection or calibration system.

3.7 Calibration Concepts

This chapter is concluded with two calibration concepts, as part of the design of a tracker station since future investigation into a tracker station calibration will be essential.

3.7.1 Camera Test Concept

Since the incident beam spot position relative to the centre of rotation of the gimbal is extremely critical, a concept was also considered to measure this error concurrently, allowing for real time error correction. Zeng and Song (1999) do however also report on a fringe position method for this measurement purpose. Here, a different concept is proposed.

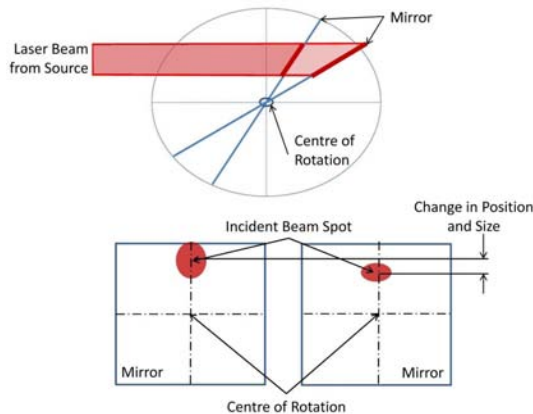


Figure 3.15: Change of Spot Position and Size Due to Centre Offset

A camera is aimed at the beam steering mirror and as the mirror rotates, the camera tracks the position of the spot. If the spot moves around, an offset exists. The detected offset can then be used to calibrate the gimbal or to modify the measured coordinates by using the kinematic model. See Figure 3.15. A camera type detector should be able to both detect a change in position and possibly shape. A challenge for this concept however is the highly reflective mirror.

A small prototype program was written in Python using OpenCV to perform an initial test. This program was able to both detect the beam spot and

track it. It was however not robust and very sensitive to ambient lighting, hence it was not developed any further.

3.7.2 Calibration Method Concept

By mounting the two axis rotation mirror on an adjustable mechanism the actual centre of rotation can be aligned with laser beam incidence point. After pointing the laser beam directly back toward the beamsplitter (i.e. the target is removed), the process is as follows:

1. Turn the mirror until the beam is approximately perpendicular to the mirror surface, which will be the case if the received signal strength is at a maximum.
2. Zero the interferometer.
3. Calibrate the mirror by moving the whole mirror around, until the change in length is minimal.
4. Rotate about the other axis and repeat the last step, until the error is minimal.

Chapter 4

Laser Tracker Kinematic Model Simulations

An understanding of the geometric errors of a gimbal beam steering mechanism was desired, both for the development of an understanding of such a gimbal and for the calibration of it, for more accurate measurements. The literature review presented the kinematic model by Zhuang and Roth (1995), which models both the mirror centre offset and the axis misalignment. This model was selected since it only has 10 parameters, compared to the 22 of Vincze *et al.* (1994), for example, and it also models a single mirror gimbal.

The model was programmed with Python and various test simulations were run with the model. The two main groups of simulations done are tests to determine the effect of parameter errors or target point position on the measured coordinates and tests to determine the effect of parameter fitting for a system.

The whole algorithm and process is first presented, after which the individual tests and results are discussed. Note that the simulations are done using numerical methods. Analytical methods are the other possibility and the results found with these simulations are compared with analytical results, as found in literature.

4.1 Simulation Process and Algorithm

There are three groups of variables in the simulations: measurement, system and gimbal parameter variables. The measurement variables are the length and two angles measured with each coordinate. The system variables are the TP (Target Point) coordinates and the gimbal parameter variables are the 10 parameters, which describe the gimbal, as defined in the kinematic model.

The principle of most of the simulations done is to start by defining a set of actual target point coordinates, then to determine the required measurements to obtain these target points, after which uncertainty or errors are added to simulate various effects. The simulations were done with the following virtual

experiment as basis: a target is mounted on a bridge type CMM and is then tracked, each TP is a coordinate where the CMM head stops and where the CMM coordinates (relative to the mirror centre of rotation) are stored along with the length and angle measurements of the tracker.

All measurements are influenced by geometric and random uncertainties. The geometric uncertainties of the gimbal is modelled and compensated for, with the parameters. The actual CMM TP's are however also subject to the CMM uncertainty and calibration accuracy. Yet for these simulations the CMM is assumed perfect, isolating the results to the gimbal performance. The CMM TP and the TP calculated from the measurements are compared and errors or uncertainty are included during the TP recalculation process with the virtual measurements. Here either a single uncertainty can be added to see the effect of a parameter or measurement error, or a general error can be added, with which the whole system response can be judged.

The required measurements are solved using a non-linear least squares optimizer (the same one was used for the multilateration), which minimizes the error between the required TP and the calculated TP. The same is done with the parameter fitting.

4.2 Simulations

For the simulation a TP set had to be generated. A quick test was done by plotting the generated points in a three dimensional plot area, which helped to ensure that the program worked appropriately, see Figure 4.1.

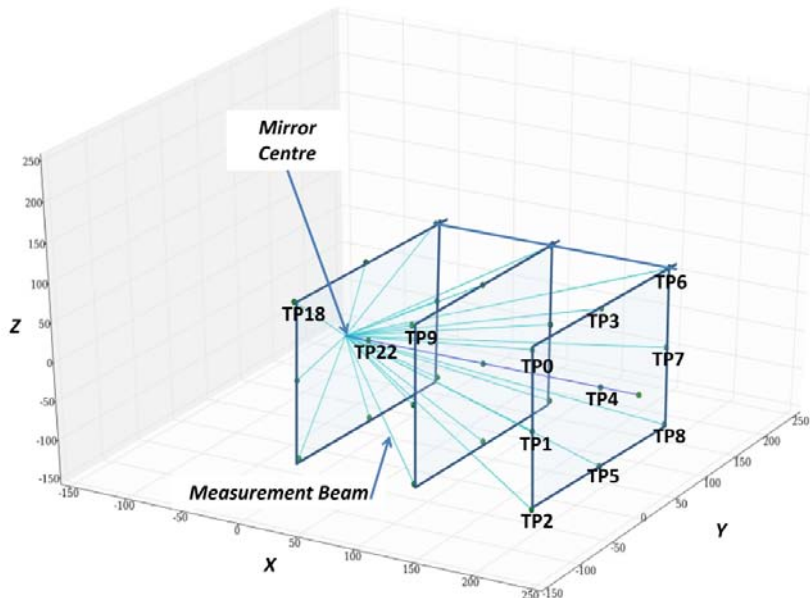


Figure 4.1: Example of a 25 Target Point (TP) Set

4.2.1 Effect of Parameter Errors

The effect of errors in the 10 parameters was investigated with a Monte Carlo analysis. Each parameter was perturbed: a small random error was added to its ideal value, while the rest remained unchanged. The TP set was then recalculated. This was done for each parameter, and repeated a sufficient number of times to ensure a convergent result. This test shows which parameter has the greatest effect, and where these effects dominate the uncertainty budget. This assumes that the parameters' effects on the final coordinates are sufficiently independent.

Figure 4.2 shows the total error caused by each parameter on average for all the coordinates. The noise added to the three angle parameters (α_1 , α_2 and $\Delta\theta_2$) were scaled down a 100 times and the noise added to the incident beam direction components (b_X and b_Y) were scaled down 50 times. The scaling was done so that the effect of all parameters can be presented in one graph. From this graph the three angle parameters, which determine the orthogonality of the two mirror axes (refer to Section 2.5) are seen to be the most critical.

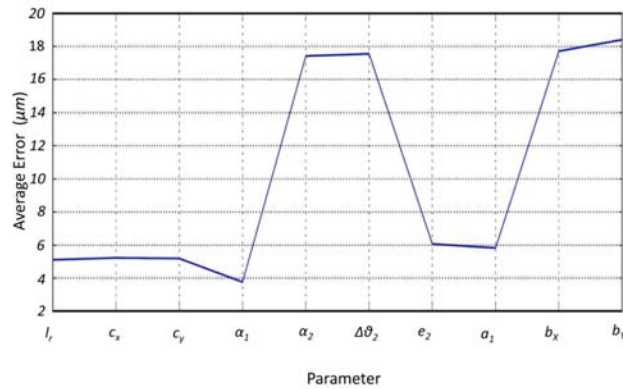


Figure 4.2: Total Individual Error per Parameter

The graphs in Figure 4.3 show the error caused by each parameter individually for each target point. This gives a representation of where in space each parameter has the greatest effect. It can be used for calibration planning by determining the best locations for target point placement. The target points are numbered, starting at the furthestmost point (see Figure 4.1). Point 22 is the closest to the origin and the error at this point is therefore the least.

An ellipsoid (see Figure 4.4a) depicting the covariance for each point was also generated from the above method with principle component analysis (Smith, 2002). These covariance ellipsoids show that greatest uncertainty area lies in a plane orthogonal to the beam direction (see Figure 4.4b). By considering Figure 4.2, it is clear that the reference length parameter does not have

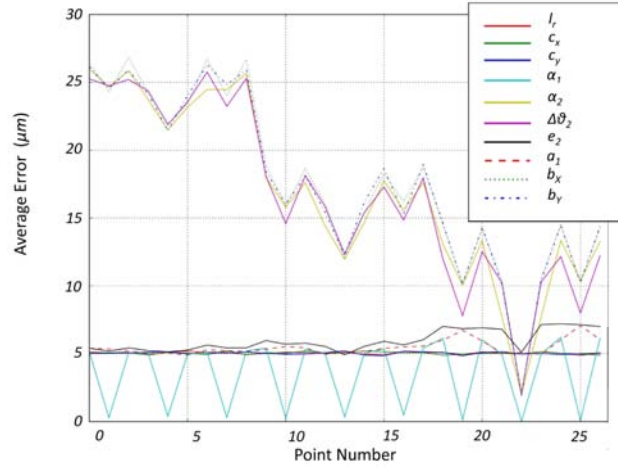


Figure 4.3: Total Individual Error per Parameter per Point

such a significant effect as the angles, which supports the idea that uncertainty in the direction of beam is less.

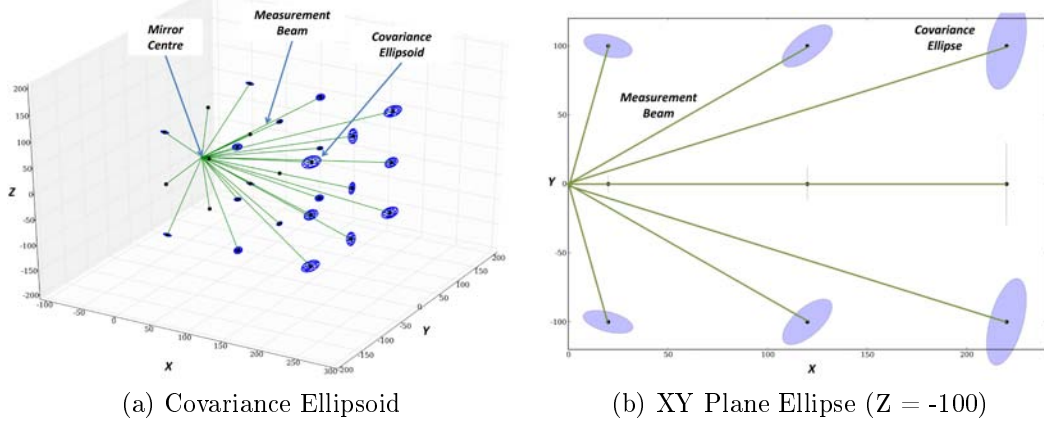


Figure 4.4: Principle Component Analysis

A target point spatial effect analysis simulation was done, in a similar fashion to the perturbation analysis. A general error was added to the all the parameters instead of a small error to a single parameter. The contour plots in Figure 4.5 show the result of this Monte Carlo analysis. The result is as expected, since the error increases away from the measurement origin, defined as the centre of rotation of the gimbal.

4.2.2 Calibration of Parameters

For an actual measurement, the system's parameters must first be identified. This can be done by measuring a target point set, determined by an external

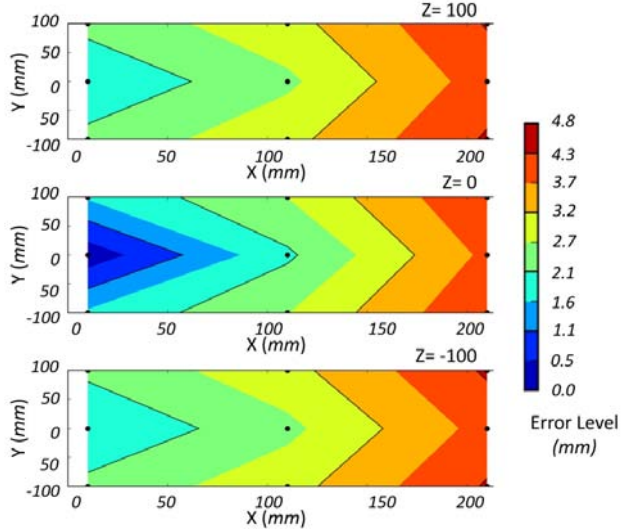


Figure 4.5: Error Contour

device such as a CMM. A parameter set can then be fitted to the measurements and the target points. Simulations for this process were done to see the fit accuracy and fit effect on the final measured coordinates.

A number of simulations were run and the fit was found to work satisfactory, by comparing the actual parameters with the fitted set. The fit approximately reduced the square root of the sum of the differences between actual and the fit parameters squared to 0.05 nm, on average for 2400 simulations, after an average random error of 0.180 mm was added, within 56 function calls in general. For the above mentioned parameter fit error, an average root sum squared error of 200 nm was found on the coordinates of the all target points.

4.2.3 Effect of Measurement Errors

The three measurement parameters were also perturbed, in a similar fashion as the gimbal parameters. The result is shown in Figure 4.6a. The two gimbal angles can be seen to contribute significantly more uncertainty than the length measurement. This again gives more support for using multilateration, since the effect of the angles is greater and the accuracy of their measurement is less than the interferometric length measurement.

4.2.4 Effect of Gimbal and Measurement Errors

The total uncertainty caused by either the gimbal errors or measurement errors were compared and is shown in Figure 4.6b. Here it is clear that the measurement error also has a much greater impact than the gimbal system parameters errors'.

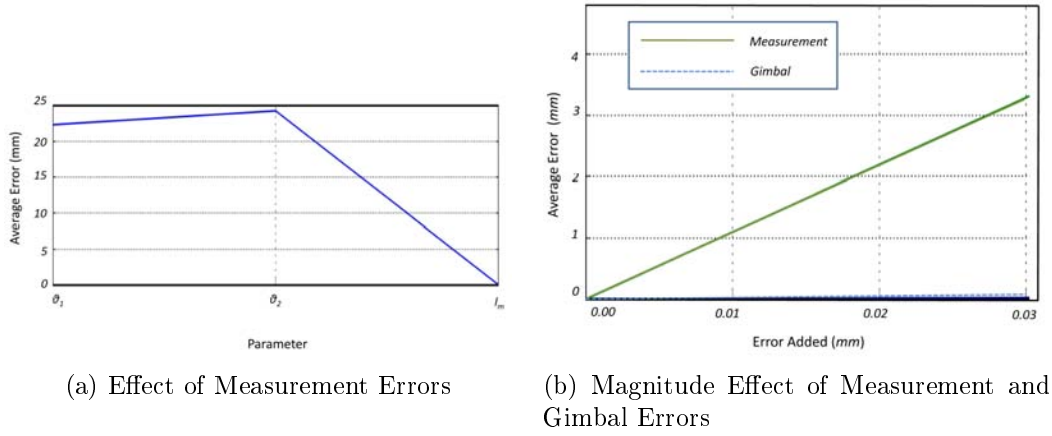


Figure 4.6: Measurement Error Analysis

4.3 Implications of the Simulation Results

The simulations give some interesting insights into the gimbal accuracy.

Not only does angle encoders, in principle, give less accurate results than the interferometric length measurement, but the angle measurements themselves cause a greater measurement uncertainty than the length measurement (see Figure 4.6a). A multilateration setup, which does not use angle measurements, will therefore have a clear accuracy advantage over the conventional trackers. Or the angles can only be used, as described by Zhuang *et al.* (2003), to update the parameters used for coordinate calibrations in real time. It is clear from the results that the measurement accuracy must be improved before it makes sense to improve the gimbal parameter accuracy, see Figure 4.6b. Yet again the greatest contributor to the measurement error is the angles of the gimbal mirror.

From the gimbal parameters perturbation it is seen that the axis orthogonality error has the greatest effect on measurement accuracy. These parameters can be determined through the fit algorithm. The accuracy of this fit, along with the reference CMM repeatability and accuracy, will however play a role in the parameter accuracy. These results compared well to the results presented in Zhuang and Roth (1995).

This kinematic model however is focused only on the gimbal, and does not consider the effects of errors in the target (for example non-parallel reflection, or centre of reflector offset) or of the PSD. For the next prototype work from Vincze *et al.* (1994), Teoh *et al.* (2002) and Lin *et al.* (2005) must also be considered.

Chapter 5

Sequential Multilateration Algorithm Tests

Sequential multilateration and SMR accuracy tests were performed at the NMISA in Pretoria, using their SMX 4000/4500 laser tracker. This chapter reports on the multilateration algorithm developed and its results.

5.1 Experiment Introduction

The main tools of the sequential multilateration experiments were a laser tracker, a bridge type CMM, *pucks* (place holders for the retroreflector) and the algorithm, which was used to fit the data to the expected model. Sequential multilateration implies that only one tracker station was used to measure the distance to each target point from at least four different positions.

Four experiments were performed and they can be grouped into two categories: setup one and setup two. In setup one pucks were mounted to the walls, floor or other objects, while with setup two a CMM was used to position the retroreflector. The laboratory environment in which these tests were performed were controlled with an air conditioning system.

5.1.1 Hardware Used

For all the experiments a commercial laser tracker was used and its performance is critical for the interpretation of the results. See the Table 2.1, in the literature review chapter for the tracker specifications.

The laser tracker is connected to a PC loaded with software, which is used to collect the desired data. The relative interferometric distance for each measurement point was obtained from the tracker program and imported to the multilateration algorithm.

A calibrated CMM was used for setup two, with a repeatability of $(2.4+3L)$ μm , where L is the distance moved in any of the CMM axes.

The *pucks* are round magnetic SMR¹ (Spherically Mounted Retroreflector) holders. These pucks were glued to surfaces (walls, floors etc) with a standard glue gun. A special puck was also used, which has a tapped hole in the middle, for mounting the puck to the CMM head, for the CMM tests.

5.2 The Algorithm

The multilateration algorithm was written in Python, using a special toolbox called *scipy.optimize*. The algorithm's goal is to determine both the target point and measurement stations' coordinates given all the length measurements from each tracker to each target point. The required inputs for this algorithm are presented first, after which the program flow and algorithm itself is presented. This algorithm is based on work presented mainly by Takatsuji *et al.* (1998), Takatsuji *et al.* (2000) and Zhang *et al.* (2005). Here system variables refers to the tracker station coordinates, target point coordinates and initial lengths for each tracker, while the measurement variables refer to the measured distance for each tracker.

The current program requires the following initial inputs:

1. Array of all the measured target coordinates (*XYZ*), from all the tracking stations. From this the measurement lengths are determined. One of the sets of target coordinates is also used for the initial values of target points. Note that this will most likely not be the same as the fit's target points, as the coordinate system of fit will differ from that of the laser tracker's coordinate system.
2. An array with the initial values of the system, or laser tracker positions.

5.2.1 Overall Program Flow

In Figure 5.1 the basic program flow is described. The first step is data initialization, the second is data fitting and the last step is output production. The data fitting is done with a non-linear least squares optimizer, which uses a modified version of the Levenberg-Marquardt algorithm. The function name is (*leastsq*) and it is found in the *SciPy* toolbox, in the *optimize* module, which utilises the *MINPACK* library.

5.2.2 The Levenberg-Marquardt Algorithm

The *scipy.optimize.leastsq* uses a modified version of the Levenberg-Marquardt solver, which is a damped Newton-Gaussian optimizer. It is an iterative method for minimizing the residual, and is defined as follows (Rao, 1996):

¹Also called a corner cube air path retroreflector.

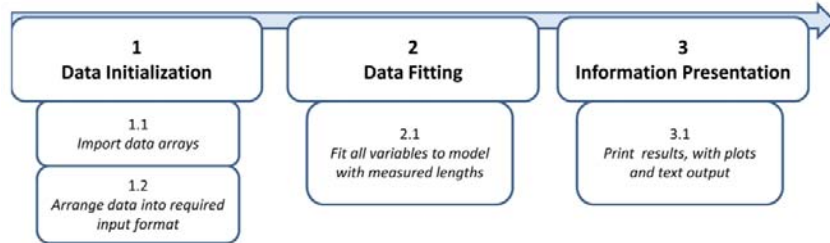


Figure 5.1: Overall Multilateration Algorithm Process

$$(J^T J + \mu I)\delta = J^T[f(x)] \quad \text{with } \mu \geq 0 \quad (5.2.1)$$

with the Jacobian (J), step δ , cost function $f(x)$ and damping factor μ , the algorithm minimizes the residual defined as:

$$F(x) = \frac{1}{2} \sum_{i=1}^m (f(x))^2 \quad (5.2.2)$$

5.3 The Experiments

Each of the four experiments was conducted with an unique purpose. The general purpose however of all the tests were to investigate the application of sequential multilateration for the measuring of a three dimensional coordinate (see Figure 2.17). The procedure for the measurements are explained first, after which the tests performed with setup one and setup two are presented.

The procedure for single measurement sessions starts with turning the laser tracker on (after doing the physical setup), which takes about 30 minutes and is required for the laser source to stabilise. The laser tracker software (on a PC connected to tracker) then runs a start up to routine, to check and calibrate the system (this also takes a few minutes).

The measurement can only begin after this start up sequence. This requires taking the SMR from the home position to the target position, without breaking the laser beam, since the tracker is a relative distance measurement device only. The tracker tracks the SMR automatically, as it is moved to a target point. At the target point a key is pressed on the PC and the measurement is taken and stored, after which the SMR can be moved to the next target point.

If the beam is broken the SMR must be returned to the home position and the tracker must then *home* itself again. During testing it was found that sufficient time must be allowed for this automatic homing process, as removing the SMR too quickly from the home position could cause measurement errors.

For a sequential multilateration test with the tracker it was required that all the target points had to be measured, after which the tracker had to be

moved to a new position. This had to be done at least four times. The tracker is a heavy device and requires two people to safely reposition it while it is activated. Changing the height of the tracker is a challenging exercise and the tracker had to be turned off to accomplish this. The tripod, on which the tracker is mounted, could only give about a 300 mm height difference.

5.4 Experiments with Setup One

For the first two experiments pucks were glued to the walls and floor of a room and the SMR was moved by hand to each new position, with at least two pucks on each of the three walls and also three on the floor of the room. This was done to help get an orientation of the target points, creating approximate *reference planes*, which could be used during results assessment. For each of the two experiments the laser tracker was moved to four different locations (three at the same height, and the last one higher) and at each position all the target points were measured.

For most of the measurements the SMR was placed in a puck. The SMR was also placed on two different types of length bars. One type was a cylindrical bar with magnetically tipped ends, each with hemispherical cavities for the SMR to be fixed into. The other type was a thin flat block made from a special material with a low coefficient of heat expansion, which had four placeholders each with three studs to place a SMR on.

5.4.1 First Experiment

The aim of this experiment was to see if the fit-algorithm worked. For this experiment all the tracker positions were relatively close to each other and there were 12 target points, requiring a total of 48 measurements.

5.4.1.1 Results

The design history of the optimization algorithm showed that it does reduce the initial error (absolute sum of the residual error vector) and that it also converges to a local minimum. This confirms that the algorithm finds a fit for the data (initial values and interferometric lengths) to the expected model. It converges within 7 iterations to an average fit error of $1.36 \mu\text{m}$ per measurement.

The error plot (Figure 5.2) illustrates the final residual term, i.e. the difference between the measured interferometric lengths and the calculated three dimensional distance from the determined tracker and target point coordinates.

The final error plot shows fit errors are in the magnitude of 5 to $10 \mu\text{m}$, which proves that the program finds a fit in the order of magnitude of the laser tracker repeatability. Sets of target measurements for each laser tracker

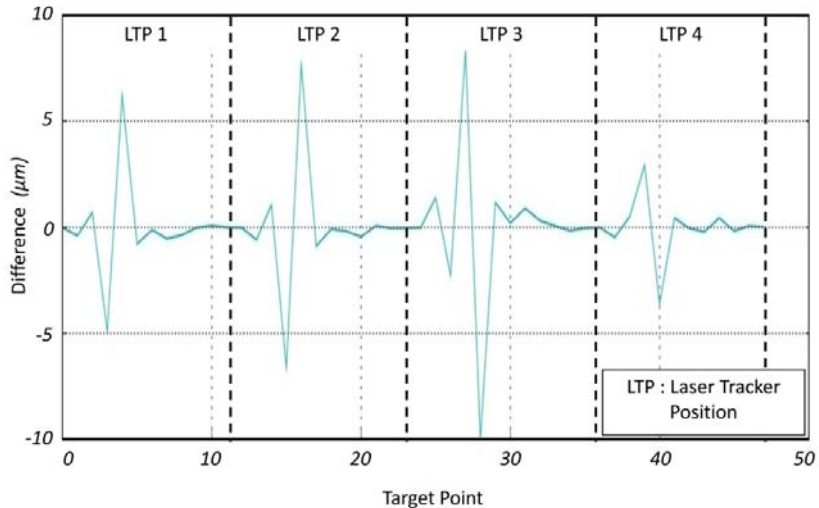


Figure 5.2: Final Error for the Fit (Experiment 1)

position can also be discerned, as for every 12 sequential target points the graph has the same form.

The repeated peaks are the target points where the length bar with magnetic ends was used. It seems reasonable to assume the reason for this is that by keeping the SMR in position by hand (as the magnets were not strong enough to keep the SMR in place) caused these errors. Holding the SMR can reduce the accuracy and repeatability of the measurement in three ways: (1) vibrations by the hand holding the SMR, (2) temperature related deformation of the SMR and (3) a reduction of repeatability due to human error by not holding the SMR at precisely the same position.

After the fit was accomplished, three dimensional distances between specific points were calculated. The tracker coordinate measurements were assumed perfect and compared with the calculated distance. For example: the distance between target point five and eight is according to the tracker software: 3061.105 mm, while with the fit it is found to be 3061.539 mm, which gives a difference of 433 μm . This however does not give an indication as to whether the fit is functioning or not, as the tracker is assumed perfect.

Length comparisons were further investigated by generating an additional plot where one point is selected as the reference point. All the distances between this point and the other points are calculated for the fit and compared to the tracker results, for a specific tracker position. After the calculation the maximum error was determined for that specific reference point.

Figure 5.3 shows this error for laser tracker position one and show that there is a big difference between the calculated distance of the tracker and fit. Since the tracker is accurate, it is not reasonable to assume that the fit improves the measurement results in the order of millimetres. There have to

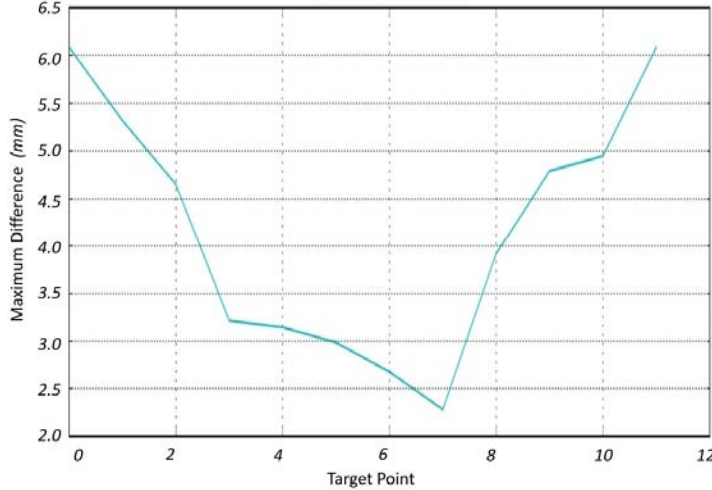


Figure 5.3: Three Dimensional Error Analysis (Tracker Position 1)

be another reason which explains this difference, as the fit self showed good results.

The amount by which the initial lengths were adjusted, which would in turn scale all the other lengths proportionally, were therefore also investigated. It was found that initial length parameters were adjusted in order of millimetres as well. This result stresses the precise determination of the home position is critical for the accuracy of the multilateration solution.

Lastly a plot of the actual solution in three dimensional space (in millimetres) was made to visualize to solution (Figure 5.4).

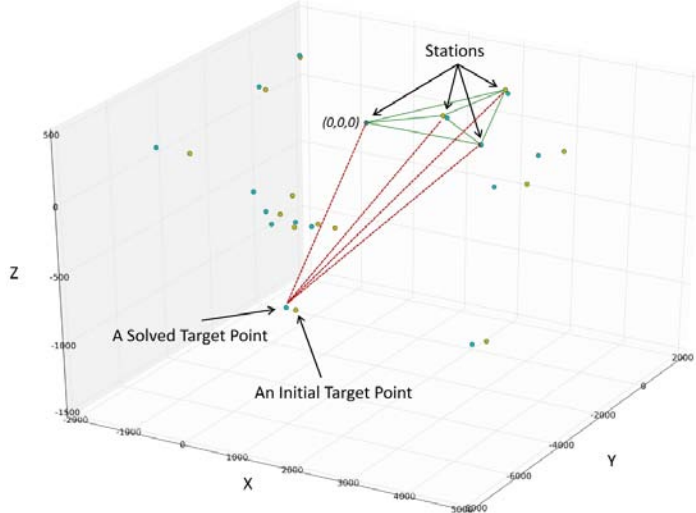


Figure 5.4: Three Dimensional Plot (Experiment 1)

5.4.2 Second Experiment

In the first experiment all the tracker positions were at the same side of the room, and only a tripod adjustment was used to obtain a height difference. For the second experiment however, the tracker positions were pushed into the corners of the room, as allowed by the *direct line of sight to all the target positions* restriction. For the last tracker position the tracker was placed on a table, to increase the height difference. For this experiment 14 target positions were chosen, requiring 56 measurements in total.

5.4.2.1 Results

The plots appeared similar to experiment one. The algorithm converged to an average $6.60 \mu\text{m}$ per point, which is in the same order of magnitude of experiment one ($1.36 \mu\text{m}$). The residual error plot is again shown (Figure 5.5) for this experiment.

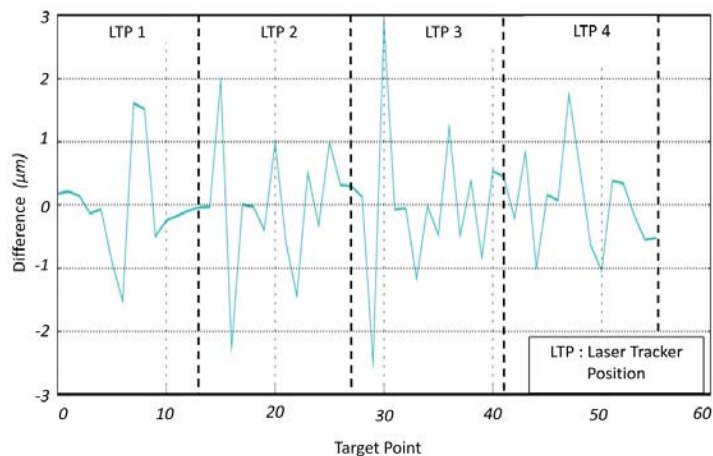


Figure 5.5: Final Error for the Fit (Experiment 2)

5.4.2.2 Difference Between Analytical and Numerical Jacobian

The least squares optimization function accepts either a numerical approximation for the Jacobian matrix of the system or a user defined analytical function. It was found that the algorithm with the analytical Jacobian in general converges within 8 function calls, while the numerical approximation method required 268. The analytical method also gave an more accurate fit, with a difference of $2.40 \times 10^{-7} \text{ mm}$ between the two methods' final total residual error.

5.4.3 Conclusion of Setup One

Experiments one and two showed that the algorithm does find a fit, however there are still unacceptably large errors when determining the actual three dimensional distance. A possible explanation has been given with respect to the initial lengths.

The influence of the method of Jacobian determination calculations has been discussed. It is suggested that the analytical method is always used, since it reduces the number of required iterations.

From the results the influence of repeatability of target points positioning in sequential multilateration becomes clear. The error with the magnetically tipped length bars showed that the SMR should be placed securely, without the need of holding it by hand.

5.5 Experiments with Setup Two

Instead of using pucks glued to a room and repositioning the SMR each time, a puck mounted to a CMM was used for this setup.

5.5.1 Third Experiment

The CMM was pre-programmed to move to different positions at which measurements were taken and the third experiment involved moving the CMM head to 20 predefined points, consisting of an array of five by four coordinates: five in the horizontal and vertical plane (YZ), with four points in each corner and one in the centre of the rectangle formed by the other four. These rectangular sets were copied in the horizontal direction (X) forming an ordered set of target points (see Figure 5.6).

The purpose of the experiment was to compare the tracker, fit and CMM distance of movement and investigate the performance of the fit against that of the tracker, by assuming that the CMM movement (repeatability) is perfect. The tracker was again moved to different positions to get an idea if tracker positions have an influence on the measurement results.

The trackers were positioned in six different positions, with only two positions at an equal higher height. However only the tripod was used to achieve the height difference. Any four of these six tracker positions could be used each time to determine the fit, provided they are not on the same height.

The tracker positions can be seen in Figure 5.7. Here LTP (Laser Tracker Position) for the fifth and sixth positions (LTP 5 and LTP 6) are the two which are raised higher than the rest. The red dashed line represents the *initial lengths*, as used by the program, while the black dots and lines represents the target coordinates and the path of the CMM head.

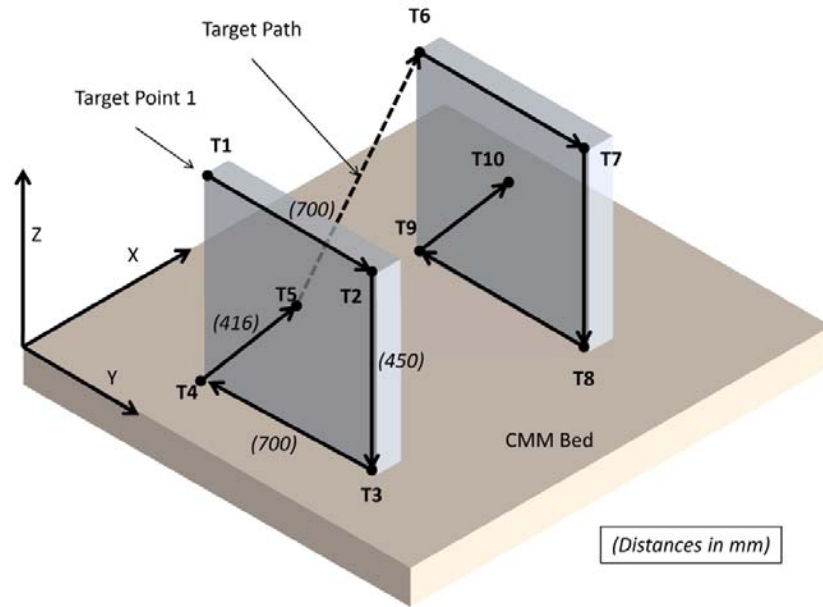


Figure 5.6: A Target Coordinate Set Created by CMM Movement

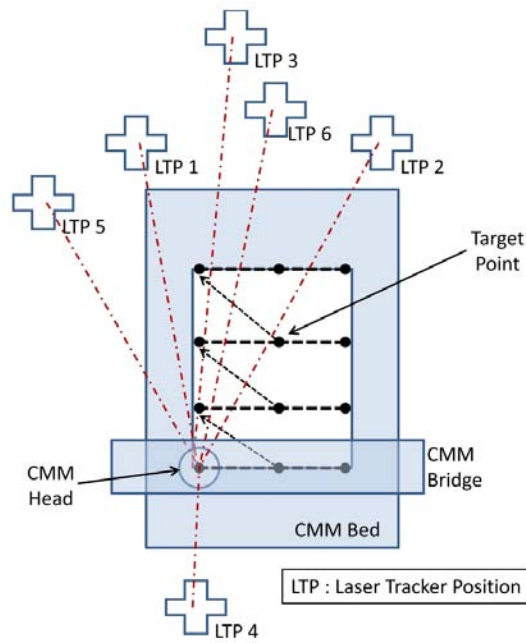


Figure 5.7: Setup for Experiment Three

5.5.1.1 Results

The error with the fit for setup two was similar to the ones for setup one, with the number of iterations and final residual sum in the range of 8 and 0.029093 mm or an average of $1.47\mu\text{m}$ per target measurement.

The three dimensional length error was again calculated and similar errors were found, as was with setup one. The focus of the experiment was to analyse the difference between the expected distances moved by the CMM head with all the different laser tracker positions and also with the fit. Five distances were selected for comparison purposes: two 700 mm horizontal distances, one 450 mm vertical distance, a diagonal from the fourth to the fifth point (for each set of five) and lastly the horizontal (X direction) distance between each set of five points' fourth target point.

The advantages of this setup is that the SMR is placed only once in the puck, which reduces any heat expansion and other human influence factors. The accuracy of the measurement is then only a factor of the laser tracker, CMM repeatability and the puck's ability hold the SMR fixed in precisely the same position.

Figure 5.8 shows an average for four different combinations of laser tracker positions. Similar results were obtained for other combinations as well. The error for the fit with the vertical 450 mm movement is the greatest. The fit for the 200 mm horizontal movement though is the best and is also more accurate than the tracker result.

The 200 mm (Figure 5.8e) is a great example of the desired result for the sequential multilateration, the other results still need to be investigated. Note that these tests assume that the CMM movement is perfectly repeatable.

5.5.2 Fourth Experiment

The last experiment involved several small tests and they are:

1. Repeated measurements of the first tracker position in the third experiment (repeated three times).
2. A test to check the influence of the movement of the CMM bridge on a measurement while the SMR is placed on the CMM.
3. A test to check the SMR, and the repeatability of it, at different angles about the laser axis.
4. A quick test was done by keeping the SMR completely stationary in a puck while taking measurements.

The purpose of experiment four was to get more data with this specific setup and to investigate the repeatability of the laser tracker (including the SMR and puck) along with the CMM setup.

5.5.2.1 Results

The repeated measurements for the first tracker position is shown in Figure 5.9. The results are for 21 points, which includes a last point, where the CMM

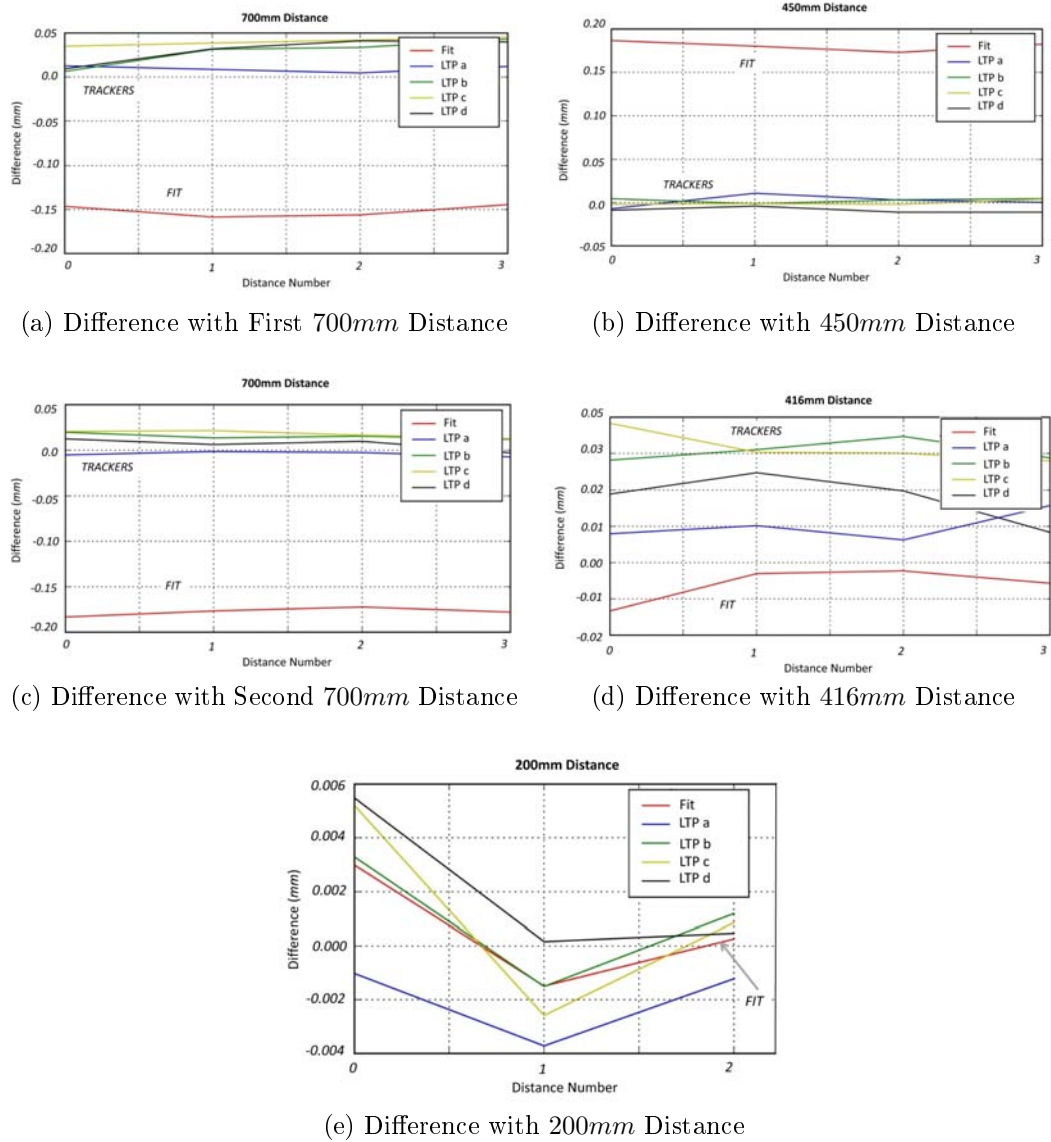


Figure 5.8: Example of the Average Error for the Fit and Laser Trackers for the Five Distances

head was returned to its starting position. This plot shows the tracker and CMM setup repeatability to be in the order of micrometers. It also shows that the repeatability increases with a decrease of distance, which agrees with the Monte Carlo kinematic model prediction (see Figures 4.5 and 4.3).

The tracker is not fixed to the CMM and is not swayed by the CMM movement, unlike the CMM bed, which is. A test was done by placing a puck (with an SMR in it) on the CMM bed and then taking repeated measurements (11 in total) while moving the bridge to the two extremes of its movement ability, in the X direction. A displacement of about 30 μm were found, while

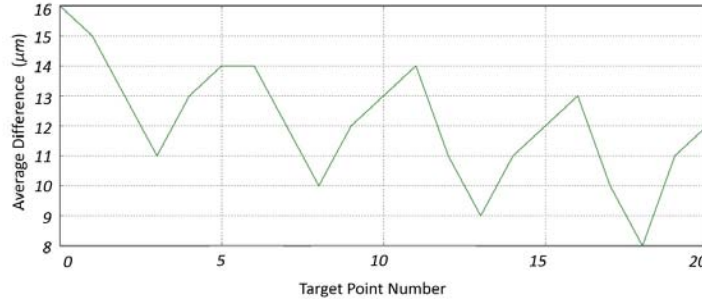


Figure 5.9: Repeated Measurements for Tracker Position One

the puck and tracker are seemingly completely still.

A test was also done by placing the SMR on a tripod a certain distance away. Measurements were taken by rotating the SMR about the laser axis and also by rotating it about the axis perpendicular to the laser beam axis. Repeated measurements were also taken.

SMR Repeatability					
Rotation relative to laser axis		X*	Y*	Z*	Length*
Around Axis					
Minimum		3245.100	55.855	-40.162	3245.829
Maximum		3245.115	55.873	-40.140	3245.844
Difference		0.015	0.018	0.022	0.015
Perpendicular to Axis					
Minimum	3243.401	55.036	-39.776	3244.112	
Maximum	3243.411	55.059	-39.758	3244.122	
Difference	0.010	0.023	0.018	0.010	
No Rotation					
At 3244 mm					
Minimum		3243.400	55.062	-39.769	3244.111
Maximum		3243.407	55.067	-39.754	3244.118
Difference		0.007	0.005	0.015	0.007

* All dimensions in mm

Table 5.1: SMR Tests

The SMR rotation tests shows errors, which are greater than the CMM repeatability, by rotating the SMR in the puck, (Table 5.1). The difference between the maximum and minimum values were however less than $25 \mu\text{m}$, as specified by the SMR calibration requirement. Eight measurements were taking for the rotation about the laser axis and four for the rotation perpendicular to the laser axis.

A quick tracker repeatability test was also performed by just taking several sequential measurements, without any movements or rotations. This test showed (Table 5.1) that the tracker interferometric length repeatability, as

setup in the lab, was less than $10 \mu\text{m}$, which is in the same range as the CMM repeatability.

5.6 Discussion of Results

As stated, four experiments were performed. The first two experiments' aim was to check if the algorithm works and to get an idea of the whole operation methodology. From the tests it was found that the algorithm does find a fit, which reduces the residual error vector satisfactorily.

In the algorithm, room is made for the *initial lengths*, and this is very important to note. The LTS gives an interferometric measurement, which necessitates knowledge of a reference length. The initial lengths were forced into the algorithm by taking the first measurement of each tracker as the reference and then deducting it from all the other measurements, for that specific tracker. These lengths are then exposed in the algorithm as variables, and are modified along with the other variables until a suitable fit is found. The initial lengths then acts as a scale for all the other measurements. Note that a suitable fit is found, but if these initial lengths are changed in the order of magnitude of millimetres, then it need to be asked whether the system still fits to the actual setup.

A promising result was found by the fifth distance with the CMM setup. The distance was calculated to be more accurate than all the laser tracker measurements, assuming that the CMM repeatability is perfect.

However, since the CMM uncertainty is not taken into consideration, nor the laser tracker errors, no final conclusion based on these experiments can be made with regards to the success or failure of the multilateration concept.

Chapter 6

Conclusion

The introduction identified three specific outcomes for this thesis (for NMISA): (1) to provide a starting point for LTS development for NMISA, (2) to build and test a prototype laser tracker and also (3) to develop a sequential multilateration algorithm for NMISA. All three of these outcomes have been successfully accomplished with this project.

These outcomes could only be accomplished after experience in the following areas were gained: electronic design (amplifier and microcontroller electronics), mechatronic design (ADC, microstepping stepper motor control, sensor integration and control systems), multilateration, optics (interferometry and PSDs), programming design¹ (microcontroller programming, GUI, communication between microcontroller and GUI), kinematic modelling as well as some miscellaneous tools and metrology concepts.

The above is mentioned to place the scope of the project in context, as well as give guidance as to some of the required skill areas for the further development of a multilateration laser tracking system.

Firstly (for outcome number (1)), the introduction and literature review of this report pointed out that dimensional metrology is critically important for an industrial nation and that currently, one of the most accurate system for three dimensional coordinate measurements is a multilateration type laser tracking system, which uses heterodyne fringe counting interferometry. The introduction chapter also placed the project into financial context for the NMISA, by referring to the current need of CMM calibrations in the automobile industry and the metre traceability chain. Furthermore, the report identifies the various components of such a system, work done previously, the operational principles and the various uncertainty sources.

Kinematic modelling of a gimbal type tracker station was done, based on a model found in literature (see Section 2.5). The model used defines the system with only 10 parameters, however this does not include target and PSD error's. The model was used to both analyse the effect of identified parameters and

¹No details on the programming were reported on, yet it did require a lot of project time.

to see if the parameters could be solved or fitted to a virtual tracker through simulation studies.

For this system the critical deadpath error was identified, as the interferometry system assumes that the distance between the mirror and the source remains constant, i.e. the change in the length measured is only due to the change of distance between the mirror and target point. It was shown that gimbal axes misalignment and mirror offset causes this error, with the misalignment being the biggest contributor, according to the results of the kinematic model.

The results of the model showed however that the two measured angles for each target point have the greatest impact on the system accuracy. This further motivates the use of multilateration. This model showed that the measurement error increases, in general, along with the radial distance away from the centre of rotation of the beam steering mechanism and that greater measurement uncertainty exist in the area perpendicular to the beam direction, incident on the target.

Secondly, a prototype tracker station was developed and tested. Tests showed that the system can track a target, be it slowly² moving in a space about 300 mm away from the tracker in a volume of at least $200 \times 200 \times 200$ mm³. It was decided that this is sufficient evidence for the working of the prototype station. Testing of the prototype showed that fast direction change, very small step size and accurate positioning are the critical parameters for the beam steering mechanism.

Finally, for the third project outcome, a multilateration algorithm was developed and tested. The algorithm found a fit for the given measured lengths. Sequential multilateration tests were also performed with a commercial laser tracker by mounting a target onto a CMM head and repositioning the laser tracker.

These tests however assumed that the CMM movement is perfect and completely repeatable and did not take the tracker uncertainties into consideration. Still, the tests did show that the current laser tracking technology is very accurate and that a multilateration technique can possibly improve this accuracy.

This project therefore satisfies the outcomes for NMISA. For the international field of three dimensional metrology, with a multilateration based laser tracking system, this project showed that a Python based (open source) algorithm can be used for the multilateration algorithm. The effect of the home position determination was also shown as critical. Furthermore, it also detailed the effects of the various parameters on measurement uncertainty.

²The exact speed was not measured. The operational speed of a LTS is critical, yet was not defined as an specification for this project, since the goal was only a functional tracker station

Appendices

Appendix A

Mathematics and Other Kinematic Models

A.1 Note on Homogeneous Transformations

Homogeneous coordinates are used in robotics and computer graphics. For example a robotic arm can be modelled in two dimensions with each link of the arm having its own frame or coordinate system. The whole arm also has its own world coordinate system. Each local frame which represents the orientation of each link can be represented in the world coordinate system through transformations (Poole, 2006).

A point in 2D is rotated θ degrees about the origin with the following 2×2 transformation rotation matrix:

$$\begin{bmatrix} \cos\theta & -\sin\theta \\ \sin\theta & \cos\theta \end{bmatrix} \quad (\text{A.1.1})$$

and it is translated with distance a and b , with a 2×1 transformation matrix:

$$\mathbf{V} = \begin{bmatrix} a \\ b \end{bmatrix} \quad (\text{A.1.2})$$

The translated point coordinates then becomes:

$$T(\mathbf{X}) = \mathbf{X} + \mathbf{V} \quad (\text{A.1.3})$$

$$T(\mathbf{X}) = \begin{bmatrix} x + a \\ y + b \end{bmatrix} \quad (\text{A.1.4})$$

Where $T(X)$ is a non-linear transformation (the same can be done for the rotation). The transformation is non-linear though, as $T(\mathbf{0})! = \mathbf{0}$. This is why homogeneous coordinates are used: it linearizes the transformations by defining the 2D point coordinates as:

$$\begin{bmatrix} x \\ y \\ 1 \end{bmatrix} \quad (\text{A.1.5})$$

The same translation as above is then rather done with:

$$\begin{bmatrix} 1 & 0 & a \\ 0 & 1 & b \\ 0 & 0 & 1 \end{bmatrix} \begin{bmatrix} x \\ y \\ 1 \end{bmatrix} = \begin{bmatrix} x+a \\ y+b \\ 1 \end{bmatrix} \quad (\text{A.1.6})$$

The rotation is now accomplished with:

$$\begin{bmatrix} \cos\theta & -\sin\theta & 0 \\ \sin\theta & \cos\theta & 0 \\ 0 & 0 & 1 \end{bmatrix} \begin{bmatrix} x \\ y \\ 1 \end{bmatrix} = \begin{bmatrix} x\cos\theta - y\sin\theta \\ x\sin\theta + y\cos\theta \\ 1 \end{bmatrix} \quad (\text{A.1.7})$$

For three dimensional coordinate systems the homogeneous coordinates are given by 4×4 matrices. A notable use of these transformations is the change of basis. If there is one point, which is known, in two coordinate systems (with coincident origins, but different orientations) that point can then be defined in:

$$\mathbf{P} = [a \ b \ c] \begin{bmatrix} 1 & 0 & 0 \\ 0 & 1 & 0 \\ 0 & 0 & 1 \end{bmatrix} \quad (\text{in frame 2}) \quad (\text{A.1.8})$$

$$\mathbf{P} = [a \ b \ c] \begin{bmatrix} u_x & v_x & w_x \\ u_y & v_y & w_y \\ u_z & v_z & w_z \end{bmatrix} \quad (\text{in frame 1}) \quad (\text{A.1.9})$$

$$\begin{bmatrix} x \\ y \\ z \\ 1 \end{bmatrix} = \begin{bmatrix} u_x & v_x & w_x & 0 \\ u_y & v_y & w_y & 0 \\ u_z & v_z & w_z & 0 \\ 0 & 0 & 0 & 1 \end{bmatrix} \begin{bmatrix} a \\ b \\ c \\ 1 \end{bmatrix} \quad (\text{homogeneous}) \quad (\text{A.1.10})$$

where $\{a,b,c\}$ and $\{u,v,w\}$ are unit vectors for the specific frame. From this it can be seen that the elements of the top left 3×3 homogeneous coordinate matrix is the basis vectors of the local frame expressed in the coordinates of the new frame.

Two definitions of homogeneous transformation matrices are used in the following text, a translation ($\text{Trans}()$) and a rotation ($\text{Rot}()$):

$$\text{Trans}(a, b, c) = \begin{bmatrix} 1 & 0 & 0 & a \\ 0 & 1 & 0 & b \\ 0 & 0 & 1 & c \\ 0 & 0 & 0 & 1 \end{bmatrix} \quad (\text{A.1.11})$$

(A.1.12)

$$\text{Rot}(z, \theta) = \begin{bmatrix} \cos\theta & -\sin\theta & 0 & 0 \\ \sin\theta & \cos\theta & 0 & 0 \\ 0 & 0 & 1 & 0 \\ 0 & 0 & 0 & 1 \end{bmatrix} \quad (\text{A.1.13})$$

(A.1.14)

$$Rot(x, \theta) = \begin{bmatrix} 1 & 0 & 0 & 0 \\ 0 & \cos\theta & -\sin\theta & 0 \\ 0 & \sin\theta & \cos\theta & 0 \\ 0 & 0 & 0 & 1 \end{bmatrix} \quad (A.1.15)$$

(A.1.16)

$$Rot(y, \theta) = \begin{bmatrix} \cos\theta & 0 & \sin\theta & 0 \\ 0 & 1 & 0 & 0 \\ -\sin\theta & 0 & \cos\theta & 0 \\ 0 & 0 & 0 & 1 \end{bmatrix} \quad (A.1.17)$$

A.2 Kinematic Modeling: Other Models

A.2.1 Geometric Model of a LTS

The geometric model of a LTS by Vincze *et al.* (1994) is the first model to be discussed. The system is modelled by attaching a coordinate system (or frame) rigidly to each part. By doing this, seven coordinate frames are needed for the various beam incident points from the laser beam source to the target centre and six transformations are used to relate these frames (this section is taken based on Vincze *et al.* (1994)).

The entire system transformation (\mathbf{A}_0^6), from first frame to the target centre, is:

$$\mathbf{A}_0^6 = \mathbf{A}_0^4 \mathbf{A}_4^5 \mathbf{A}_5^6$$

with \mathbf{A}_0^4 calculated from \mathbf{A}_0^1 and \mathbf{A}_0^3 , where:

$$\mathbf{A}_0^3 = \mathbf{A}_0^1 \mathbf{A}_1^2 \mathbf{A}_2^3$$

The first transformation positions the vertical axis of the gimbal joint relative to the laser beam, with three rotational and translational parameters:

$$\mathbf{A}_0^1 = Trans(\Delta a_1, \Delta b_1, \Delta d_1) Rot(z, \Delta\theta_1) Rot(y, \Delta\beta_1) Rot(x, \Delta\alpha_1)$$

The second transformation relates the two axes of the gimbal joint,

$$\mathbf{A}_1^2 = Rot(z, q_2 + \Delta\theta_2) Trans(\Delta a_2, 0, \Delta d_2) Rot(x, \Delta\alpha_2)$$

with q_2 the angle of the vertical axis.

The third transformation places the plane mirror (assumed perfectly flat) relative to the horizontal axis.

$$\mathbf{A}_2^3 = Rot(z, q_3 + \Delta\theta_3) Trans(\Delta a_3, 0, 0) Rot(y, \Delta\beta_3)$$

where q_3 is angle of the horizontal axis.

The fourth transformation mirrors the beam and uses the interferometric length to calculate a point on the target base plane. This is a translation a in the direction of the laser beam to mirror surface:

$$\mathbf{A}_0^3 \cdot Trans(0, b, d) \cdot (0, 0, 0, 1)^T = (a, 0, 0, 1)$$

where b and d is the intersection point in the mirror plane. The translation is found by solving a .

The fifth transformation is used to reach a point on the base plane of the target with:

$$\mathbf{A}_0^4 = Trans(a, 0, 0) Rot(k, 2 \cdot \phi) Trans(q_4 + \Delta q_4 - a, 0, 0)$$

where k is the normal of the laser beam direction of coordinate system 0, as taken from \mathbf{A}_0^1 , and the normal of normal of mirror surface from \mathbf{A}_0^3 , ϕ is the angle between these two vectors, and the interferometric length (Δq) with an offset parameter (Δq_4).

The last two transformations translate the base plane to the correct base point of the target, with two error tracking signals (q_5, q_6 in direction of y, z respectfully), as detected by the PSD:

$$\mathbf{A}_4^5 = Trans(0, \Delta d_5 + d_{5y} \cdot q_5, d_{5z} \cdot q_5)$$

$$\mathbf{A}_4^6 = Trans(0, d_{6y} \cdot q_6, \Delta d_6 + d_{6z} \cdot q_6)$$

with offset parameters ($\Delta d_5, \Delta d_6$) and scaling parameters ($d_{5y}, d_{5z}, d_{6y}, d_{6z}$).

This model describes a LTS with 22 parameters and includes the PSD offsets in the target point calculation.

A.2.2 Alternative Single Beam Model

Teoh *et al.* (2002) uses the same technique as described by Vincze *et al.* (1994). In this model an error value is added to the ideal parameter value for geometric error analysis, with:

$$p = p_{ideal} + \Delta p$$

In this model the gimbal axis is mechanically decoupled and three mirrors are used in the tracking head: one stationary one to direct the beam to the next one, which only rotates about the vertical axis and reflects the beam to the third mirror, which rotates about the horizontal axis and point the beam toward the retroreflector (this section is taken based on Teoh *et al.* (2002)).

If it is assumed that all geometric errors are compensated for in the calculations, the model is given as:

$${}^W \mathbf{A}_R = \mathbf{A}_0 \mathbf{A}_1 \mathbf{A}_2 \mathbf{A}_3 \mathbf{A}_R \quad (\text{A.2.1})$$

where

$$\mathbf{A}_o = Trans(x_{X0}, y_{Y0}, z_{Z0}) \quad (A.2.2)$$

$$\mathbf{A}_1 = Trans(0, 0, a_{Z1})Rot(0, 90^\circ, 0)Rot(0, 90^\circ, 0) \quad (A.2.3)$$

$$\mathbf{A}_2 = Trans(0, 0, a_{Z2})Rot(90^\circ, 0, 0)Rot(0, -q_1, 0) \quad (A.2.4)$$

$$\mathbf{A}_3 = Trans(0, 0, a_{Z3})Rot(90^\circ, 0, 0)Rot(0, q_2, 0) \quad (A.2.5)$$

$$\mathbf{A}_R = Trans(0, 0, a_{ZR})Trans(a_{XR}, 0, 0)Trans(0, a_{YR}, 0) \quad (A.2.6)$$

Here a_{XR} and a_{YR} are determined from the PSD sensor as deviations from the centre of the retroreflector as:

$$a_{XR} = \frac{X_{PSD}}{2} \quad a_{YR} = \frac{Y_{PSD}}{2} \quad (A.2.7)$$

And a_{ZR} is the distance between the mirror and retroreflector, defined as:

$$a_{ZR} = l_{reading} - l_{mirror} \quad (A.2.8)$$

where $l_{reading}$ is the current measurement and l_{mirror} is the distance between the laser head and mirror. The target position can be determined from the ${}^W\mathbf{A}_R$ transformation as:

$$x = -\sin(q_1)a_{XR} + \cos(q_1) + a_{Z2} + a_{X0} \quad (A.2.9)$$

$$y = \sin(q_1)\cos(q_2)a_{XR} + \sin(q_1)\sin(q_2)a_{ZR} + \cos(q_1)a_{YR} + \quad (A.2.10)$$

$$+ \cos(q_1)a_{ZR} + a_{Y0} \quad (A.2.11)$$

$$z = -\cos(q_1)\cos(q_2)a_{XR} - \cos(q_1)\sin(q_2)a_{ZR} + \quad (A.2.12)$$

$$+ \sin(q_1)a_{YR} + \sin(q_1)a_{Z3} + a_{Z1} + a_{Z0} \quad (A.2.13)$$

with a_{Z0} , a_{Y0} , a_{X0} the x , y , and z coordinates of the laser tracking head and a_{Z1} , a_{Z2} , a_{Z3} the distances between the various tracking head mirrors.

A.2.3 Multiple Beam Model

A multiple beam model is reviewed next. In Zhuang *et al.* (2003) relatively less accurate gimbal angle measurements are also incorporated for the self calibration. It is then shown that by using these angular measurements to predict the mirror centre offset, that large errors can be avoided (this section is taken from Zhuang *et al.* (2003)).

A.2.3.1 Modelling a Ideal Three-Beam LTS

The three beam LTS can be modelled, without any mirror centre offset or gimbal axis misalignment, as follows (Zhuang *et al.*, 1992):

$$(\mathbf{r}_p - \mathbf{r}_k) \cdot (\mathbf{r}_p - \mathbf{r}_k) = l_k^2, \quad k = 1, 2, 3 \quad (\text{A.2.14})$$

where \mathbf{r}_p and \mathbf{r}_k is the coordinates of the target point centre and k 'th tracker station in the world coordinate system, respectfully. The distance between these two points are l_k for the k 'th tracker. The target position is the intersection point of spheres with their centres at each tracker mirror centre and with radius equal to the length of the relative measured distance. There are multiple points of intersection, but only one solution will make practical sense.

If the distances are known, as well as the point of laser beam incidence on the tracking mirror, the target point coordinates can be calculated. For three tracker stations let A , B and C be the rotation centre of the each tracker mirror with A the origin of the world coordinate system. With B on the x axis and C on xy -plane of the world coordinate system, the coordinates are solved as:

$$r_{p,x} = \frac{(l_1^2 - l_2^2 + r_{2,x}^2)}{2r_{2,x}} \quad (\text{A.2.15})$$

$$r_{p,y} = \frac{(l_1^2 - l_3^2 + \mathbf{r}_3 \cdot \mathbf{r}_3 - 2r_{p,x}r_{3,x})}{2r_{3,y}} \quad (\text{A.2.16})$$

$$r_{p,z} = \pm (l_1^2 - r_{p,x}^2 - r_{p,y}^2)^{0.5} \quad (\text{A.2.17})$$

A.2.3.2 Incorporating Angle and Length Measurements

For a three tracker LTS, assign to each mirror centre as an origin to a frame: $\{1\}$, $\{2\}$ and $\{3\}$. Let $\{1\}$ be the world coordinate system. Then assign the actual point of laser incidence on the tracker mirror for each tracker as: A , B and C with frames $\{A\}$, $\{B\}$ and $\{C\}$, but with each axis parallel to its tracker base frame, e.g. x -axis of frame $\{A\}$ parallel to frame $\{1\}$ x -axis.

Now, to use the model described above, place a frame $\{A'\}$ with its origin at point A , with point B on its x -axis, and point C in its xy -plane. Let c_k be the coordinates of laser beam incidence for the k 'th tracker, which is dependent on 10 parameters of a single beam laser tracker, as well as the distance and angle measurements.

The target coordinates can be determined if the following is known: c_k , the transformation matrix from $\{k\}$ to $\{1\}$ and the measured distances. The target is now determined by:

$${}^1\mathbf{r} = {}^1\mathbf{T}_A {}^A\mathbf{T}_{A'} \mathbf{r} \quad (\text{A.2.18})$$

with

$${}^A\mathbf{T}_{A'} = \begin{bmatrix} {}^A\mathbf{R}_{A'} & 0 \\ 0 & 1 \end{bmatrix} \quad (\text{A.2.19})$$

$${}^1\mathbf{T}_A = \begin{bmatrix} I & c_1 \\ 0 & 1 \end{bmatrix} \quad (\text{A.2.20})$$

$$r_x = \frac{(l_1^2 - l_2^2 + {}^{A'}c_{2,x}^2)}{2 {}^{A'}c_{2,x}} \quad (\text{A.2.21})$$

$$r_y = \frac{(l_1^2 - l_3^2 + {}^{A'}\mathbf{c}_3 \cdot {}^{A'}\mathbf{c}_3 - 2r_x {}^{A'}c_{3,x})}{2 {}^{A'}c_{3,y}} \quad (\text{A.2.22})$$

$$r_z = \pm (l_1^2 - r_x^2 - r_y^2)^{0.5} \quad (\text{A.2.23})$$

The beam incidence point is transformed to the $\{\mathbf{A}'\}$ frame as follows:

$${}^{A'}\mathbf{c}_2 = {}^{A'}\mathbf{R}_A {}^A\mathbf{c}_2 \quad (\text{A.2.24})$$

$${}^{A'}\mathbf{c}_3 = {}^{A'}\mathbf{R}_A {}^A\mathbf{c}_3 \quad (\text{A.2.25})$$

where

$${}^{A'}\mathbf{R}_A = \{\mathbf{x}^T, \mathbf{y}^T, \mathbf{z}^T\} \quad (\text{A.2.26})$$

$$\mathbf{x}^T = \begin{pmatrix} \| {}^A\mathbf{c}_2 \| \\ 0 \\ 0 \end{pmatrix} \quad (\text{A.2.27})$$

$$\mathbf{z}^T = \frac{{}^A\mathbf{c}_2 \times {}^A\mathbf{c}_3}{\| {}^A\mathbf{c}_2 \times {}^A\mathbf{c}_3 \|} \quad (\text{A.2.28})$$

$$\mathbf{y}^T = \mathbf{z}^T \times \mathbf{x}^T \quad (\text{A.2.29})$$

$${}^A\mathbf{c}_k = {}^A\mathbf{T}_1 {}^1\mathbf{T}_k \mathbf{c}_k, k = 2, 3 \quad (\text{A.2.30})$$

This model in Zhuang *et al.* (2003) is then used to do a sensitivity analysis. This is done by perturbing eq. A.2.14.

Appendix B

Summary of All Relevant Datasheets

Datasheet List			
Manufacturer	Component	Supplier	Name
Hamamatsu	SiPIN Photodiodes http://sales.hamamatsu.com/assets/pdf/parts_S/S5980_etc.pdf	N/A	S5981
Linear	Operational Amplifier http://docs-europe.electrocomponents.com/webdocs/05aa/0900766b805aab5b.pdf	RS Components	LT1490
Mantech	Geared DC Motor http://www.mantech.co.za/ProductInfo.aspx?Item=14M0846	Mantech	QJT-12JS
McLennan	Geared Stepper Motor http://docs-europe.electrocomponents.com/webdocs/0030/0900766b800305e5.pdf	RS Components	P542-M48
Microchip	Microcontroller http://www.microchip.com/wwwproducts/Devices.aspx?dDocName=en010337	Avnet	dsPIC30f4011
Microchip	12bit ADC http://www.microchip.com/wwwproducts/Devices.aspx?dDocName=en010533	Avnet	MCP3204
National	LD 5V Power Regulator http://www.mantech.co.za/ProductInfo.aspx?Item=LM2940CT05	Mantech	LM2940
NSK	Thrust Bearing http://docs-europe.electrocomponents.com/webdocs/0093/0900766b80093233.pdf	RS Components	Thrust bearing, single direction
ST	Stepper Motor Controller http://www.mantech.co.za/ProductInfo.aspx?Item=L297	Mantech	L297
ST	Dual Full Bridge Driver http://www.mantech.co.za/ProductInfo.aspx?Item=35M1867	Mantech	L298
TI	Positive to Negative Converter http://focus.ti.com/docs/prod/folders/print/ptn04050a.html	TI	PTN04050a

Table B.1: Summary of All Relevant Datasheets

Appendix C

PCB Schematics

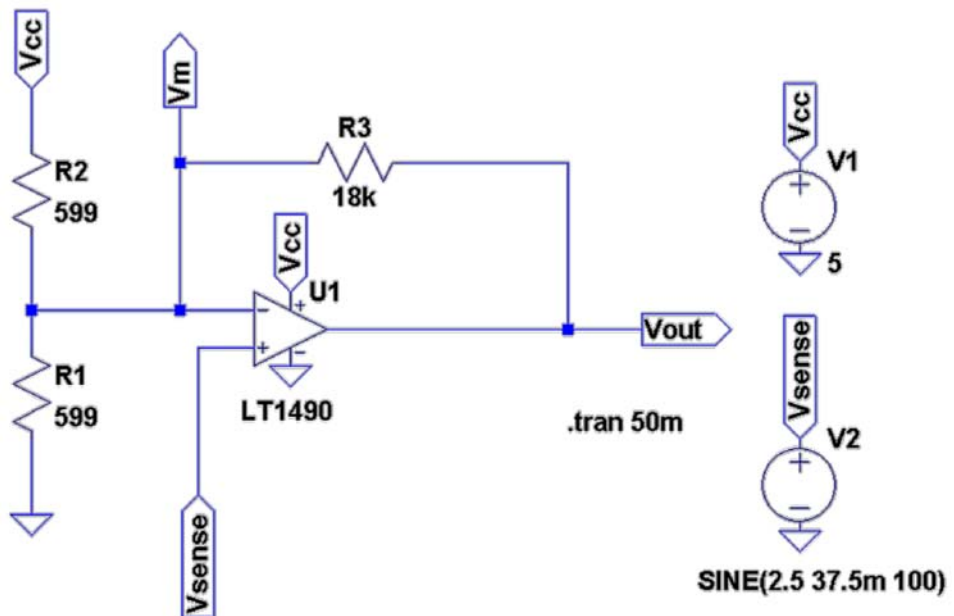


Figure C.1: Amplification Prototype Schematic 1 and 2

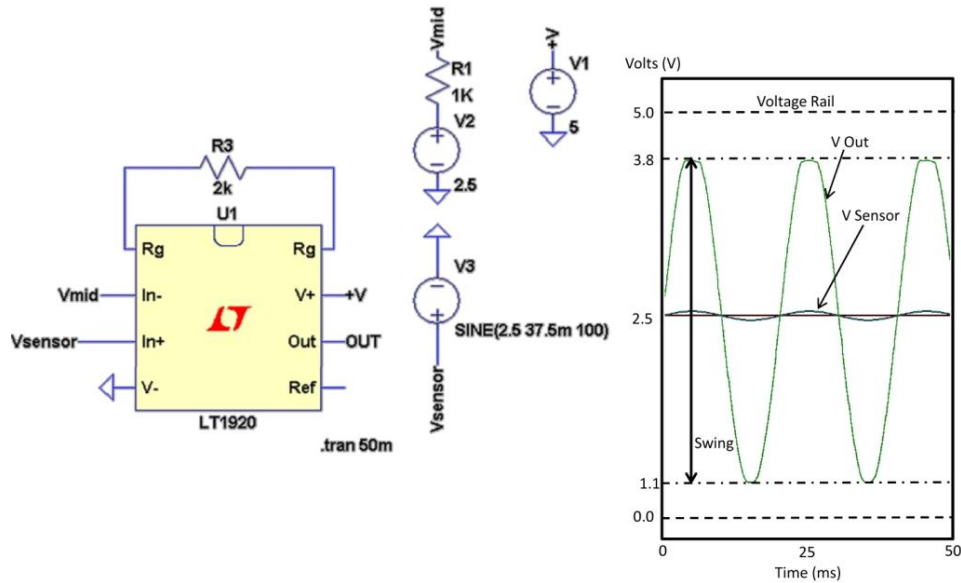


Figure C.2: Amplification With a Instrumentation Amplifier

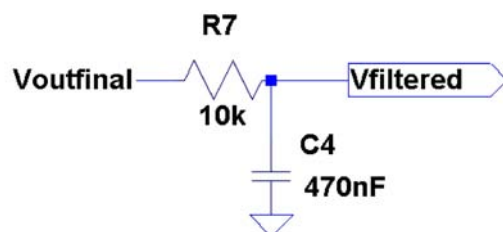


Figure C.3: Low Pass Anti-Aliasing Filter

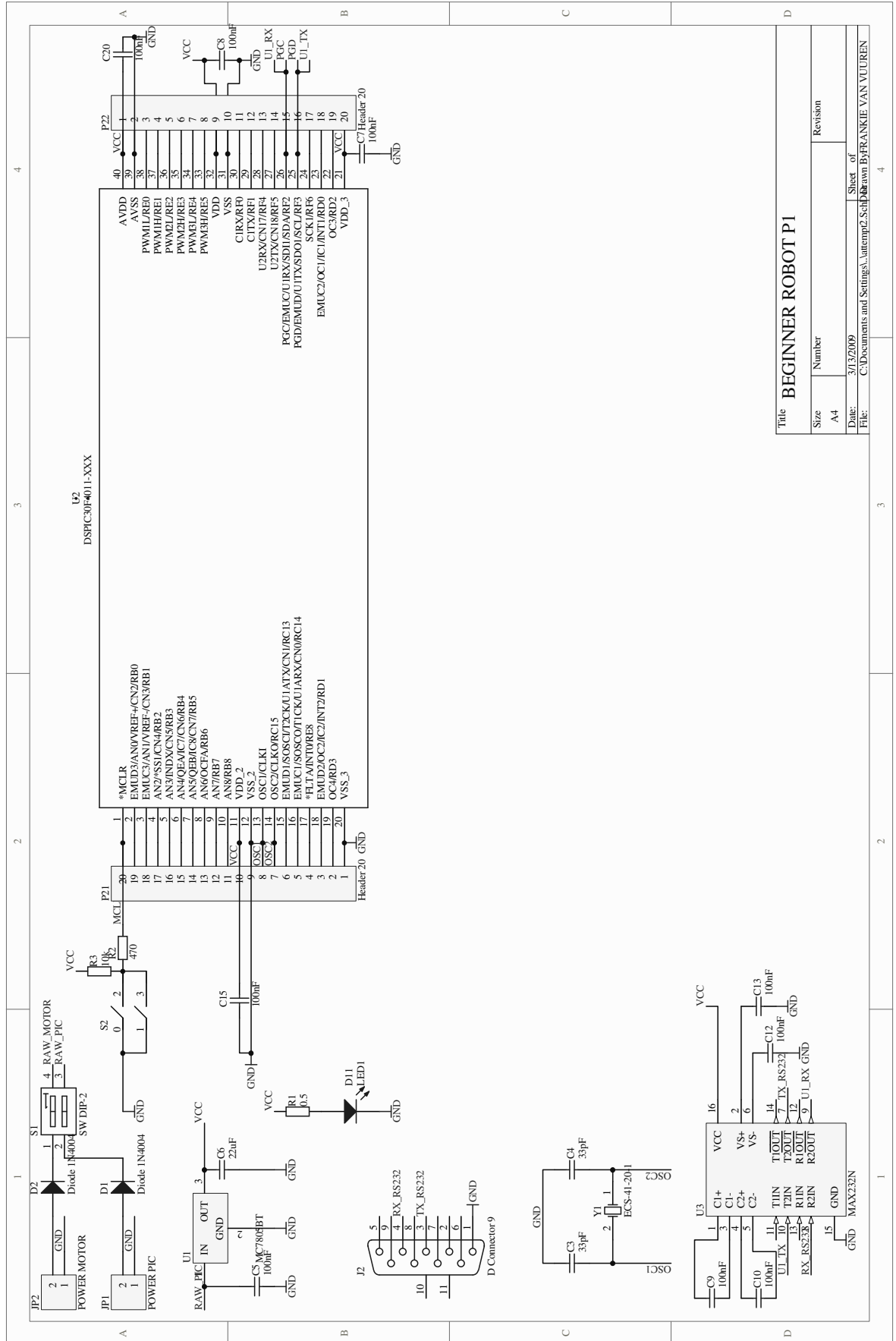


Figure C.4: Main Board Schematic (p1)

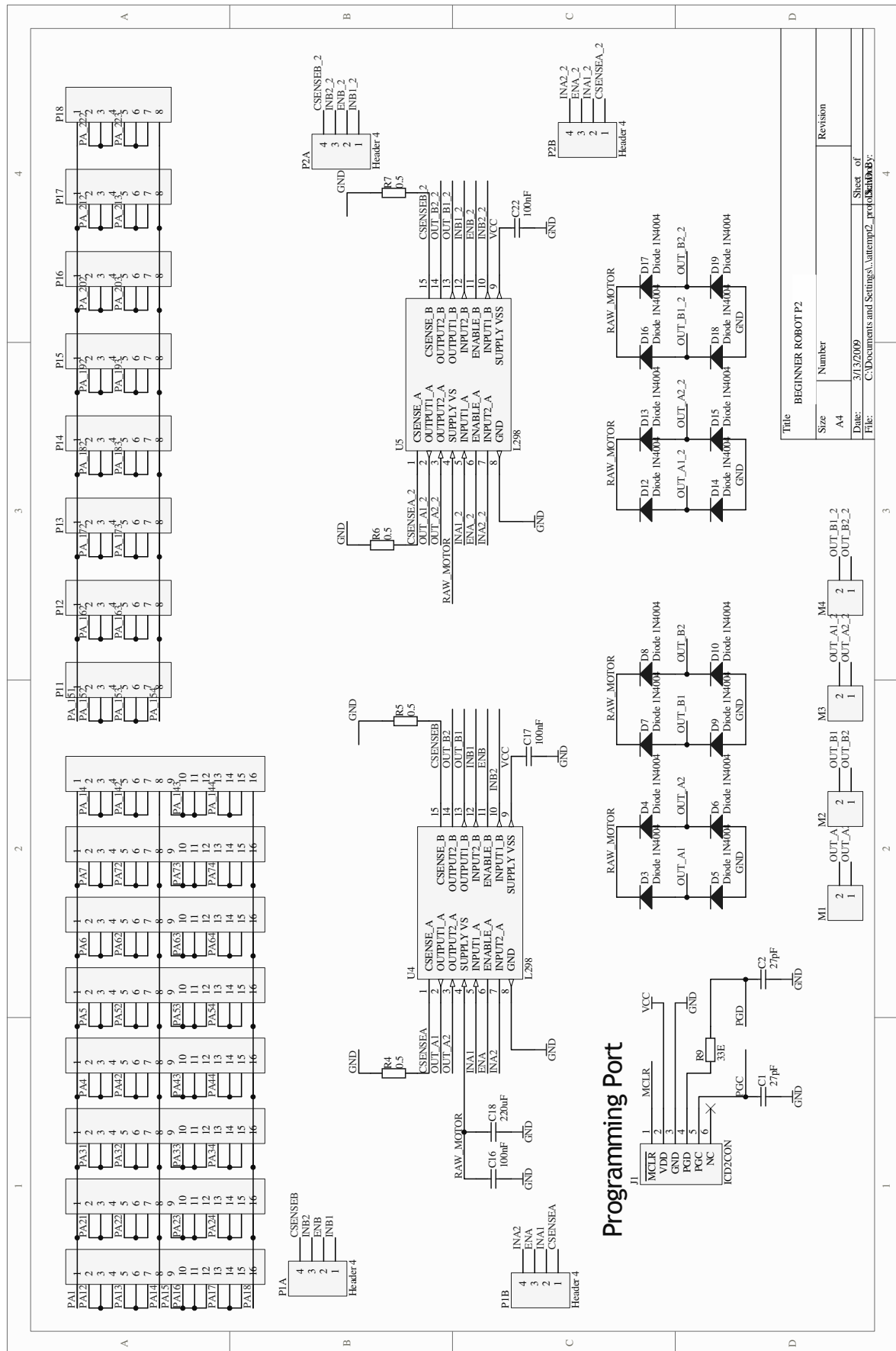


Figure C.5: Main Board Schematic (p2)

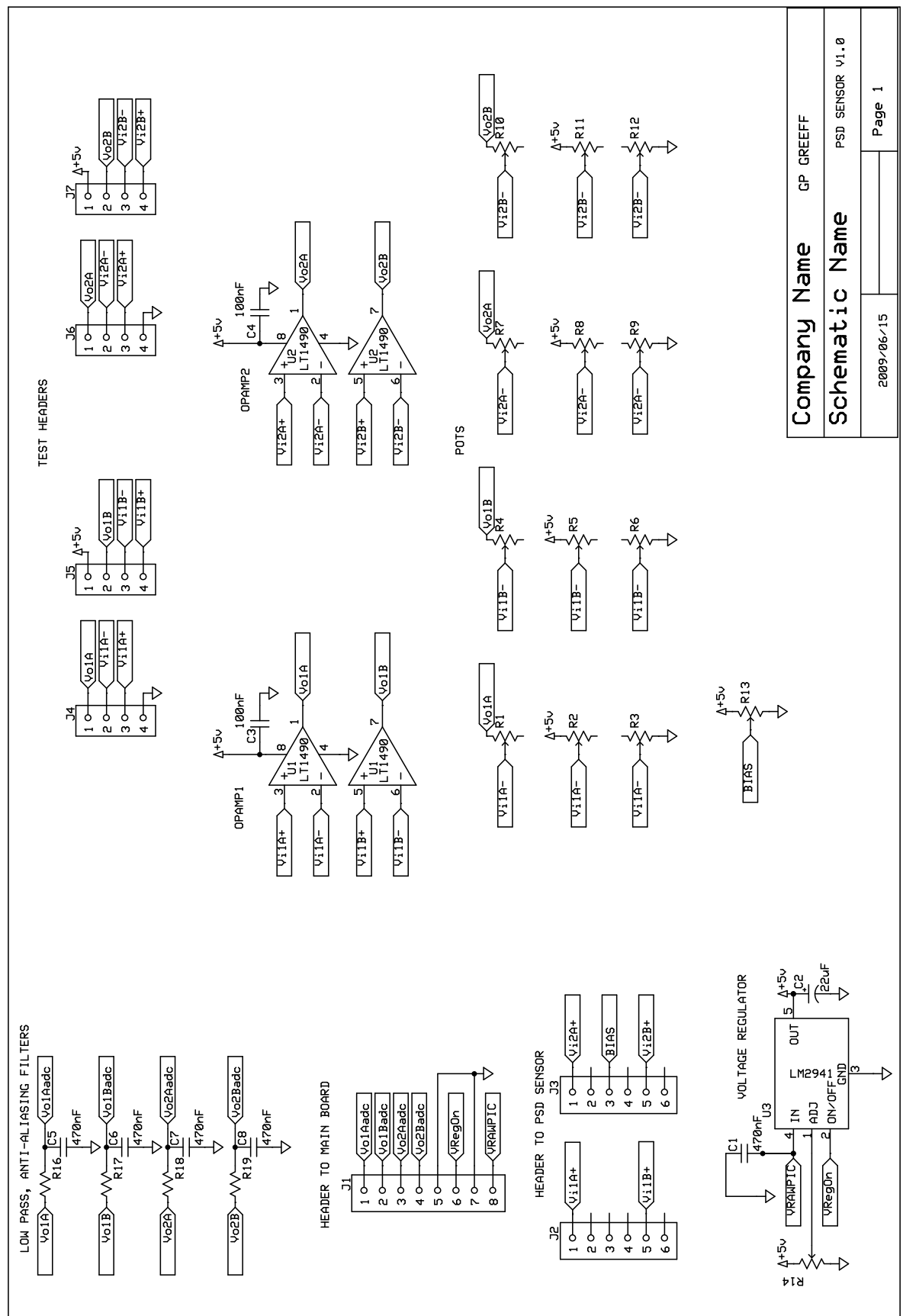


Figure C.6: First Amplifier Schematic

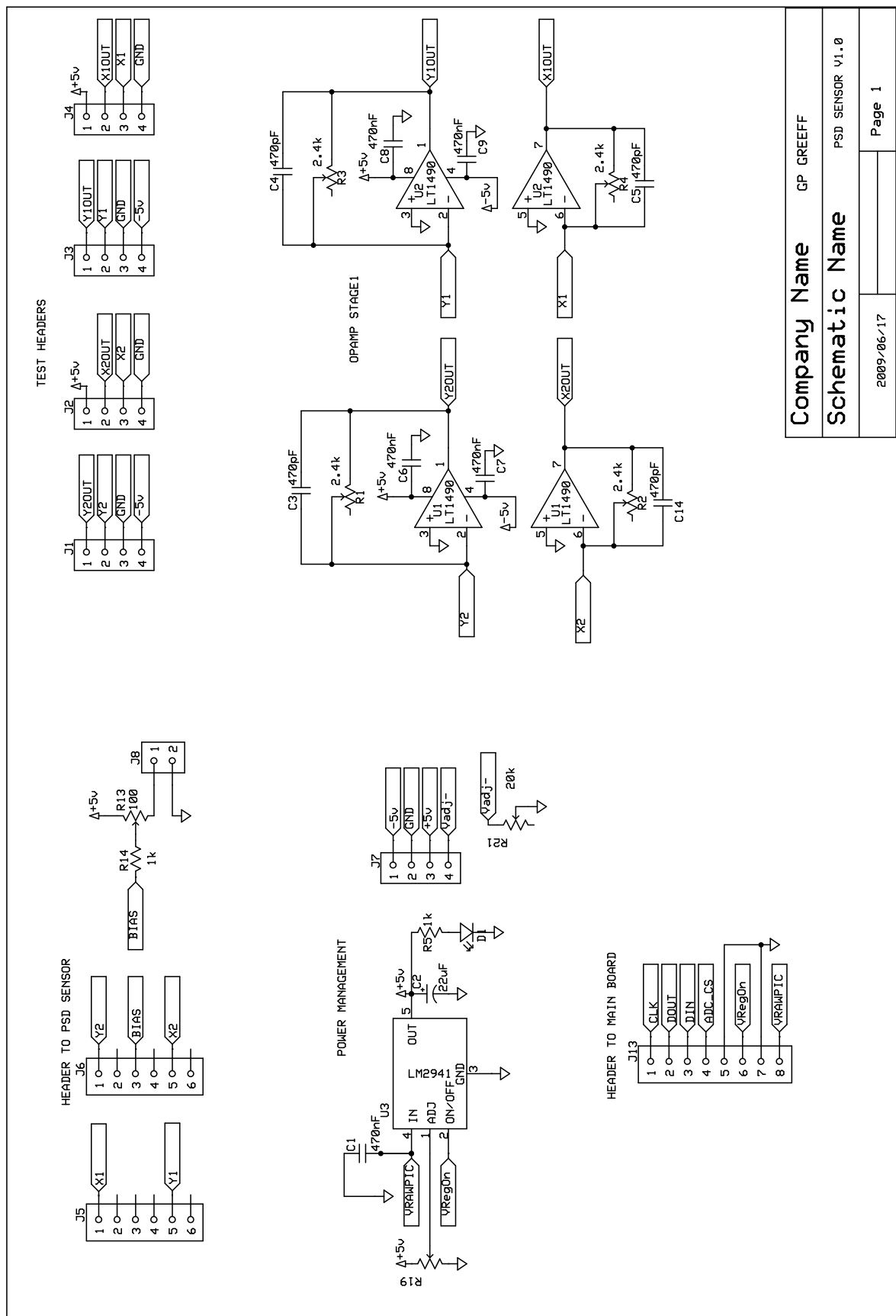


Figure C.7: Final Amplifier Schematic (p1)

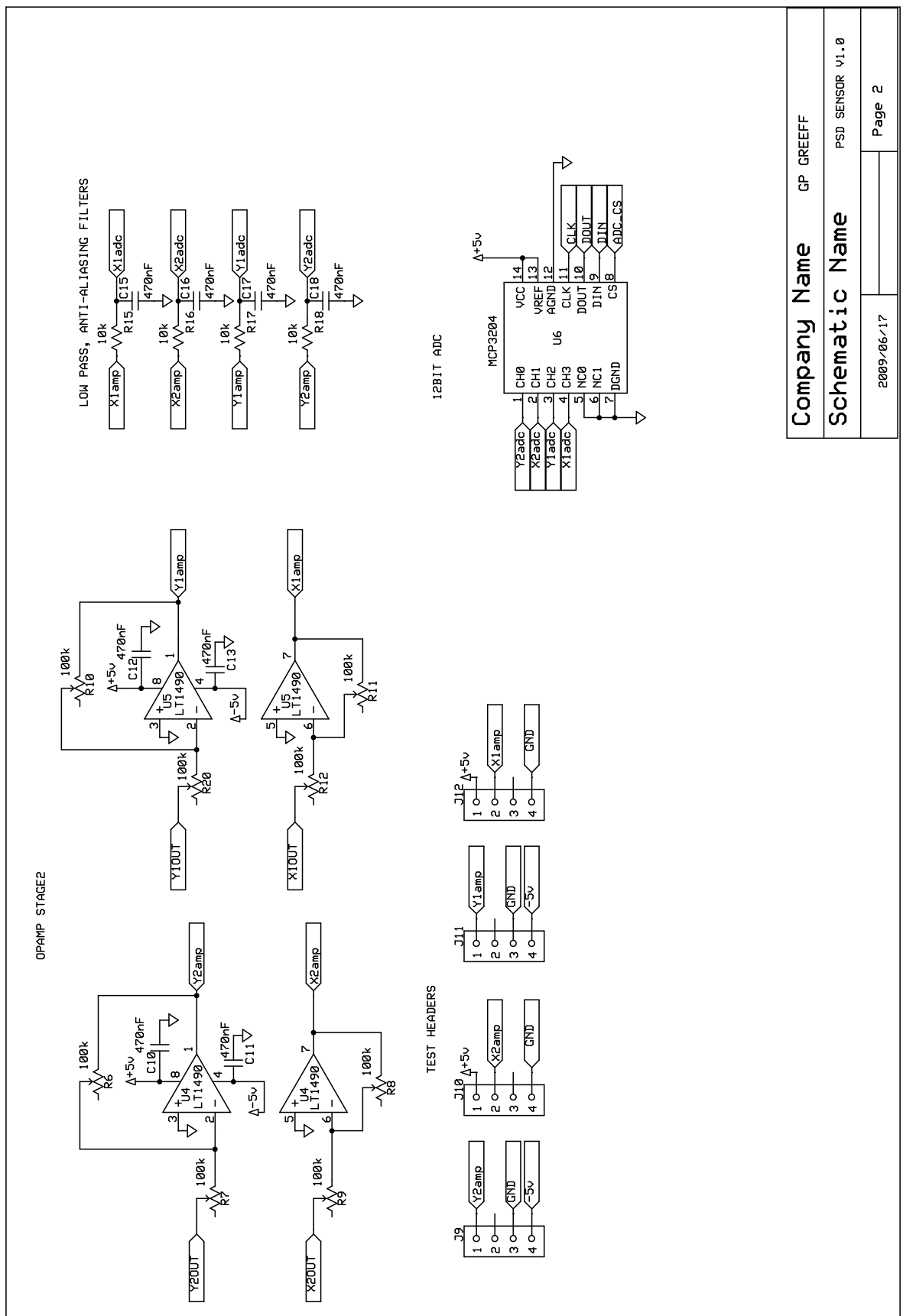


Figure C.8: Final Amplifier Schematic (p2)

Company Name	GP GREEFF
Schematic Name	PSD SENSOR v1.0
2009-06-17	Page 2

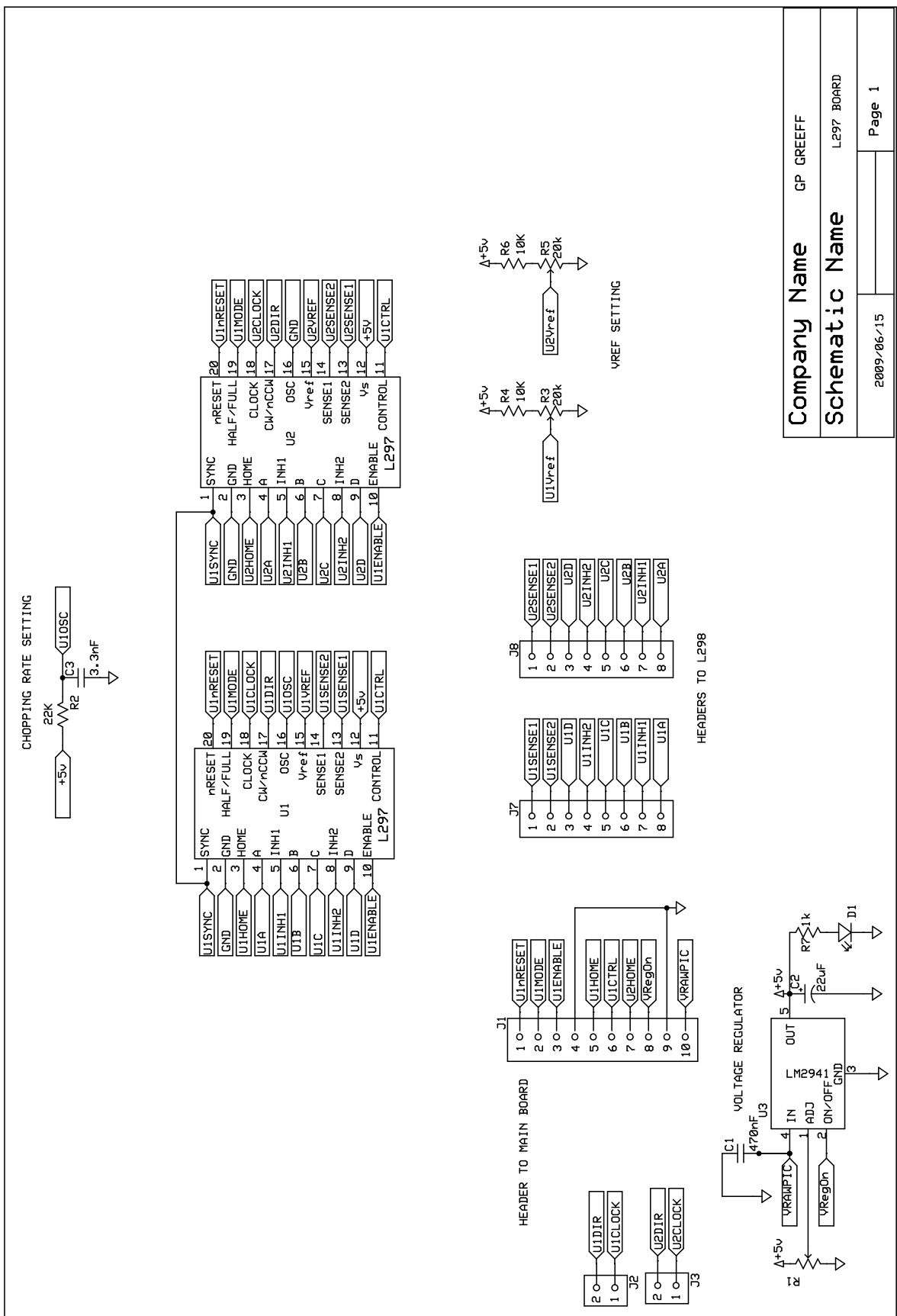


Figure C.9: Stepper Motor Controller Schematic

Appendix D

Gimbal Prototype 2 Drawings

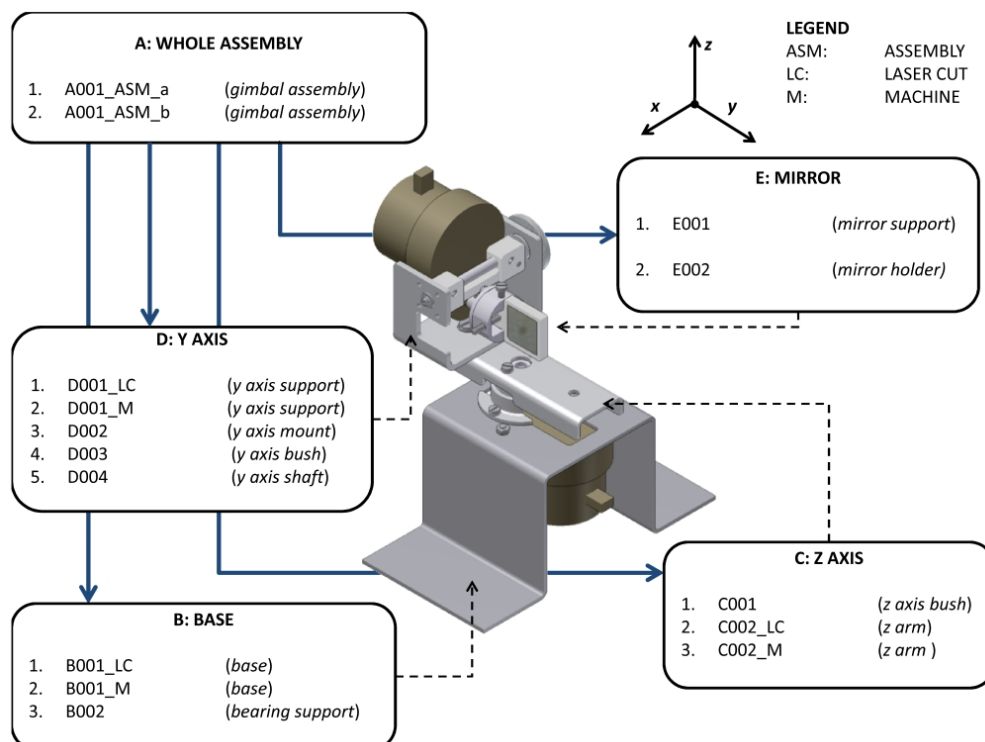


Figure D.1: Gimbal Prototype 2 Drawing Tree

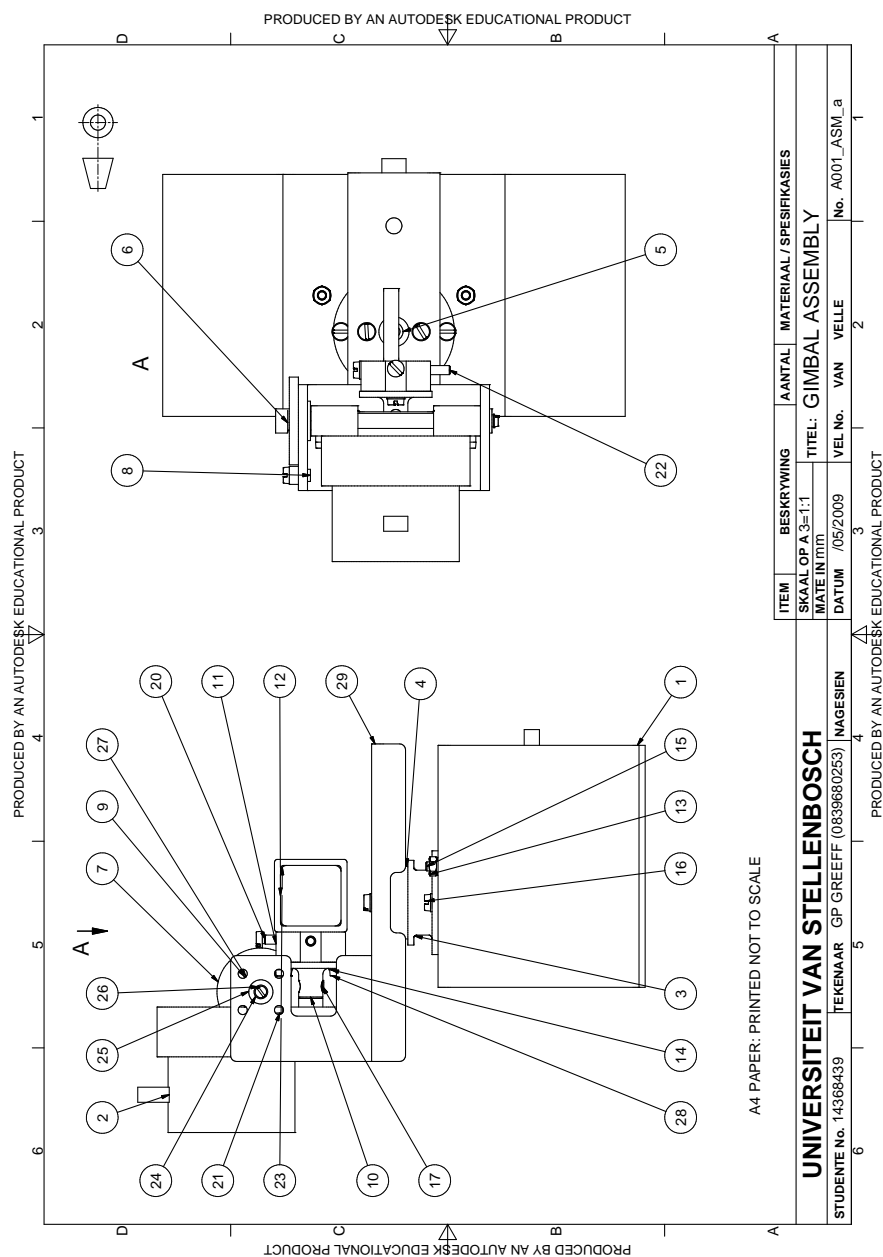


Figure D.2: A001 Gimbal Assembly p1 (Not Printed to Scale)

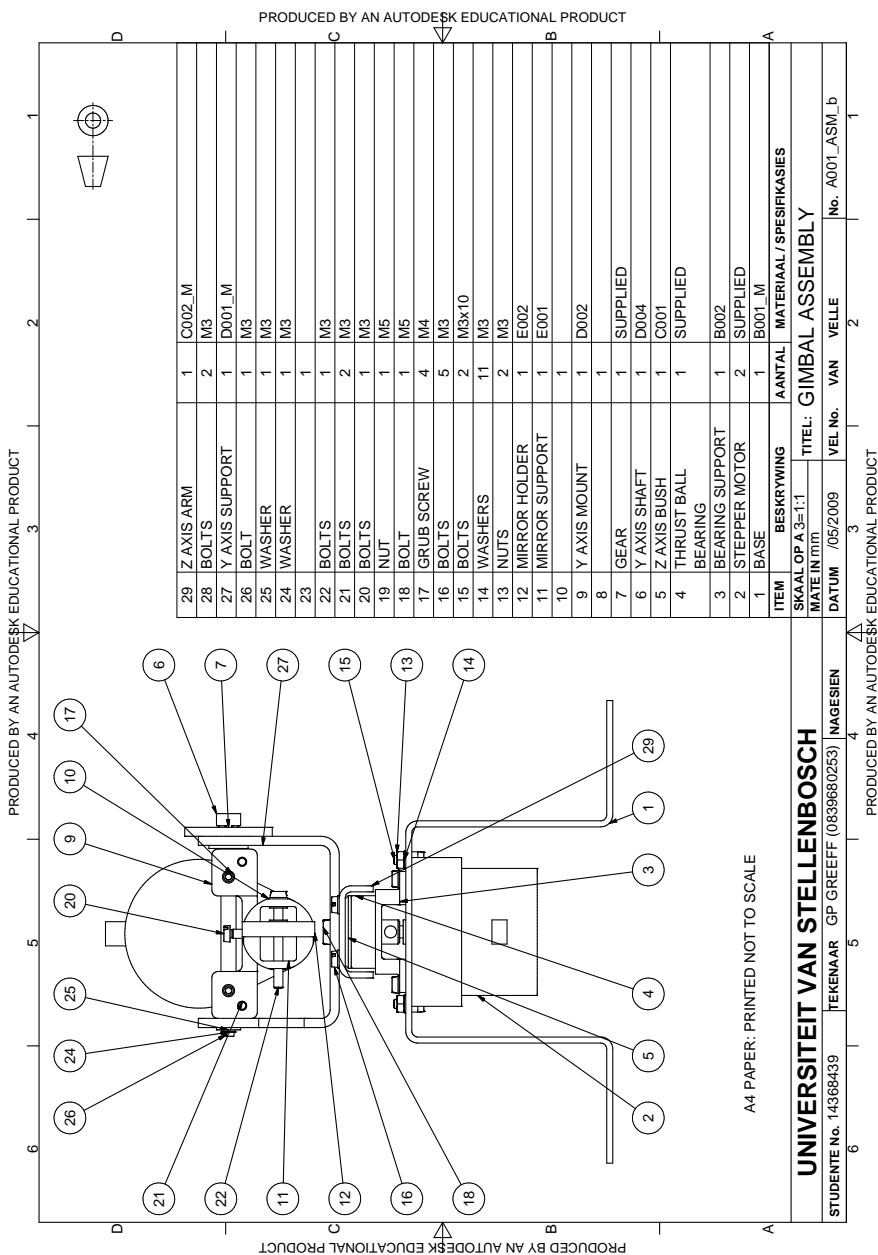


Figure D.3: A001 Gimbal Assembly p2 (Not Printed to Scale)

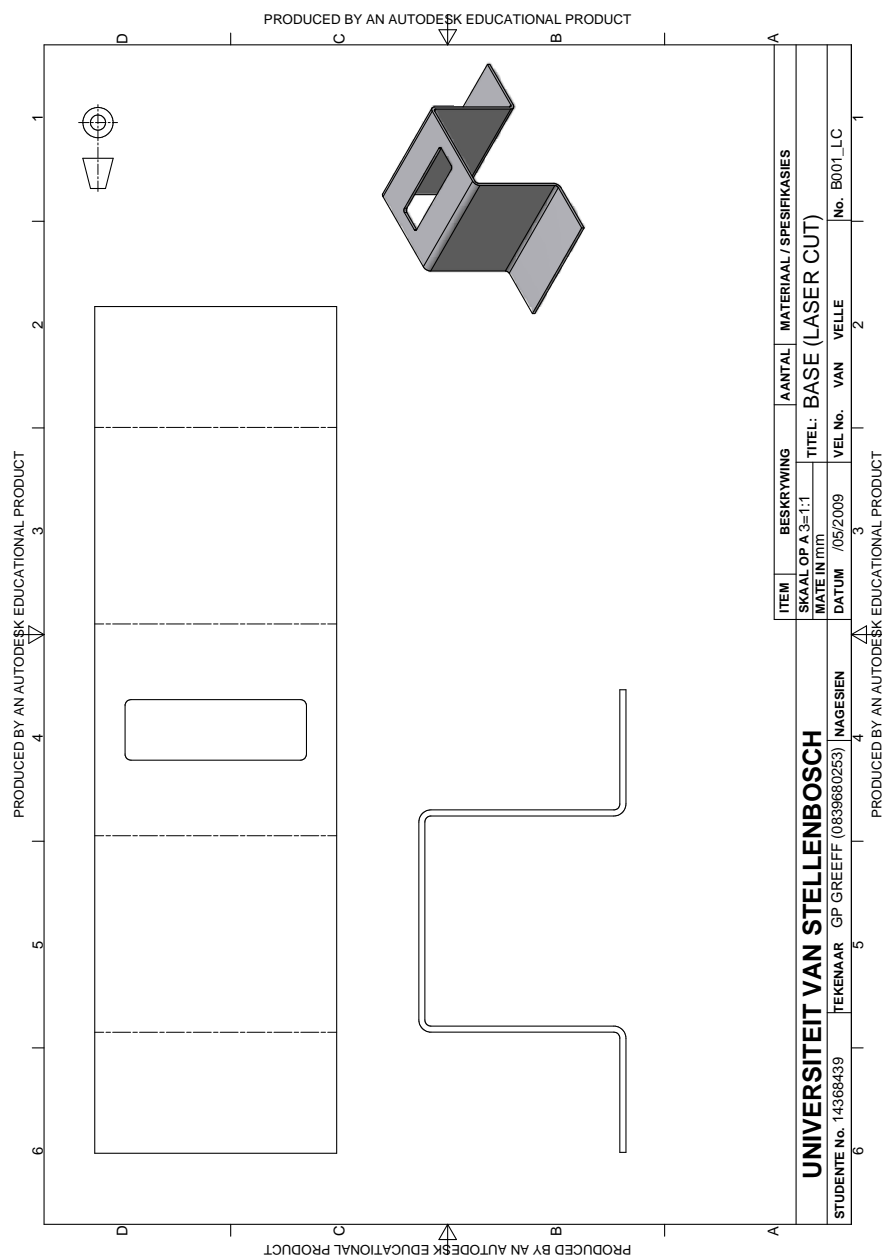


Figure D.4: B001 Laser Cut Base (Not Printed to Scale)

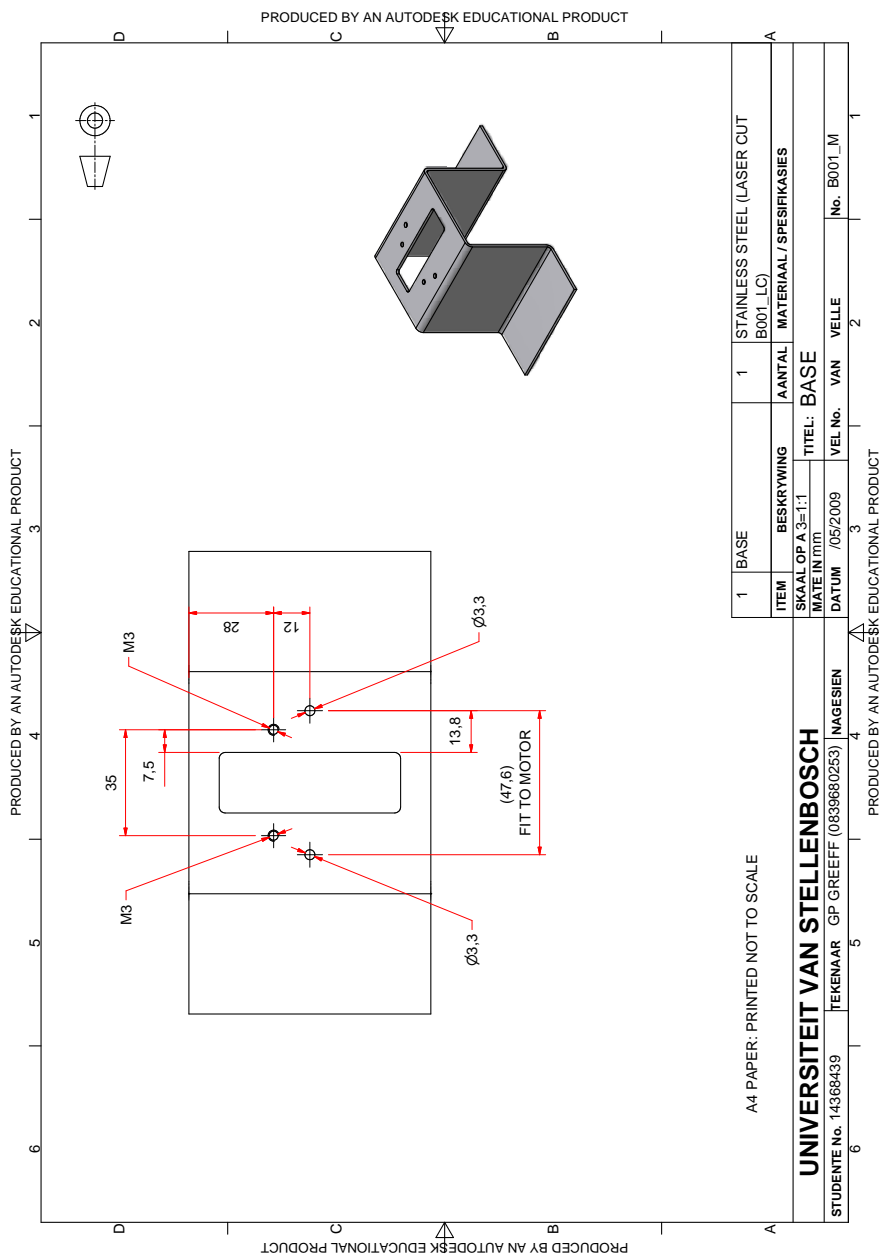


Figure D.5: B001 Machined Base (Not Printed to Scale)

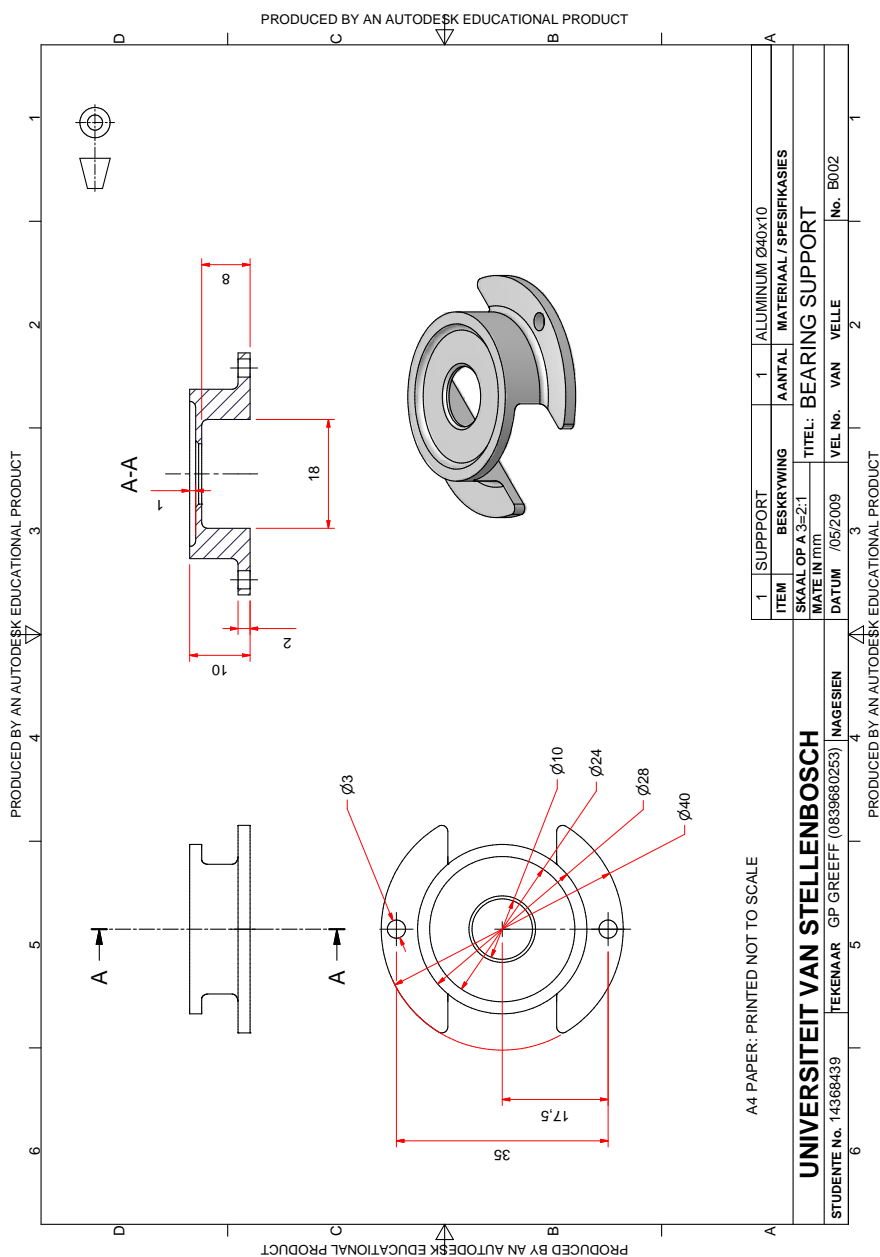


Figure D.6: B002 Bearing Support (Not Printed to Scale)

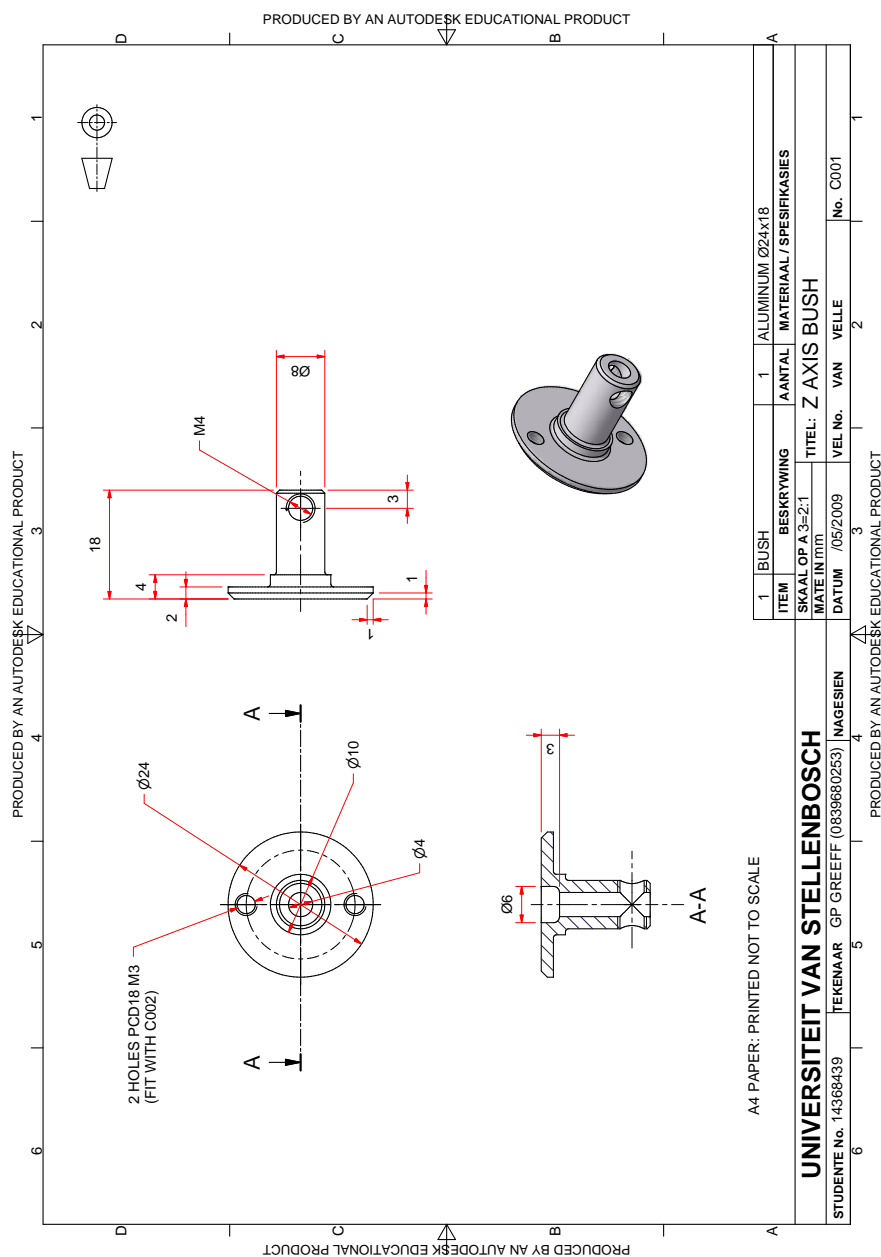


Figure D.7: C001 Z Axis Bush (Not Printed to Scale)

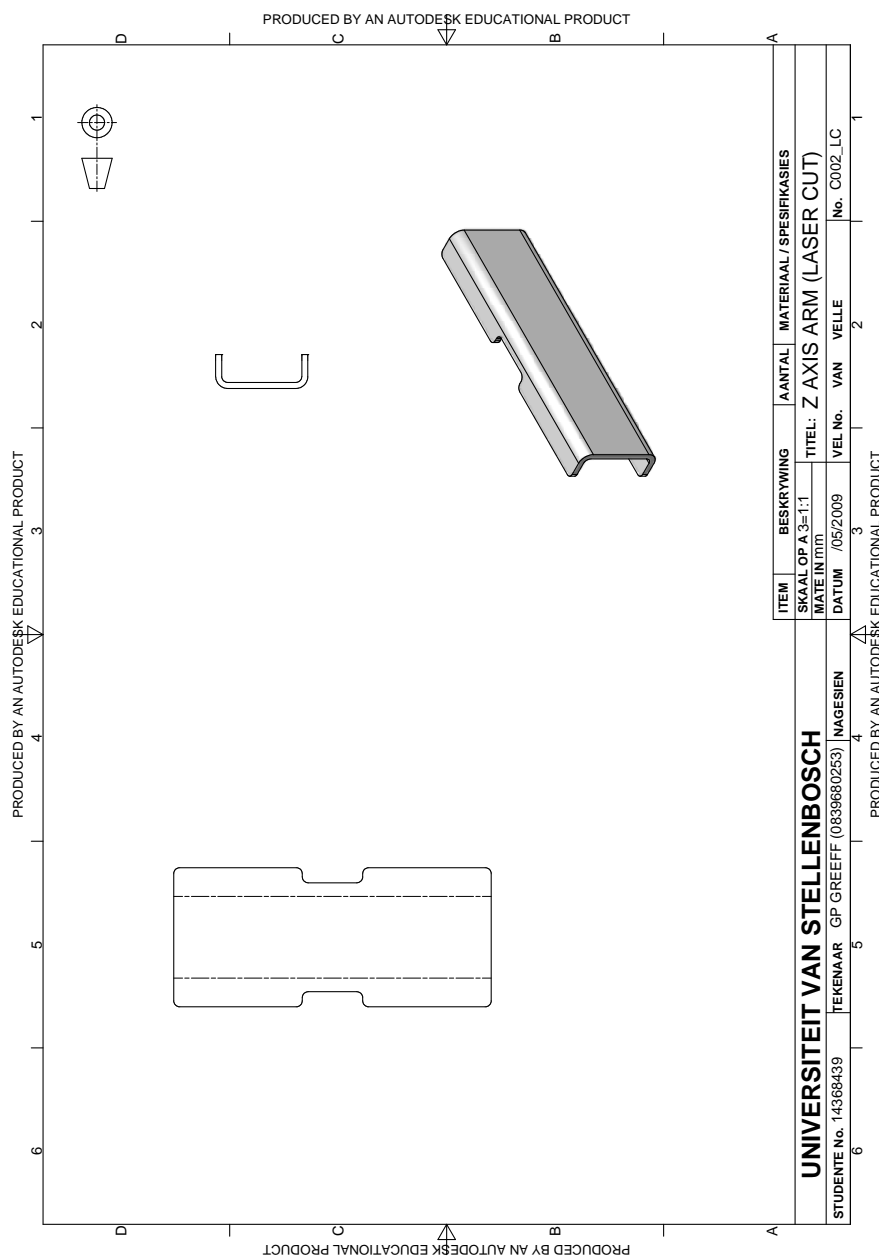


Figure D.8: C002 Laser Cut Z Axis Arm (Not Printed to Scale)

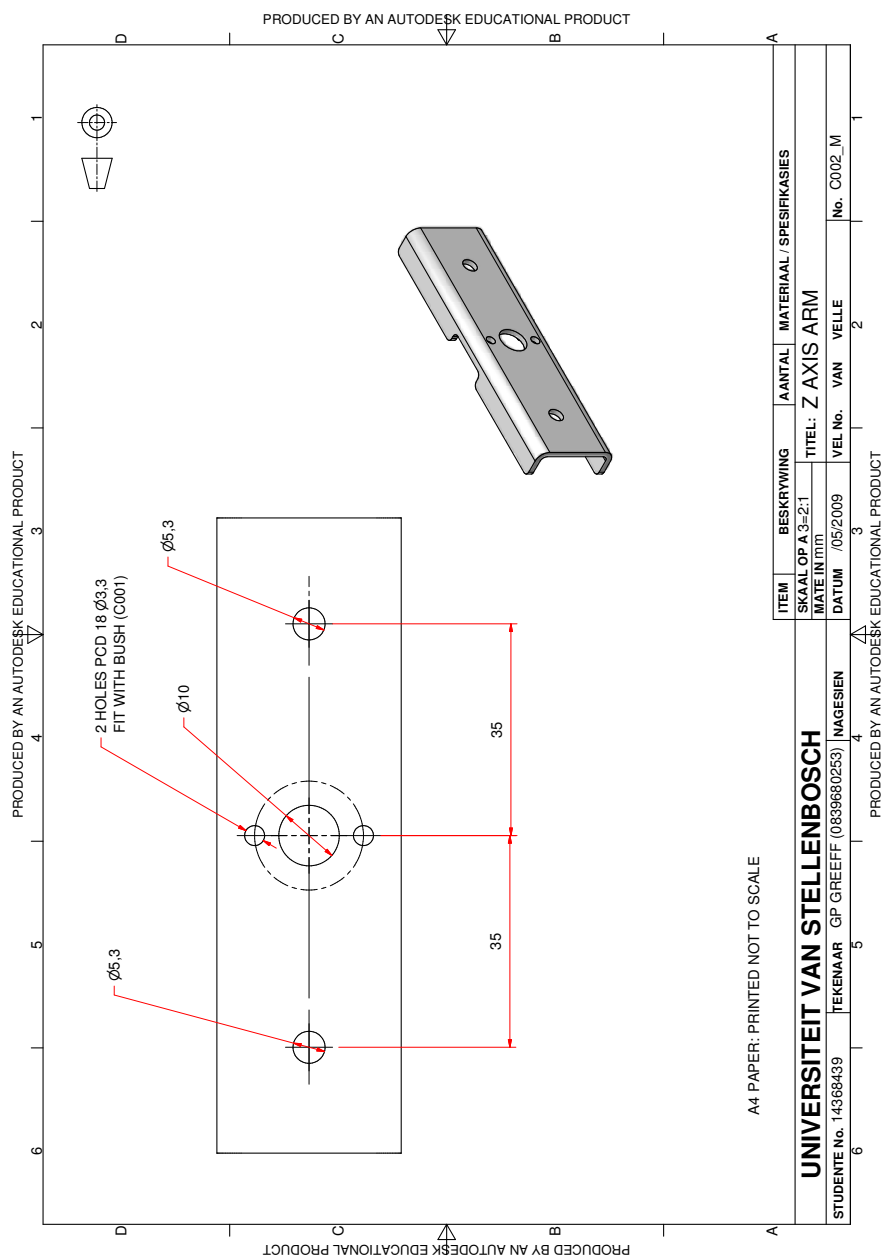


Figure D.9: C002 Machined Z Axis Arm (Not Printed to Scale)

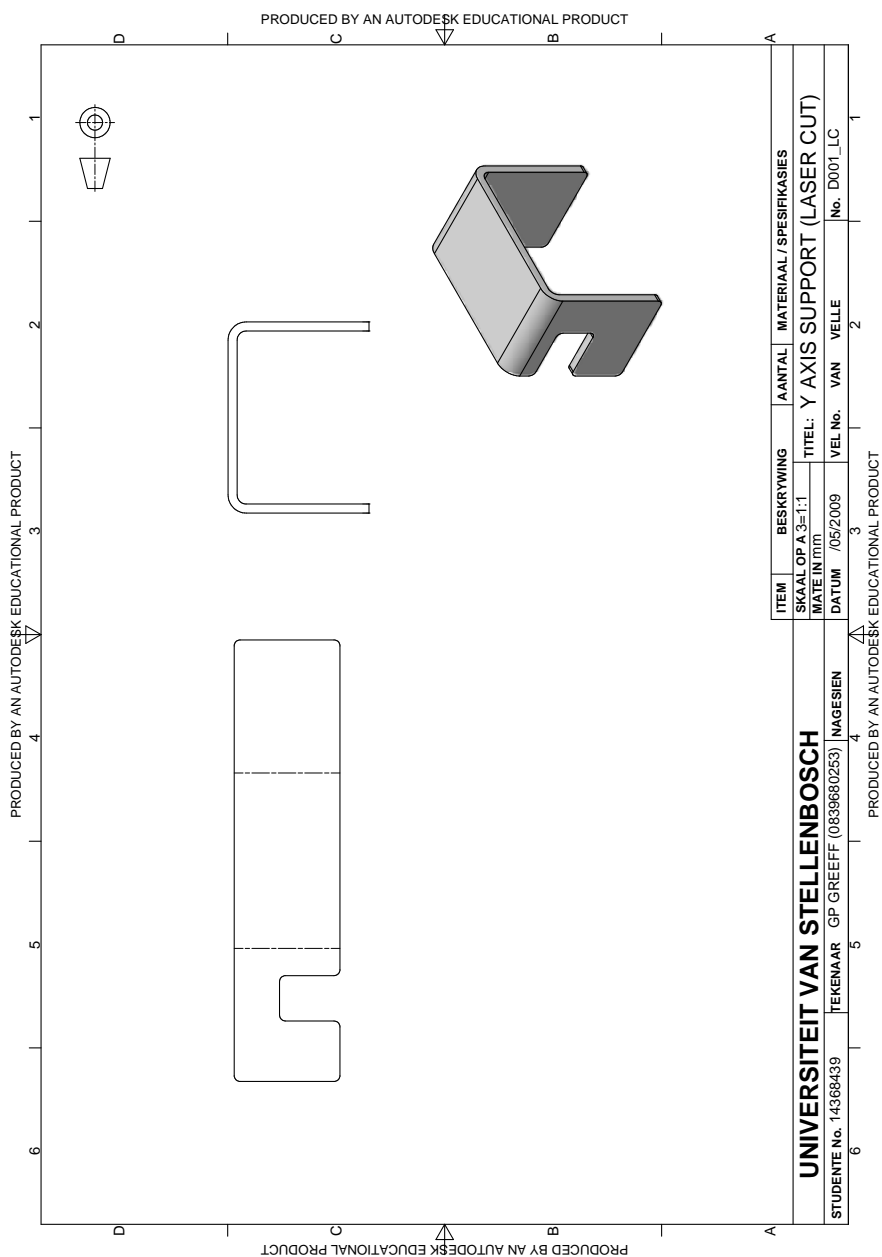


Figure D.10: D001 Laser Cut Y Axis Support (Not Printed to Scale)

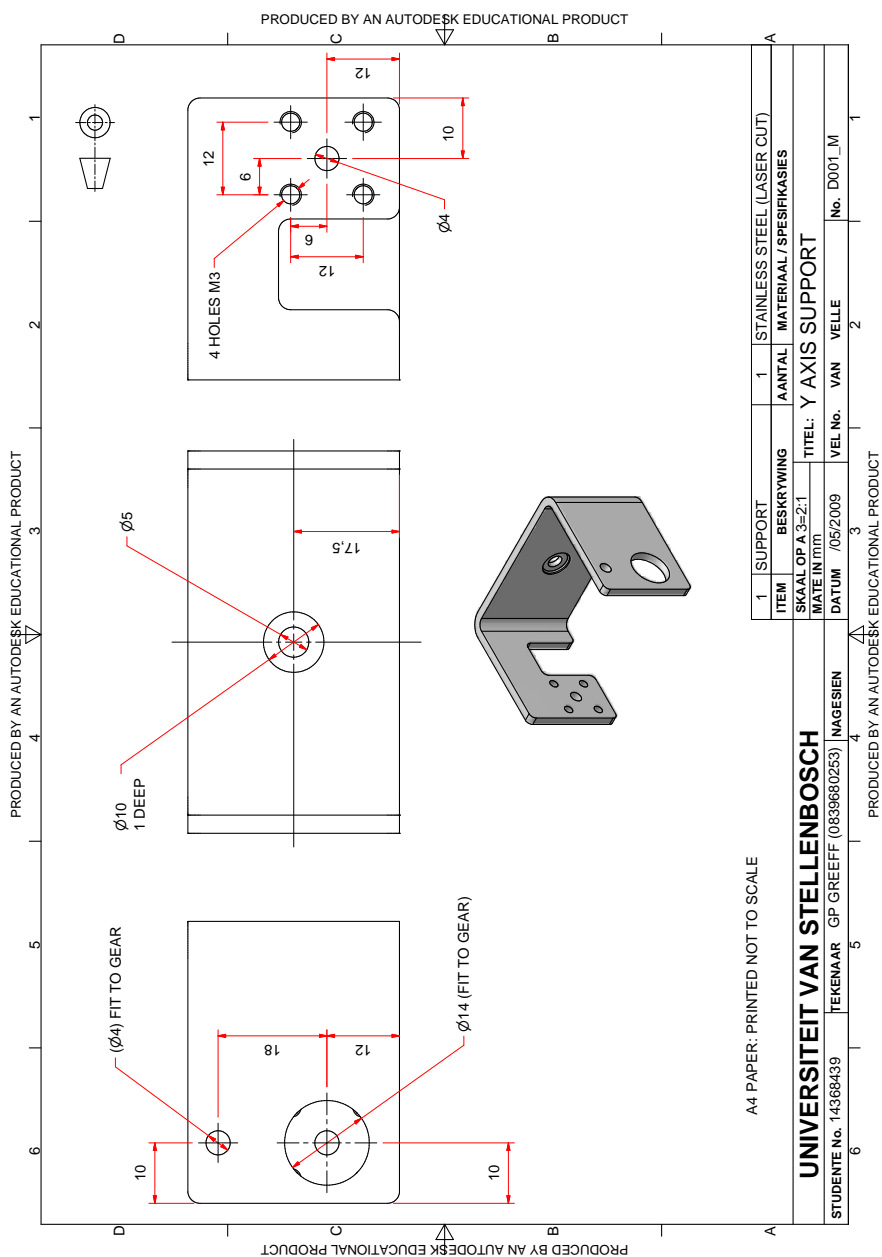


Figure D.11: D001 Machined Y Axis Support (Not Printed to Scale)

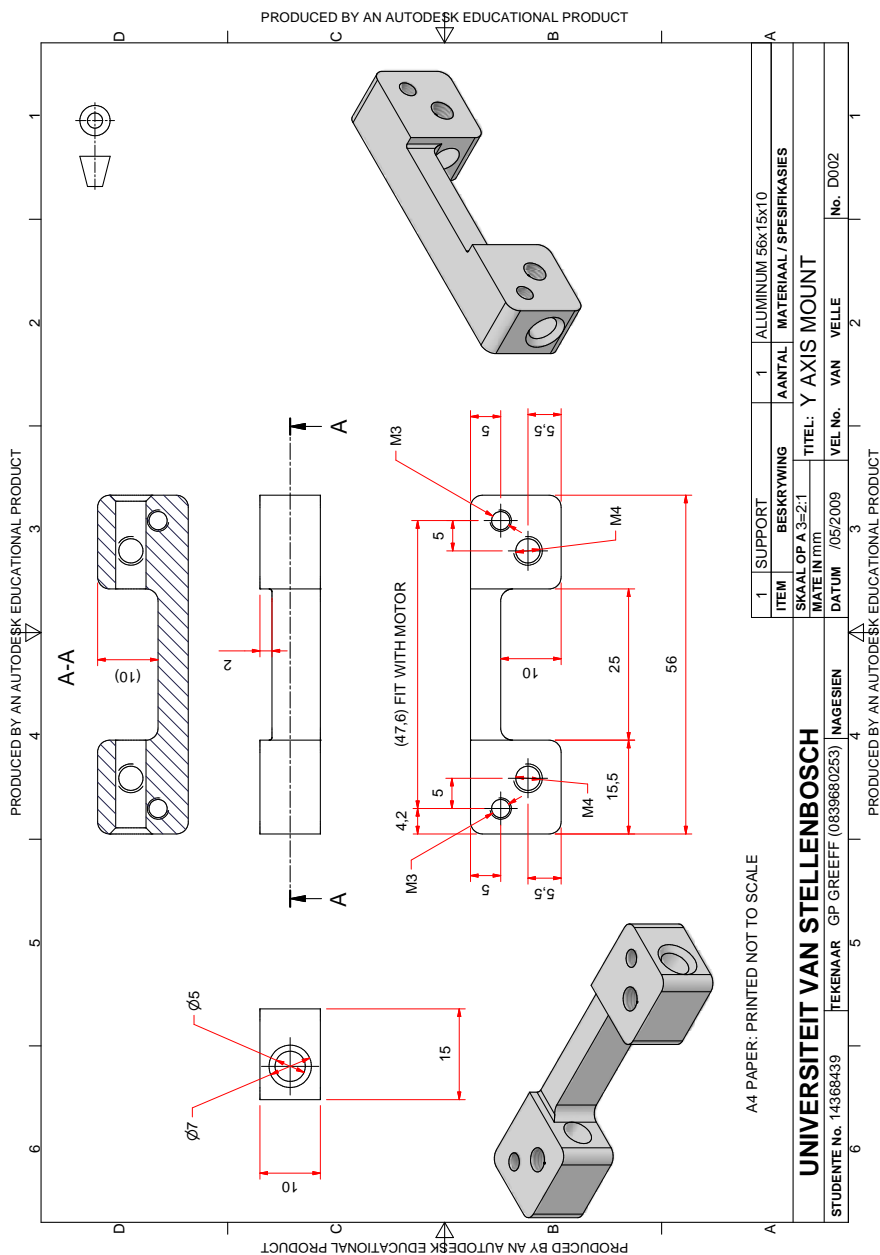


Figure D.12: D002 Y Axis Mount (Not Printed to Scale)

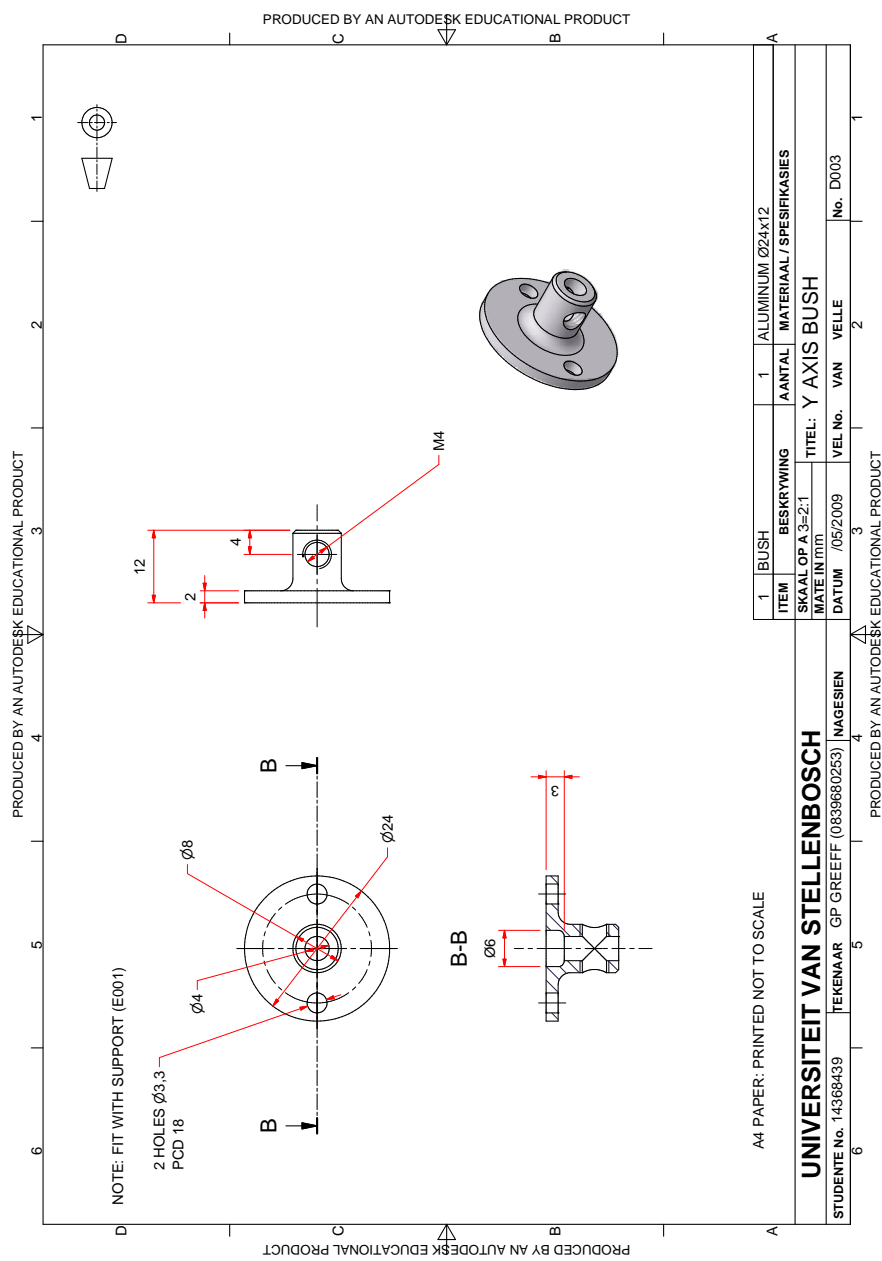


Figure D.13: D002 Y Axis Bush (Not Printed to Scale)

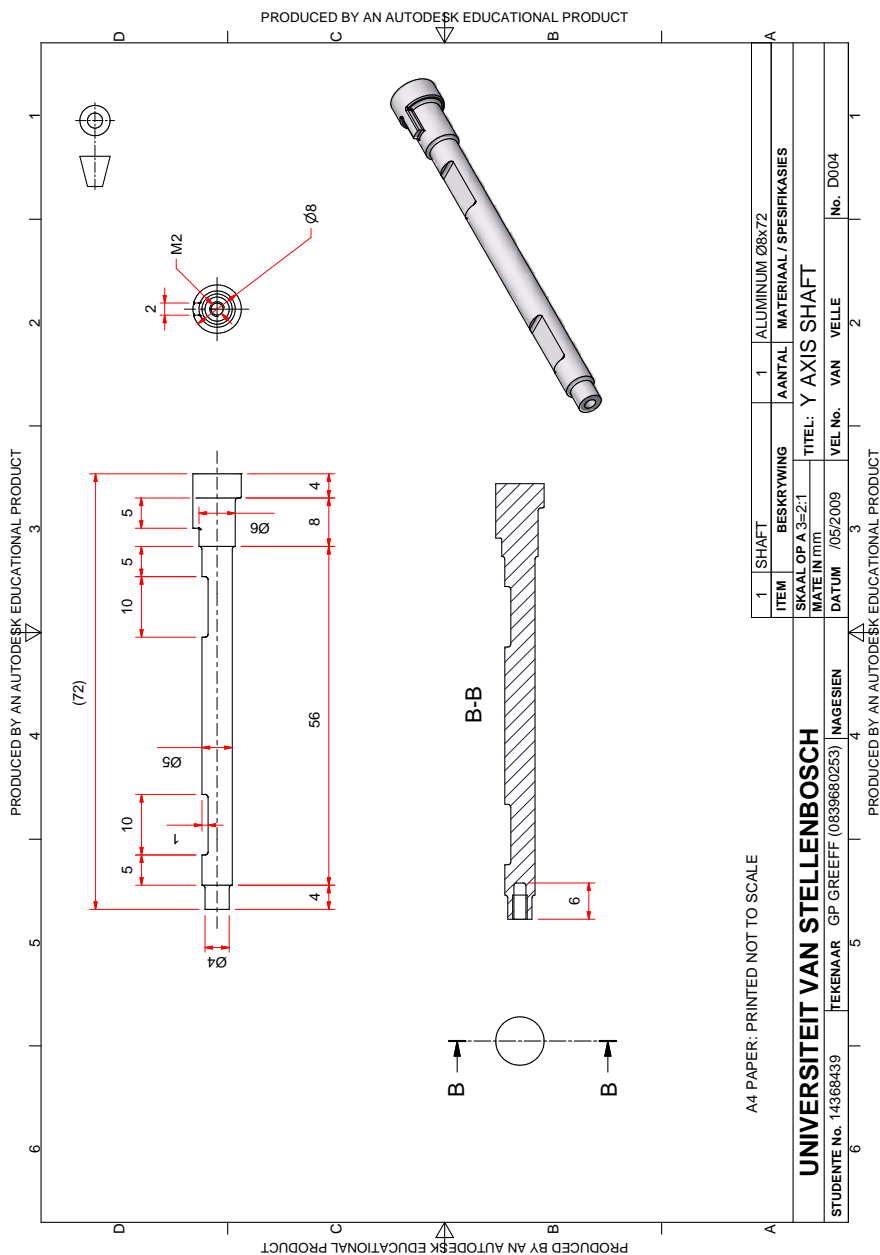


Figure D.14: D004 Y Axis Shaft (Not Printed to Scale)

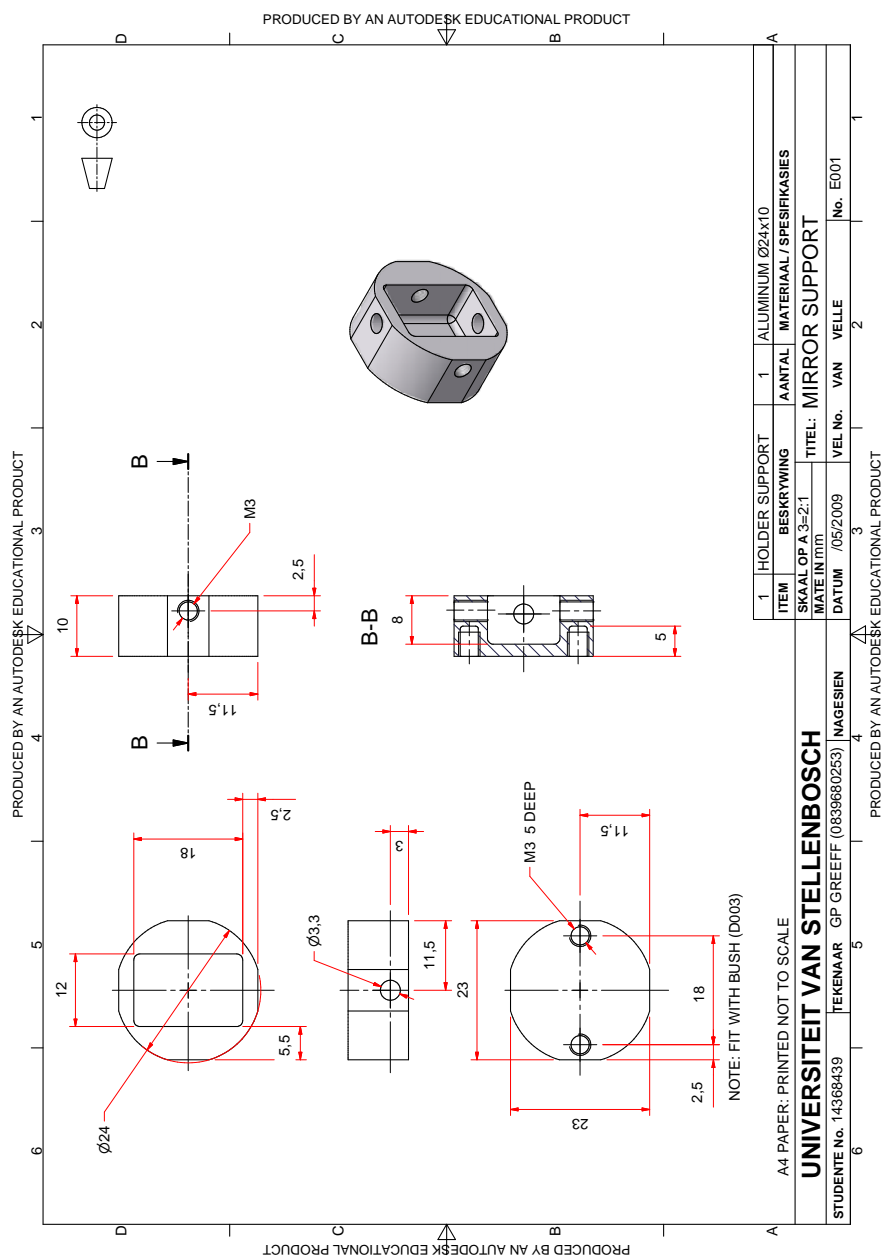


Figure D.15: E001 Mirror Support (Not Printed to Scale)

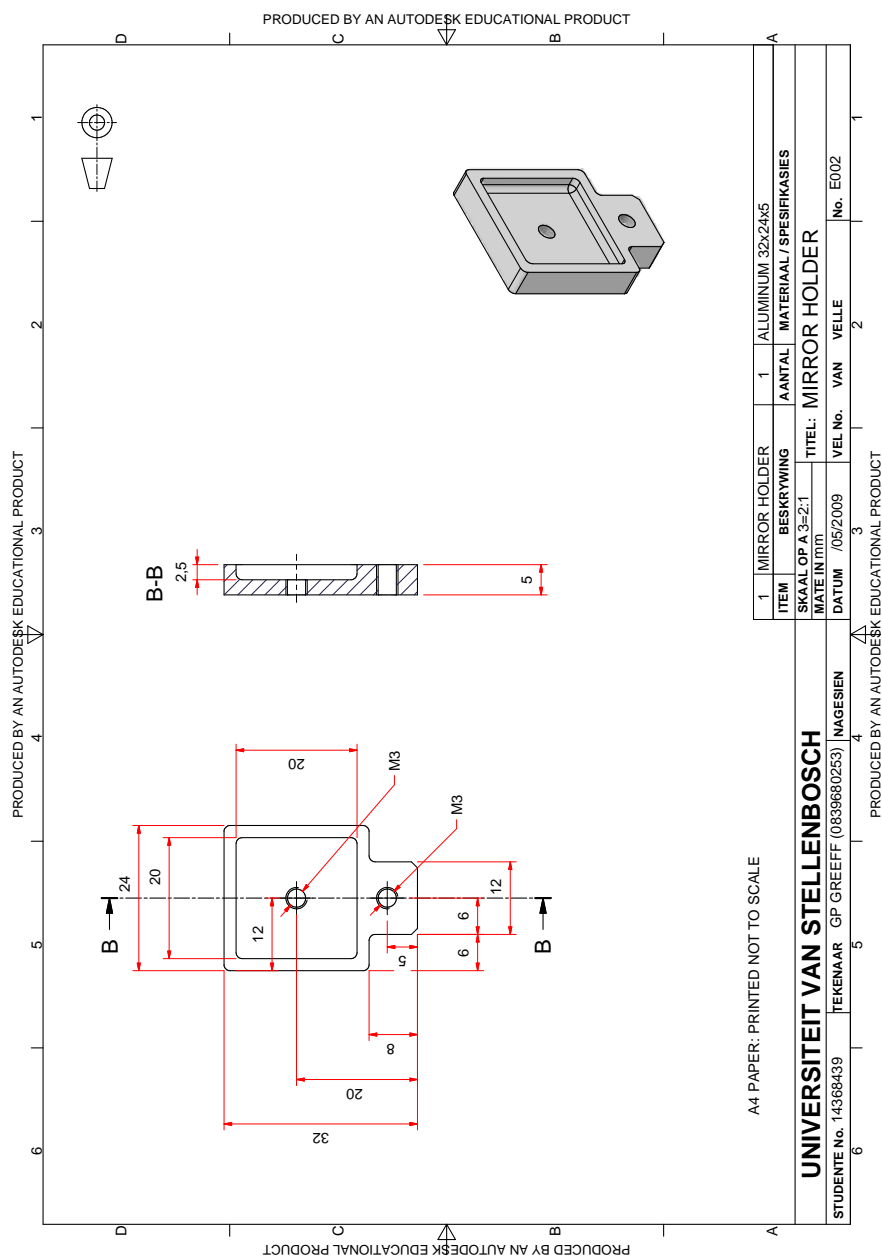


Figure D.16: E002 Mirror Holder (Not Printed to Scale)

Appendix E

Cost Summary

	Project Component	Component	Quantity	Cost	Total	Notes
Mechanics	Gimbal Prototype 1	Geared DC Motor CJT-12JS	2	R 94.08	R 188.17	Supplied by Mantech Electronics
		Laser Cut Components (6 parts)	1	R 174.55	R 174.55	Fabrinox
	Gimbal Prototype 2	McLennan Servo Supplies, Geared Stepper Motor P542-M48-G23	2	R 629.91	R 1 259.81	Supplied by RS Components
		Laser Cut Components (3 parts)	1	R 109.71	R 109.71	Fabrinox
		RHP, Thrust Bearing	1	R 115.89	R 115.89	RS Components
		Gears, bolts, nuts, grub screws, allen keys	1	R 100.00	R 100.00	RS Components, Eikestad Bolt & Nut cc
	Main PCB	PCB	1	R 147.06	R 147.06	North Tech Services cc
		Mircochip, dsPIC30f4011	1	R 0.00	R 0.00	Avnet, free sample
		TI, MAX232	1	R 0.00	R 0.00	Supplied by TI, free sample
		ST, L298 Dual Bridge Driver	2	R 40.96	R 81.92	Supplied by Mantech Electronics
		National Semiconductor, Regulator LM2940CT	1	R 22.42	R 22.42	Supplied by Mantech Electronics
		Diodes	16	R 1.14	R 18.24	Supplied by Mantech Electronics
Electronics	Stepper Motor Controller	L297 Stepper Motor Controller	2	R 35.46	R 70.92	Supplied by Mantech Electronics
		PCB	1	R 0.00	R 0.00	E&E Department PSB Manufacturing
		National Semiconductor, Regulator LM2940CT	1	R 22.42	R 22.42	Supplied by Mantech Electronics
	Sensor Board	PCB	1	R 0.00	R 0.00	E&E Department PSB Manufacturing
		National Semiconductor, Regulator LM2940CT	1	R 22.42	R 22.42	
		TI, PNT04050a converter TI	1	R 0.00	R 0.00	Supplied by TI, free sample
		Mircochip, MCP32041 12Bit ADC	1	R 0.00	R 0.00	Supplied by Avnet, free sample
		Hamamatsu, Si PIN Photodiode S5981	1	R 0.00	R 0.00	Supplied by NMISA
	Miscellaneous	Linear Technology, LT1490 opamp	4	R 49.93	R 199.72	Supplied by RS Components
		LED, crystal, switches, DB9 connection, connections, veroboard	1	R 200.00	R 200.00	Supplied by Avnet, Mantech electronics or RS Components
		TOTAL	44	R 1 765.95	R 2 733.25	<i>Excluding labour and delivery costs</i>

Figure E.1: Summary of the Project Costs

List of References

- Aerotech (2009). AOM360D Series Motorized Optical Mounts. Datasheet, Aerotech, Inc., Aerotech, Inc., 101 Zeta Drive Pittsburgh, PA.
Available at: <http://www.aerotech.com/products/pdf/AOM360D.pdf>
- API (2008). API Retroreflector. Datasheet, Automated Precision Inc.
Available at: <http://www.apisensor.com/>
- API (2009). Tracker3 Laser Tracking System. Datasheet, Automated Precision Inc.
Available at: <http://www.apisensor.com/>
- Bai, Y., Zhuang, H. and Roth, Z. (2005). Fuzzy logic control to suppress noises and coupling effects in a laser tracking system. *IEEE Transactions on Control Systems Technology*, vol. 13, no. 1, pp. 113–121.
- BIPM (2006). The International System of Units (SI). Standard, Bureau International des Poids et Mesures, 1, Boulevard Ney, 75018 Paris, France.
- Born, M. and Wolf, E. (1999). *Principles of Optics*. 7th edn. Cambridge University Press, Cambridge, U.K.
- Bridges, B. and Hagan, K. (2001 August). Laser tracker maps three-dimensional features. Magazine Article 8/01, American Institute of Physics. P28, 29, 31-33.
- Claudiu, C. (2003). Tiny bootloader.
Available at: <http://www/etc.ugal.ro/cchiculita/software/picbootloader.htm>
- Condit, R. and Jones, D.W. (2004). Stepping motors fundamentals. Application Note AN907, Microchip Technology Inc.
- Cuypers, W., Gestel, N.V., Voet, A., Kruth, J.-P., Mingneau, J. and Bleys, P. (2009). Optical measurement techniques for mobile and large-scale dimensional metrology. *Optics and Lasers in Engineering*, vol. 47, no. 3-4, pp. 292 – 300. ISSN 0143-8166. Optical Measurements.
- Edwards, I. (1988). Using photodiodes for position sensing. Application note, United Detector Technology.
- Estler, W., Edmundson, K., Peggs, G. and Parker, D. (2002). Large-scale metrology - an update. *CIRP Annals - Manufacturing Technology*, vol. 51, no. 2, pp. 587 – 609.

- Fan, K., Liu, C., Wu, P., Chen, Y. and Wang, W. (2007). The Structure Design of a Micro-precision CMM with Abbe Principle. In: *Proceedings of the 35th International MATADOR Conference: formerly the International Machine Tool Design and Research Conference*, vol. 12, p. 297. Springer.
- FARO (2009). SMX Laser-Tracker 4000/4500. Product specification, FARO Swiss Holding GmbH.
Available at: <http://www.faro.com/lasertracker/home/>
- Fletcher, S., Longstaff, A. and Myers, A. (2005). Investigation into the accuracy of a proposed laser diode based multilateration machine tool calibration system. In: *Journal of Physics: Conference Series*, vol. 13, pp. 398–401. Institute of Physics Publishing.
- Gallagher, B.B. (2003). *Optical shop applications for laser tracking metrology systems*. Master's thesis, Department of Optical Sciences, University of Arizona.
- Geosystems, L. (2009). PCMM system specifications Leica absolute tracker and leica T-products. Datasheet, Leica Geosystems. Datasheet.
Available at: <http://www.leica-geosystems.com/>
- Hamamatsu (2002). Position sensitive diodes. Technical report, Hamamatsu Photonics K.K., Solid State Division.
- Hecht, E. (1997). *Optics*. 3rd edn. Addison-Wesley Pub Co, Reading, MA.
- Hughes, E., Wilson, A. and Peggs, G. (2000). Design of a high-accuracy CMM based on multi-lateration techniques. *CIRP Annals - Manufacturing Technology*, vol. 49, no. 1, pp. 391–394.
- Jain, S. (2003). A survey of laser range finding. Technical brief.
Available at: <http://citeseerx.ist.psu.edu/viewdoc/summary?doi=10.1.1.130.6167>
- Jiang, H., Osawa, S., Takatsuji, T., Noguchi, H. and Kurosawa, T. (2002). High-performance laser tracker using an articulating mirror for the calibration of coordinate measuring machine. *Optical Engineering*, vol. 41, no. 3, pp. 632–637.
- Johnson, R. and Lentz, C. (2003 March). 2D optical position sensor. Magazine Article Issue 152, Circuit Cellar.
Available at: <http://www.circuitcellar.com/archives/titledirectory/141to160.html>
- Kruger, O.A. (2004). NMISA Research and development report. Development report, NMISA.
- Lau, K.C., and Hocken, R.J. (1987). Three and five axis laser tracking systems. Patent 4714339.

- Lewis, A. (2006). CMM developments at the National Physical Laboratory. Presentation, NPL.
Available at: http://www.cenam.mx/cmu-mm/Evento_2006/Presentaciones/Lewis-ClubMMC2006.pdf
- Lin, P., Lu, C. et al. (2005). Modeling and sensitivity analysis of laser tracking systems by skew-ray tracing method. *Journal of Manufacturing Science and Engineering*, vol. 127, p. 654.
- NMISA (2008). Homepage of the NMISA.
Available at: <http://www.nmisa.org/>
- Norgia, M., Giuliani, G. and Donati, S. (2007). Absolute distance measurement with improved accuracy using laser diode self-mixing interferometry in a closed loop. *IEEE Transactions on Instrumentation and Measurement*, vol. 56, no. 5, p. 1894.
- OSI (2007). Position Sensing Photodiodes. Application note, OSI Optoelectronics.
Available at: http://www.osiopoelectronics.no/tech_app_notes.php
- Poole, D. (2006). *Linear Algebra: A Modern Introduction*. 2nd edn. Brooks/Cole Pub Co, Toronto, Canada.
- Rako, P. (2004). Photodiode amplifiers: Changing light to electricity. Technical report, National Semiconductor Corporation, Strategic Applications Engineer Amplifier Group.
Available at: <http://www.national.com/onlineseminar/2004/photodiode/PhotodiodeAmplifiers.pdf>
- Rao, S. (1996). *Engineering optimization: theory and practice*. 3rd edn. Wiley-Interscience, New York.
- Rhee, H. and Kim, S. (2002). Absolute distance measurement by two-point-diffraction interferometry. *Applied optics*, vol. 41, no. 28, p. 5921.
- Schmidt, S. (2006). Applications dictate gimbal selection. Technical report, Laser Focus World.
- Schneider, C. (2004). Lasertracer—a new type of self tracking laser interferometer. Technical report, IWAA, Geneva, Switzerland.
Available at: <http://www.slac.stanford.edu/econf/C04100411/papers/054.PDF>
- Schwenke, H., Franke, M. and Hannaford, J. (2005). Error mapping of CMMs and machine tools by a single tracking interferometer. *CIRP Annals - Manufacturing Technology*, vol. 54, no. 1, p. 475.
- Shirinzadeh, B. (1998). Laser-interferometry-based tracking for dynamic measurements. *Industrial Robot*, vol. 25, no. 1, pp. 35–41.

- Smith, L. (2002). A tutorial on principal components analysis. Tech. Rep., Cornell University.
Available at: <http://users.ecs.soton.ac.uk/hbr03r/pa037042.pdf>
- Takatsuji, T., Goto, M., Kirita, A., Kurosawa, T. and Tanimura, Y. (2000). The relationship between the measurement error and the arrangement of laser trackers in laser trilateration. *Measurement Science and Technology*, vol. 11, no. 5, pp. 477–83.
- Takatsuji, T., Goto, M., Kurosawa, T. and Tanimura, Y. (1998). The first measurement of a three-dimensional coordinate by use of a laser tracking interferometer system based on trilateration. *Measurement Science and Technology*, vol. 9, no. 1, pp. 38–41.
- Teoh, P., Shirinzadeh, B., Foong, C. and Alici, G. (2002). The measurement uncertainties in the laser interferometry-based sensing and tracking technique. *Measurement*, vol. 32, no. 2, pp. 135–150.
- Umetsu, K., Furutnani, R., Osawa, S., Takatsuji, T. and Kurosawa, T. (2005). Geometric calibration of a coordinate measuring machine using a laser tracking system. *Measurement Science and Technology*, vol. 16, no. 12, pp. 2466–2472.
- Vincze, M., Prenninger, J. and Gander, H. (1994). A laser tracking system to measure position and orientation of robot end effectors under motion. *The International Journal of Robotics Research*, vol. 13, no. 4, p. 305.
- Watson, J. (sa). A new approach to large scale measurement using four tracking interferometers. Tech. Rep., Itek Optical Systems, A Division of Litton Industries, 10 Maguire Road Lexington MA 02173 USA.
- Yongbing, L., Guoxiong, Z. and Zhen, L. (2003). An improved cat's-eye retro-reflector used in a laser tracking interferometer system. *Measurement Science and Technology*, vol. 14, no. 6, pp. 36–40.
- Yu, F. and Yang, X. (1997). *Introduction to Optical Engineering*. Cambridge University Press, New York , U.S.A.
- Zeng, L. and Song, D. (1999). Fringe position method for measuring the position of a tracking mirror. *Measurement Science and Technology*, vol. 10, no. 2, pp. N13–N16.
- Zhang, D., Rolt, S. and Maropoulos, P. (2005). Modelling and optimization of novel laser multilateration schemes for high-precision applications. *Measurement Science and Technology*, vol. 16, no. 12, pp. 2541–2547.
- Zhang, G., LI, X., Lin, Y., Liu, S., Liu, X., LI, X., Guo, J., Qiu, Z., Zhao, S., Jiang, C. and Fan, Y. (2003). A study on the optimal design of laser-based multilateration systems. *CIRP Annals - Manufacturing Technology*, vol. 52, no. 1, pp. 427 – 430.

- Zhuang, H., LI, B., Roth, Z. and Xie, X. (1992). Self-calibration and mirror center offset elimination of a multi-beam laser tracking system. *Robotics and autonomous systems*, vol. 9, no. 4, pp. 255–269.
- Zhuang, H., Motaghedi, S., Roth, Z. and Bai, Y. (2003). Calibration of multi-beam laser tracking systems. *Robotics and Computer-Integrated Manufacturing*, vol. 19, no. 4, p. 301.
- Zhuang, H. and Roth, Z. (1995). Modeling gimbal axis misalignments and mirror center offset in a single-beam laser tracking measurement system. *The International Journal of Robotics Research*, vol. 14, no. 3, p. 211.